Volume 70A
Number 5
Sept.–Oct. 1966

Physics and Chemistry

U.S. DEPARTMENT OF COMMERCE

SECTION A

JOURNAL OF RESEARCH

NATIONAL BUREAU OF STANDARDS

Journal of Research

of the

National Bureau of Standards

A. Physics and Chemistry

Sept.–Oct. • 1966

VOLUME • 70A

NUMBER • 5

Editor: C. W. Beckett

Associate Editors: D. D. Wagman
J. M. Richardson

Publication dates:
Feb. 1, Apr. 1, June 1, Aug. 1, Oct. 1, Dec. 1, 1966

JOURNAL OF RESEARCH

The National Bureau of Standards Journal of Research reports research and development in the fields of activity shown at right. Also included from time to time are survey articles on topics closely related to the Bureau's scientific and technical program.

The Journal is published in three separate sections as follows:

A. Physics and Chemistry

Contains papers of interest primarily to scientists working in these fields. Issued six times a year. Annual subscription: domestic, $5.00; foreign, $6.00. Single copy, $1.00.

B. Mathematics and Mathematical Physics

Presents studies and compilations designed mainly for the mathematician and the theoretical physicist. Issued quarterly. Annual subscription: domestic, $2.25; foreign, $2.75. Single copy, 75c.

C. Engineering and Instrumentation

Reports research and development results of interest chiefly to the engineer and the applied scientist. Issued quarterly. Annual subscription: domestic, $2.75; foreign, $3.50. Single copy, 75c.

The National Bureau of Standards is a principal focal point in the Federal Government for assuring maximum application of the physical and engineering sciences to the advancement of technology in industry and commerce. Its responsibilities include development and maintenance of the national standards of measurement, and the provision of means for making measurements consistent with those standards; determination of physical constants and properties of materials; development of methods for testing materials, mechanisms, and structures, and making such tests as may be necessary, particularly for government agencies; cooperation in the establishment of standard practices for incorporation in codes and specifications; advisory service to government agencies on scientific and technical problems; invention and development of devices to serve special needs of the Government; assistance to industry, business and consumers in the development and acceptance of commercial standards and simplified trade practice recommendations; administration of programs in cooperation with United States business groups and standards organizations for the development of international standards of practice; and maintenance of a clearinghouse for the collection and dissemination of scientific, technical and engineering information. The scope of the Bureau's activities is suggested in the following listing of its three Institutes and their organizational units.

Institute for Basic Standards. Applied Mathematics. Electricity. Metrology. Mechanics. Heat. Atomic Physics. Physical Chemistry. Laboratory Astrophysics.* Radiation Physics. Radio Standards Laboratory.* Radio Standards Physics & Radio Standards Engineering. Office of Standard Reference Data.

Institute for Materials Research. Analytical Chemistry. Polymers. Metallurgy. Inorganic Materials. Reactor Radiations. Cryogenics.* Materials Evaluation Laboratory. Office of Standard Reference Materials.

Institute for Applied Technology. Building Research. Information Technology. Performance Test Development. Electronic Instrumentation. Textile and Apparel Technology Center. Technical Analysis. Office of Weights and Measures. Office of Engineering Standards. Office of Invention and Innovation. Office of Technical Resources. Clearinghouse for Federal Scientific and Technical Information.**

*Located at Boulder, Colo. 80302.
**Located at 5285 Port Royal Road, Springfield, Va. 22151.

U.S. DEPARTMENT OF COMMERCE
John T. Connor, Secretary

NATIONAL BUREAU OF STANDARDS
A. V. Astin, Director

Order all publications from the Superintendent of Documents
U.S. Government Printing Office, Washington, D.C. 20402

Use of funds for printing this publication approved by the Director of the Bureau of the Budget (June 22, 1966).

JOURNAL OF RESEARCH of the National Bureau of Standards—A. Physics and Chemistry
Vol. 70A, No. 5, September–October 1966

Orientation of Calcium Molybdate ($CaMoO_4$) and Other Single Crystals Having the Scheelite Structure*

E. N. Farabaugh, H. S. Peiser, and J. B. Wachtman, Jr.

Institute for Materials Research, National Bureau of Standards, Washington, D.C. 20234

(May 20, 1966)

Values of interplanar angles useful in distinguishing the [100] from the [110] direction in $CaMoO_4$ are given to facilitate orientation by analysis of back-reflection Laue patterns. The distinction between the [001] and [00$\bar{1}$] directions in the scheelite structure is discussed and examples of physical properties dependent upon this distinction are given. The [001] direction is defined in terms of the crystal structure and a procedure for identifying [001] using Laue patterns is described. The same distinction applies to certain nonpolar directions of all crystals belonging to the following nonenantiomorphous point groups: $\bar{1}$, m, 2/m, mmm, $\bar{3}$, 3m, $\bar{3}$m, $\bar{4}$, 4/m, 4/mmm, $\bar{6}$, 6/m, 6/mmm, m3 and m3m.

Key Words: Calcium molybdate, crystal orientation, crystallographic groups, interplanar angles, physical properties, scheelite structure, single crystal, x-ray back-reflection.

1. Introduction

A large number of phases having the scheelite structure are known [*1*].[1] The ability of these crystals to accept trivalent ions into solid solution and their optical suitability as laser ion hosts [*2*] has stimulated recent interest in this family of crystals. The growth of scheelite itself, $CaWO_4$, has been studied [*3*, *4*, *5*] and an etch pitting technique for the observation of dislocations [*6*, *7*] has been developed. Substitution of trivalent rare-earth ions has been studied [*8*, *9*] as has the effect of vacuum reduction and photolytic coloring of doped crystals [*10*, *11*]. Work has been published on a number of physical properties including electron spin resonance [*12*, *13*], plastic deformation [*14*], and sound velocity [*15*]; it appears likely that more physical properties data on scheelite structure crystals will soon be published. It is important that these data be referred to the proper crystal axes; the correct and complete crystal orientation requires that some fine distinctions be made. The structure of $CaWO_4$ belonging to space group $I4_1/a\text{–}C_{4h}^6$ with Laue symmetry 4/m has been carefully refined both by x-ray diffraction [*16*, *17*] and by neutron diffraction [*18*]; Zalkin and Templeton [*16*] point out that there are two distinct ways in which the axes may be oriented with respect to the structure and that the distinction depends upon differences in the intensity of symmetry unrelated pairs of diffracted beams of the distinct types (*hkl*) and (*khl*). The metal atoms in special positions, as will be elaborated in section 4 below, do not contribute to these differences which are for many reflection pairs quite small. Previous authors, however, do not discuss the specific process of orientation by Laue pattern analysis. We shall show that this distinction can be made from visual inspection of a back-reflection Laue pattern provided it is taken on a surface parallel to (001). Some interplanar angles useful in Laue pattern analysis have been given by Nassau [*19*] and by Frounfelker and Hirthe [*20*], but the distinction between [001] and [00$\bar{1}$] is not discussed. These angles are useful in distinguishing between [100] and [110] but the distinction depends upon small angular differences; additional angles are given in the present paper to make identification more certain. We shall illustrate the orientation procedure with angles and Laue patterns for $CaMoO_4$. The results should be applicable to any of the scheelite-structure materials. They should also serve as a general illustration of the technique for determining the sense of axes in those crystals where different senses exist and are manifested in a certain cyclic sequence of intensities of diffracted beams.

2. Relation of Axes to Point Group and Space Group Symmetry

The point group of scheelite is 4/m (C_{4h}) and the space group is $I4_1/a$. The crystallographic *c* axis is conventionally [*21*, *22*] taken parallel to the 4-axis, and the Z axis of the set of right-handed rectangular XYZ axes (to which physical properties are usually referred) may be taken in either direction along the 4-axis with different results for the sign of certain physical properties. On first thought this statement may appear incorrect; if +Z is arbitrarily chosen parallel to the 4-axis, the perpendicular mirror plane makes −Z equivalent. Clearly the Z axis is not of the type variously termed vector, polar, or uniterminal by dif-

*The work was partially supported by the U.S. Atomic Energy Commission.

[1] Italicized figures in brackets indicate the literature references at the end of this paper.

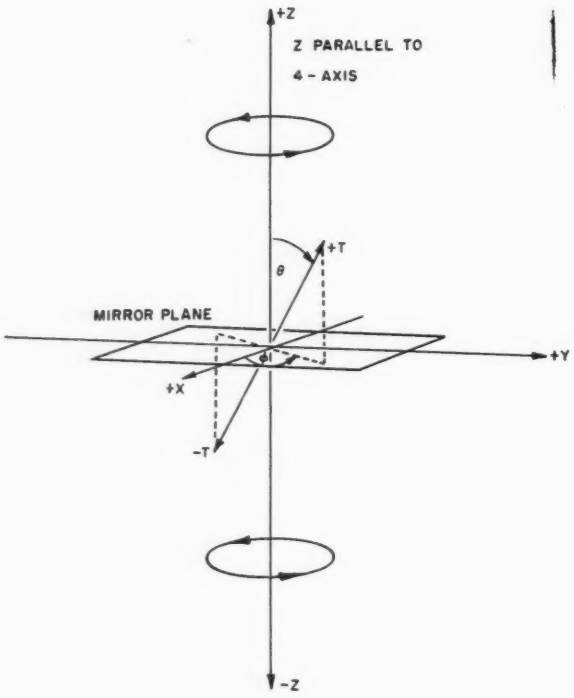

FIGURE 1. *Distinction between +Z and −Z in point group 4/m.*

ferent writers [*23*, *24*, *25*]. The +Z and −Z axes are equivalent in the sense that they are related by one or more symmetry operations of the crystal; they are, nevertheless, distinguishable as shown in figure 1. Consider any feature of the crystal (such as a particular sequence of atoms) which has a clockwise sense when viewed from the origin looking along +Z. The mirror plane requires the presence of an equivalent sequence around −Z which will have counterclockwise sense when viewed from the origin. The space group of scheelite has a glide plane instead of a mirror plane so that two equivalent sequences would be displaced perpendicular to [001] as well as reflected but the conclusion that the sequences show opposite senses of rotation when viewed from an intermediate point remains valid. To specify an arbitrary direction, T, in the usual spherical polar coordinate system of figure 1 thus requires a range of $0 \leq \theta \leq 180°$ and $0 \leq \Phi < 90°$. If measurements are made from −T to −Z to give values of θ' and Φ' (with Φ' measured in the same sense about −Z as Φ about +Z) the conversion is $\theta = \theta'$, $\Phi = 90° - \Phi'$. The choice of X fixes Y once +Z has been chosen and the stipulation made that XYZ form a right-handed rectangular system; the X axis is taken parallel to either of the two equal dimensions of the smallest unit cell [*22*].

TABLE 1. *Angles between planes in crystals of* $CaMoO_4$ c/a = *2.187*

$\{h_1k_1l_1\}$	$\{h_2k_2l_2\}$	Values of angles between $\{h_1k_1l_1\}$ and $\{h_2k_2l_2\}$
001	011	65.4°
	023	55.5°
	012	47.6°
	013	36.1°
	014	28.6°
	015	23.1°
	016	19.5°
	017	16.9°
001	111	72.1°
	223	64.1°
	112	57.1°
	113	45.9°
	114	37.7°
	115	31.4°
	116	26.9°
	117	23.6°
	118	20.6°
	1·1·10	16.5°
010	012	42.4°
	023	34.4°
	034	31.4°
	011	24.5°
	043	18.9°
	032	16.9°
	021	12.8°
	031	8.6°
	041	6.5°
110	112	32.9°
	223	25.9°
	334	23.3°
	111	17.9°
	443	13.6°
	332	12.1°
	221	9.1°
	331	6.1°
	441	4.6°
100	410	14.0
	310	18.4
	210	26.5
	110	45.0

3. Distinction Between [100] and [110] Using Angles Determined From a Laue Pattern

The usual back-reflection Laue camera [*26*] using 3 cm specimen-to-film distance gives a pattern corresponding to a spherical segment subtending about 60°. Poles lying outside this segment can be constructed from hyperbolas on the film but the angular error increases so that it is best to base identification on angles between poles corresponding to spots on the film. The center of the sector may lie anywhere in the spherical triangle with corners (001), (100), (110); angles in any of the other octants are the same so we can momentarily disregard the distinction between [001] and [00$\bar{1}$]. Evidently at least one of the poles (001), (102), (100), (113), and (110), must fall within the sector. Angles between poles lying near these reference poles are given in table 1. It should be noted that the distinction between the direction of [100] and [110] depends on differences such as 28.7 deg from (001) to (104) compared to 26.9 deg from (001) to (116) so that some care is needed. These angles are based on $c/a = 2.187$ of Swanson, Gilfrich, and Cook [*27*] for $CaMoO_4$; other scheelite structures having different c/a ratios will have somewhat different values. The tables of Frounfelker and Hirthe

[20] give values of angles for several c/a values; these tables can be used as a practical guide in making small corrections to our angular values for the variations in c/a encountered for other scheelite structures. Angles between 100 and $hk0$ are independent of c/a; angles between 100 and hkl are given by arc cot $\sqrt{2}\,(c/a)(h/l)$.

4. Distinction Between [001] and [00$\bar{1}$] Using Intensity of Spots on Laue Pattern

The pair of diffracted beams $\{hkl; khl\}$ would have equal intensities were it not for the contribution from the oxygen atoms in general positions. The unequal intensities of such pairs can be used to define a sense of rotation about Z. The result can be derived from the structure factor tables [21] for $I4_1/a$ that the intensity of a diffracted beam, $I(h, k, l)$, should obey

$$I(h, k, l) = I(\bar{k}, h, l) = I(\bar{h}, \bar{k}, l) = I(k, \bar{h}, l)$$

$$= I(\bar{h}, \bar{k}, \bar{l}) = I(k, \bar{h}, \bar{l}) = I(h, k, \bar{l}) = I(\bar{k}, h, \bar{l}).$$

These are different from the set

$$I(k, h, l) = I(\bar{h}, k, l) = I(\bar{k}, \bar{h}, l) = I(h, \bar{k}, l)$$

$$= I(\bar{k}\,\bar{h}, \bar{l}) = I(h, \bar{k}, \bar{l}) = I(k, h, \bar{l}) = I(\bar{h}, k, \bar{l}).$$

The relevant structure-factor equations are quoted in the International Tables [21].

For distinguishing [001] from [00$\bar{1}$] it is required that there is at least one pair of reflections $\{hkl; khl\}$ for which $I(hkl)/I(khl)$ differs from one by as large a factor as possible. Intensity ratios differing greatly from one will be associated with reflections for which the metal ions' contribution to the structure factor—equal for hkl and khl—is small. This condition assures the relative independence of intensity from the chemical identity of the ions, as for example a change from W to Mo ions.

Using 20 to 25 kV peak Ag x-radiation with the characteristic radiation repressed, good back-reflection pictures were obtained. Back-reflection pictures of $CaMoO_4$, figure 2, revealed several pairs of planes with intensity differences between hkl and khl easily recognizable. The following four pairs were used in the orientation determination: {2,1,11; 1,2,11}, {3,1,18; 1,3,18}, {2,1,13; 1,2,13}, and {3,2,15; 2,3,15}. Their corresponding intensity ratios, measured on a densitometer comparator, were 5, 0.7, 4, and 0.3.

In back-reflection pictures of $PbMoO_4$, the differences in intensities of hkl and khl were not as easily recognized because of the large contribution to the intensity by the Pb ion. Two sets of planes {2,1,11; 1,2,11} and {2,1,13; 1,2,13} could still be recognized as exhibiting intensity differences. The measured intensity ratios were 2 for both sets of planes. Upon examination of the structure factor equations it was found that the metal ion contribution was the smallest relative to the oxygen contribution in these two sets of planes {2,1,11; 1,2,11} and {2,1,13; 1,2,13} for both $CaMoO_4$ and $PbMoO_4$.

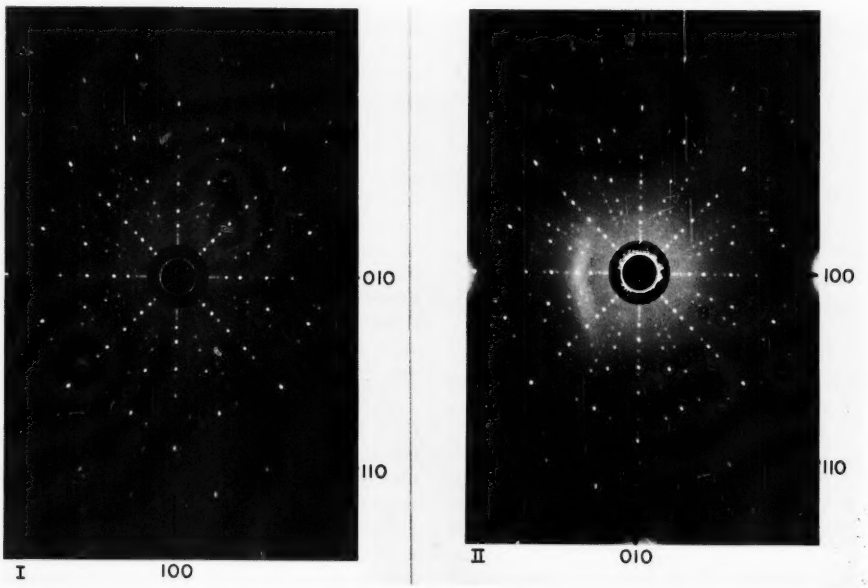

FIGURE 2. *Laue back-reflection pictures of* $CaMoO_4$ *showing the (001) and (00$\bar{1}$) orientations.*

Furthermore, when comparing intensities for pairs of reflections $\{hkl; khl\}$ for purposes of orientation it is desirable to pick a pair for which the contribution to the intensities from the oxygen in the general position is not a sensitive function of the x, y, and z parameters of the oxygen general position. These oxygen parameters are variable for different members of the crystal-chemical group of scheelite phases. Appreciable variability with solid-solution effects must be expected. Evaluation of the structure factor equations for the different pairs of planes over a range of x, y, and z's indicated that the two pairs of planes {2,1,11; 1,2,11} and {2,1,13; 1,2,13} best satisfied this condition. Thus these two pairs of planes are quite useful in determining the sense of [001] in scheelites, even in the case of the heavy cation Pb in $PbMoO_4$.

To determine the correct setting of the axes with respect to the crystal using the Laue method the ratio of the reflected intensities of each of the previously mentioned 4 pairs of reflecting planes was calculated for both $CaMoO_4$ and $PbMoO_4$.

Using the oxygen parameters specified by Sillén and Nylander [*28*] for $CaMoO_4$ ($x=0.25$, $y=0.15$, $z=0.075$) the calculated ratios for $CaMoO_4$ were not consistent with the measured ratios in that the calculated ratio $I(3,2,15)/I(2,3,15) \approx 1$. However, when the calculations were done using the data of Zalkin and Templeton [*16*] for the oxygen parameters ($x=0.2415$, $y=0.1504$, $z=0.0861$) of $CaWO_4$, the calculated intensity ratios were consistent with the measured ones. From the few data points examined here, a structure refinement for $CaMoO_4$ is indicated. Using the $CaWO_4$ oxygen parameters for the $CaMoO_4$ calculations it was found that $I(2,1,11) > I(1,2,11)$; $I(3,1,18) < I(1,3,18)$, $I(2,1,13) > I(1,2,13)$ and $I(3,2,15) < I(2,3,15)$. With this information the axes of $CaMoO_4$ can then be chosen to agree with the setting of Zalkin and Templeton, and to satisfy the above inequalities.

The same procedure was carried out with $PbMoO_4$. Using the data of Leciejewicz's refinement of $PbMoO_4$ [*29*], the intensity ratios of the two observable pairs of planes were $I(2,1,11) > I(1,2,11)$ and $I(2,1,13) > I(1,2,13)$. Thus these two sets of planes can be used to chose the correct setting of the axes consistent with the intensity ratios and the sense of [001].

Figure 2 shows two Laue patterns of $CaMoO_4$ taken with the [001] and [00$\bar{1}$] orientations respectively. In figure 2(I) (the $+c$ direction out of the plane of the picture) the spots are labeled as follows: A′=(3,1,18), A=(1,3,18), B′=(2,1,13), B=(1,2,13), C′=(2,1,11), C=(1,2,11), D′=(3,2,15) and D=(2,3,15). In figure 2(II) ($-c$ direction out of the plane of the picture) the spots are labeled as follows: A′=(3,1,$\bar{1}\bar{8}$), A=(1,3,$\bar{1}\bar{8}$), B′=(2,1,$\bar{1}\bar{3}$), B=(1,2,$\bar{1}\bar{3}$), C′=(2,1,$\bar{1}\bar{1}$), C=(1,2,$\bar{1}\bar{1}$), D′=(3,2,15), and D=(2,3,$\bar{1}\bar{5}$). It may be noted here that the differences in the intensities are somewhat diminished in making a print from the x-ray film; the intensity differences are more easily observed on the film itself. One can now choose +Z from simple inspection of these patterns. It is, however, necessary to have a flat ground parallel to (001) within a few degrees and to have the beam incident perpendicular to (001) within a few degrees. Otherwise differences in absorption corrections applicable to the non-equivalent reflections constituting a pair $\{h, k, l; k, h, l\}$ could distort the intensity relationships to such an extent that the inequalities can no longer be recognized at sight on the Laue pattern. The absorption, Lorentz, and polarization corrections (for crystals intercepting the entire beam) are the same for hkl and khl when the incident x-ray beam is parallel to [001] and the surface is (001). One can first determine the orientation, apart from the distinction between +Z and −Z, from a Laue pattern taken at random orientation and then grind a small flat parallel to (001) for a second Laue pattern.

5. Physical Properties Dependent on the Distinction Between +Z and −Z

Scalar, first rank, and symmetric second rank tensor properties do not depend on the distinction between +Z and −Z as can be seen from the fact that the matrices for these properties are the same as for the highest symmetry tetragonal point group, 4/mmm, for which the distinction between +Z and −Z vanishes. The center of symmetry possessed by 4/m makes scheelite nonpiezoelectric so that this property need not be considered. The sign of the elastic compliance $[30]s_{16}$ ($s_{16}=s_{61}$) does, however, depend on the choice of +Z; the Standards on Piezoelectric Crystals [*22*] apparently overlooks this fact. A tensile stress along X in a crystal of point group 4/m will cause an elastic deformation in which both X and Y must remain perpendicular to Z, but the angle between X and Y need not remain a right angle. Thus, in general, application of σ_{11} will cause a nonvanishing value of e_{12} and give a nonzero value of $s_{61}=4s_{1211}$. Suppose the value of s_{61} is positive for our choice of +Z and a particular choice of X. If we rotate our coordinate system 90° about Z so that X′=Y and Y′=−X we have a tensile stress $\sigma'_{22}=\sigma_{11}$ and a shear strain $e'_{12}=-e_{12}$ giving an elastic compliance $s'_{62}=4s'_{1222}=-s_{61}$. This is consistent with the requirement for crystals of point group 4/m that $s_{62}=-s_{61}$. Thus no change in the numerical values of the elastic constants results from a rotation of the coordinate system 90° about Z. If, however, we reverse the direction of Z and choose a right-handed system such that Z″=−Z, X″=X, Y″=−Y the result is $\sigma''_{11}=\sigma_{11}$, $e''_{12}=-e_{12}$ and $s''_{61}=4s''_{1222}=-s_{61}$ so that the sign of s_{61} is changed by interchanging +Z and −Z and retaining a right-handed system.

A number of tensor properties are listed by Nye [*30*] (see pp. 290–291) and some appear to be dependent on the choice of +Z. Thus it appears that some elements in the matrix of the piezo-optical tensor will depend on this choice. The situation should be considered carefully for any property more complex than a symmetrical second rank tensor and the decision made as to whether the additional trouble of determining +Z is required for correct determination of all matrix elements.

6. General Occurrence of Symmetry Related Directions Which Are Distinguishable

The effect here discussed is clearly not limited to crystals having the scheelite structure. It does not depend, for example, on the existence of a screw axis 4_1 or 4_3 parallel to z, but would apply to crystals with structures belonging to any space group in the 4/m class. It is interesting to inquire which directions in which point groups have the property of being symmetry related but distinguishable by the right or left handedness of their surroundings when viewed from a common origin. We shall term these enantiomorphous nonpolar directions keeping in mind that the concept of an enantiomorphous crystal (one whose mirror image cannot be brought into coincidence with the crystal itself by any sequence of proper rotations) is different. A nonpolar direction cannot have this enantiomorphous character if it lies in a mirror plane or if it is perpendicular to an evenfold axis. Other symmetry elements occurring in crystallographic point groups do not destroy this enantiomorphous character. Thus, for example, a general direction in any centrosymmetric point group is an enantiomorphous nonpolar direction. The general direction $[u\,v\,w]$ in m3m is equivalent to $[\bar{u}\,\bar{v}\,\bar{w}]$ in the sense that the two are symmetry related but they are nevertheless distinguishable by handedness of environment; we would require a left-handed coordinate system to write $[\bar{u}\,\bar{v}\,\bar{w}]$ for $[u\,v\,w]$. In noncentrosymmetric point groups a general direction is always polar. The special directions for both centrosymmetric and noncentrosymmetric classes require detailed examination; the results are summarized for centrosymmetric classes in table 2. All enantiomorphous nonpolar directions in centrosymmetric classes except general directions are found to be parallel to symmetry axes of order two or greater. Only four of the noncentrosymmetric point groups are found to contain enantiomorphous nonpolar directions as listed in table 3.

TABLE 2. *The enantiomorphous nonpolar directions, other than the general direction, in centrosymmetric crystals*

Centrosymmetric class	$[uvw]$ Indistinguishable opposites	$[uvw]$ Distinguishable opposites parallel to axial symmetry (order ≥ 2)
$\bar{1}$	None	None
2/m	$v=0$	[010]
mmm	u, v or $w=0$	None
$\bar{3}$	None	[001]
$\bar{3}$m	$v=2u$; $v=\frac{1}{2}u$; $v=-u$	[100]; [010]; [110]
4/m	$w=0$	[001]
4/mmm	u, v, or $w=0$, $u=\pm v$	None
6/m	$w=0$	[001]
6/mmm	u, v, or $w=0$, $u=\pm v$, $2v$, or $\frac{1}{2}v$	None
m3	u, v, or $w=0$	[±1±11]
m3m	u, v, or $w=0$, $u=\pm v$; $v=\pm w$; $w=\pm u$	None

TABLE 3. *The enantiomorphous nonpolar directions in noncentrosymmetric crystals*

Point group	Nonpolar directions with $[uvw]$ distinguishable from $[u\,v\,w]$
m	[010]
3m	[100]; [010]; [110]
$\bar{4}$	[001]
6	[001]

The authors acknowledge the work of W. S. Brower of NBS in the growth of the crystals of $CaMoO_4$ and $PbMoO_4$ used in this research.

7. References

[1] R. W. G. Wyckoff, Crystal Structures II, chap. VIII, table page 13 (Interscience Publishers, 1960).

[2] R. C. Duncan, Continuous room-temperature Nd^{3+}: $CaMoO_4$ laser, J. Appl. Phys. **36,** 874 (1965).

[3] K. Nassau and A. M. Broyer, Calcium tungstate: Czochralski growth, perfection, and substitution, J. Appl. Phys. **33,** 3064 (1962).

[4] K. Nassau, Effect of growth parameters on the threshold of $CaWO_4$: Nd crystals, Proceedings of the Symposium on Optical Masers, p. 451 (1963).

[5] B. Cockayne, D. S. Robertson, and W. Bardsley, Growth defects in calcium tungstate single crystals, Brit. J. Appl. Phys. **15,** 1165 (1964).

[6] H. J. Levinson, G. M. Loiacono, and K. Nassau, Calcium Tungstate—II. Observation of dislocations, J. Appl. Phys. **34,** 3603 (1963).

[7] A. R. Chaudhuri and L. E. Phaneus, Grown-in dislocations in calcium tungstate crystals pulled from the melt, J. Appl Phys. **34,** 2162 (1963).

[8] K. Nassau and G. M. Loiacono, Calcium Tungstate—III. Trivalent rare earth substitution, Phys. and Chem. of Solids **24,** 1503 (1963).

[9] K. Nassau, Calcium Tungstate IV—The theory of coupled substitution, Phys. and Chem. of Solids **24,** 1511 (1963).

[10] D. C. Cronemeyer and M. W. Beaubien, Coloring by vacuum reduction in Nd- and Pr-doped $CaWO_4$, Appl. Phys. Letters **4,** 85 (1964).

[11] D. C. Cronemeyer and M. W. Beaubien, Photolytic and reduction coloring of $CaWO_4$:Nd, J. Appl. Phys. **35,** 1779 (1964).

[12] G. H. Azarbayejani and A. L. Merlo, Election paramagnetic resonance of Eu^{+2} in $CaWO_4$, Phys. Rev. **137,** A489 (1965).

[13] J. Bronstein and V. Volterra, Electron paramagnetic resonance of Eu^{2+} in $CaWO_4$, Phys. Rev. **137,** A1201 (1965).

[14] A. Arbel and R. J. Stokes, Plastic deformation of calcium tungstate single crystals, Honeywell Research Report HR-64-275, July 1964.

[15] D. Gerlich, Sound velocity measurements in $CaWO_4$ single crystal, Phys. Letters **12,** 314 (1964).

[16] A. Zalkin and D. H. Templeton, X-ray diffraction refinement of the calcium tungstate structure, J. Chem. Phys. **40,** 501 (1964).

[17] R. D. Burbank, Absolute integrated intensity measurement: application of $CaWO_4$ and comparison of several refinements, Acta Cryst. **18,** 88 (1965).

[18] M. I. Kay, B. C. Frazer, and I. Almodovar, Neutron diffraction refinement of $CaWO_4$, J. Chem. Phys. **40,** 504 (1964).

[19] K. Nassau, Crystallographic angles of calcium tungstate (Tetragonal, $c/a=2.169$), Trans. AIME **218,** 959 (1960).

[20] R. E. Frounfelker and W. M. Hirthe, Crystallographic data for the tetragonal crystal system, Trans. AIME **224,** 196 (1962).

[21] N. F. M. Henry and K. Lonsdale, editors, International Tables for X-ray Crystallography Vol. **I** (Kynoch Press, Birmingham, England, 1952). See page 178 for the space group diagram and page 423 for the structure factor equations for $I4_1/a$.

[22] Standards on piezoelectric crystals, 1949, Proceedings I.R.E. **37**, 1378 (1949).
[23] W. G. Cady, Piezoelectricity (McGraw-Hill Book Co., New York, N.Y., 1946).
[24] Charles S. Smith, Macroscopic Symmetry and Properties of Crystals, p. 175 in Solid State Physics Vol. **6**, ed. by F. Seitz and D. Turnbull (Academic Press, New York, 1958).
[25] F. C. Phillips, An introduction to Crystallography, 3d ed., John Wiley & Sons, Inc., New York, N.Y. (1963).
[26] Elizabeth A. Wood, Crystal Orientation Manual, Columbia University Press (1963).
[27] H. E. Swanson, N. T. Gilfrich, and M. I. Cook, Standard x-ray diffraction patterns, National Bureau of Standards Circ. 539, Vol. **10** (1956).
[28] L. G. Sillén and A. L. Nylander, On the oxygen positions in tungstates and molybdates with the scheelite structure, Ark. Kemi, Min. Geol. **17A**, No. 4 (1943).
[29] J. Leciejewicz, Neutron crystallographic investigation of lead molybdenum oxide, $PbMoO_4$, Z. Krist. **121** [2–4] 158, (1965).
[30] J. F. Nye, Physical Properties of Crystals, Oxford University Press (1957).

(Paper 70A5–410)

JOURNAL OF RESEARCH of the National Bureau of Standards—A. Physics and Chemistry
Vol. 70A, No. 5, September–October 1966

Crystal Structure of $BaGe[Ge_3O_9]$ and Its Relation to Benitoite

C. Robbins, A. Perloff, and S. Block

Institute for Materials Research, National Bureau of Standards, Washington, D.C. 20234

(May 23, 1966)

$BaGe[Ge_3O_9]$ is trigonal, space group P3, with lattice constants $a=11.61$, $c=4.74$ Å, and $Z=3$.

The structure was established by three-dimensional Patterson and electron density syntheses. Three-dimensional least-squares refinement resulted in a final R value of 6.8 percent (observed data only).

The previously proposed structural relationship of this compound with benitoite, $BaTiSi_3O_9$, has been confirmed. The structure can be considered as composed of Ge_3O_9 rings, in which the Ge is tetrahedrally coordinated, linked through octahedrally coordinated Ge atoms to form a three-dimensional Ge-O network. All Ge polyhedra are linked by corner sharing. The Ba ions occupy positions in channels of the network.

Key Words: Barium tetragermanate, structure, benitoite, crystal, x-ray.

1. Introduction

The synthesis of three germanates of formula type $MeGe_4O_9$ (Me = Sr, Pb, Ba) was reported by Robbins and Levin [1].[1] A comparison of indexed powder patterns suggested that the compounds were isostructural. This was later confirmed by Eulenberger, Wittman, and Nowotny [2]. In addition, they reported the synthesis of two forms of $CaGe_4O_9$ designated α and β, and found the α form was isostructural with (Sr, Pb, Ba) Ge_4O_9.

Crystal chemical considerations (Robbins and Levin [1]) suggested a structural relationship with the mineral benitoite, $BaTiSi_3O_9$, whose structure was determined by Zachariasen [3]. Comparison of patterns of 1:4 germanates with indexed benitoite powder data supported this view. From these observations and a consideration of unit cell dimensions, a trial structure for the tetragermanates was obtained (Robbins and Levin [1]). To test the validity of the proposed model, the structure of $BaO \cdot 4GeO_2$ was determined.

2. Experimental Data

Single crystals in the form of needles elongated along [001] were obtained by slowly cooling a melt of composition $BaGe_4O_9$ from slightly above the congruent melting point of 1392 ± 5 °C.

Unit cell dimensions, density measurements, and optical data for this compound were reported by Robbins and Levin [1]. Their data plus the space group information are:

$a=11.61$ Å	$\omega=1.797\pm0.003$
$c=4.74$ Å	$\epsilon=1.783\pm0.003$
$S.G.=P3$	ρ (obs) $=5.1$ gcm^{-3}
$Z=3$	ρ (calc) $=5.12$ gcm^{-3}

No systematic absences were observed. Precession films were consistent with space groups P3ml or $P\bar{3}$ml. No satisfactory structure could be derived in these space groups. The possible space groups P3 or $P\bar{3}$ were then considered. The centrosymmetric choice could be eliminated on the basis of packing considerations because of the short c dimension. The assumption that the space group is P3 was confirmed by the final structure.

Integrating Weissenberg films of levels $h\ k\ l$ with $l=0, 1, 2, 3, 4$ were taken with Zr-filtered MoKα radiation ($\lambda=0.7107$ Å) using the multiple film technique. Intensities were measured with a densitometer comparator. Very weak reflections were estimated visually. The intensity data were obtained from a crystal approximately rectangular in cross section with dimensions of 0.043 mm, 0.066 mm, and a length of 0.189 mm. The linear absorption coefficient for molybdenum radiation is 222.41 cm^{-1}.

Lorentz and polarization factor corrections were applied. Since the main objective of the study was the determination of positional parameters, no corrections for absorption errors were made. The latter would be expected to affect, primarily, the thermal parameters. The data consisted of 327 observed and 435 unobserved independent reflections.

[1] Figures in brackets indicate the literature references at the end of this paper.

TABLE 1. *Final atomic parameters*[a]

	x	σ(x)	Y	σ(Y)	z	σ(z)	B	σ(B)
Ba	0.3341	0.0004	0.3334	0.0005	0.0		1.0265	0.0526
Ge(1)	.0		.0		−.0928	0.0034	0.3509	.2221
Ge(2)	.6667		.3333		.0062	.0038	.5501	.1798
Ge(3)	.3333		.6667		.1024	.0031	.2158	.1867
Ge(4)	.8148	.0007	.8200	.0006	.4111	.0025	.3859	.1570
Ge(5)	.6674	.0007	.5131	.0006	.5051	.0034	.1402	.0864
Ge(6)	.5180	.0006	.6719	.0007	.5929	.0025	.3680	.1275
O(1)	.8459	.0032	.9286	.0035	.1193	.0075	−.4341	.4651
O(2)	.5843	.0046	.4074	.0047	.2158	.0106	1.1598	.7527
O(3)	.7746	.0033	.6524	.0033	.3101	.0078	−0.1996	.5040
O(4)	.5505	.0035	.5561	.0035	.6965	.0080	.0655	.5479
O(5)	.4743	.0056	.7350	.0058	.8978	.0127	2.2502	.9361
O(6)	.9264	.0038	.8428	.0036	.6430	.0082	0.0008	.5266
O(7)	.6650	.0069	.8081	.0068	.4927	.0175	3.0732	1.2087
O(8)	.4059	.0043	.5880	.0041	.3274	.0091	1.0008	0.6433
O(9)	.7525	.0048	.4844	.0046	.7472	.0103	1.1328	.7087

[a] The standard deviations are derived from the full-matrix least-squares refinement.

3. Structure Determination

Similarities in the x-ray powder patterns and unit cell dimensions of benitoite ($BaTiSi_3O_9$) and $BaO{\cdot}4GeO_2$ led Robbins and Levin [1] to suggest that barium germanate probably exists as $BaGeGe_3O_9$ in a structural arrangement closely related to that found for benitoite by Zachariasen [3]. The large number of unobserved reflections obtained in the present study was consistent with the proposed relationship provided the Ba and Ge atoms had x and y parameters near $1/3$ and $2/3$ and z parameters near 0 or $1/2$ in the germanate cell. In benitoite Ba, Ti, and the Si_3O_9 rings all are on, or around threefold axes. The lower symmetry of the germanate permits, at most, only one of the corresponding atoms or groups to be on a threefold axis.

A three-dimensional Patterson function was computed and peaks corresponding to Ba-Ba and Ge-Ge vectors were identified and related to the proposed model. On the basis of the trial structure and space group P3, three choices of origin were possible i.e., at the center of a Ge_3O_9 group, at a Ba atom or at an octahedrally coordinated Ge atom. Using coordinates of Ba and Ge from the model, three cycles of Fourier refinement were calculated for each choice of origin. Only the model with a Ge atom at the origin on a threefold axis refined satisfactorily. Using phases based on Ba and Ge positions from the Fourier refinement, a 3-dimensional electron density map was calculated which yielded the oxygen coordinates.

The structure was refined by a full-matrix least-squares analysis of the 327 observed and 435 unobserved reflections. The final conventional R value based on the 327 observed independent reflections was 0.068. The total number of parameters varied was 62 which included x, y, and z, an isotropic temperature factor for each atom and a scale factor for each level. The final parameters from this refinement are listed in table 1. The temperature factors are not considered meaningful, primarily because of absorption. The correlation matrix from this refinement indicated that many of the variables were correlated to a moderate degree (correlation coefficients on the order of 0.5 to 0.6). The possibility that this was the source of the unrealistic temperature factors was considered. A second least-squares refinement was made in which, alternately, scale and position parameters were varied for 2 cycles with fixed temperature factors and then temperature factors were varied for 2 cycles with fixed scale and position parameters. This was repeated for a total of eight cycles. The result was identical with the first refinement to within one standard deviation. Therefore, only the parameters from the first refinement are given in this paper. Observed and calculated structure factors are reported in table 2.

Atomic scattering factors for neutral Ge and O^{-1} were taken from *International Tables for X-ray Crystallography* (1962). Values for Ba^{+2} were taken from Thomas and Umeda [4]. The barium and germanium form factors were corrected for dispersion (International Tables for X-ray Crystallography, 1962).

4. Structure Description

A projection of the structure of $BaO{\cdot}4GeO_2$ along [001] is shown in figure 1. Numbering of the atoms of the asymmetric unit is consistent with table 1. The structure is made up of rings of three GeO_4 tetrahedra linked together by GeO_6 octahedra. Barium atoms are located in channels of the network. Germanium atoms 1, 2, and 3 are octahedrally coordinated and lie on threefold axes. Germanium atoms 4, 5, and 6, in tetrahedral coordination, make up the Ge_3O_9 ring. Six rings are linked through a germanium octahedron to form the germanium-oxygen network. The two nonring oxygens of each of three equivalent GeO_4 tetrahedra are bonded to germanium atoms above and below the ring to form GeO_6 groups. Every germanium polyhedron shares all of its corners: GeO_4 tetrahedra share only corners with other polyhedra with the exception of Ge (6), which shares one edge with a barium polyhedron; each germanium octahedron shares three edges with three different barium polyhedra.

The Ge_3O_9 ring, projected along [001], is shown in figure 2. Interatomic distances, angles and standard deviations for the three germanium atoms in tetra-

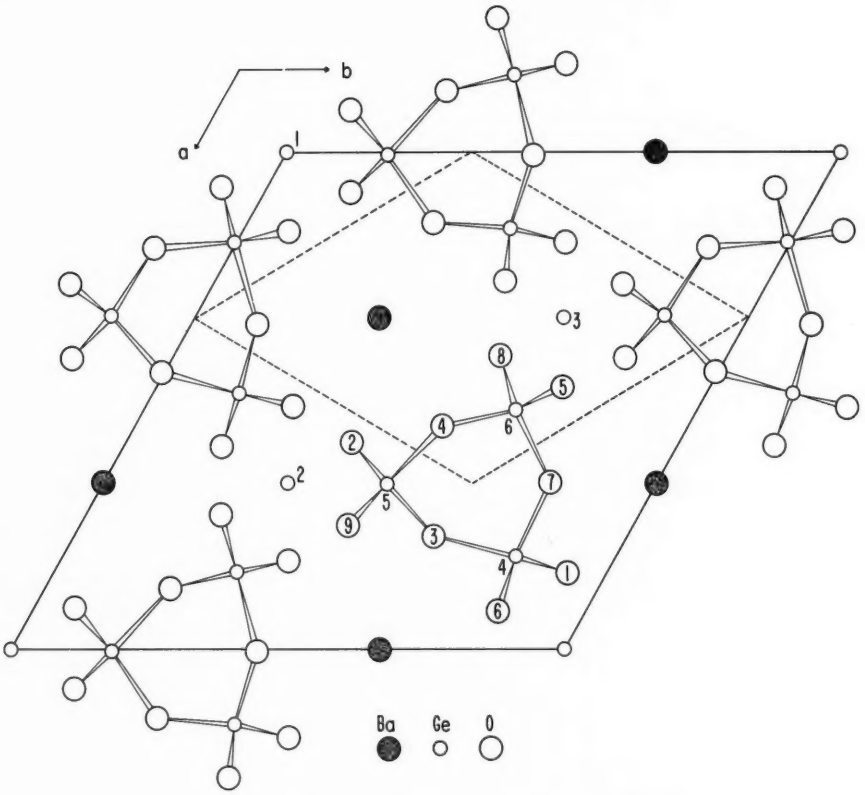

FIGURE 1. *[001] Projection of the* BaGe $[Ge_3O_9]$ *structure.*
The numbering is that of table 1.

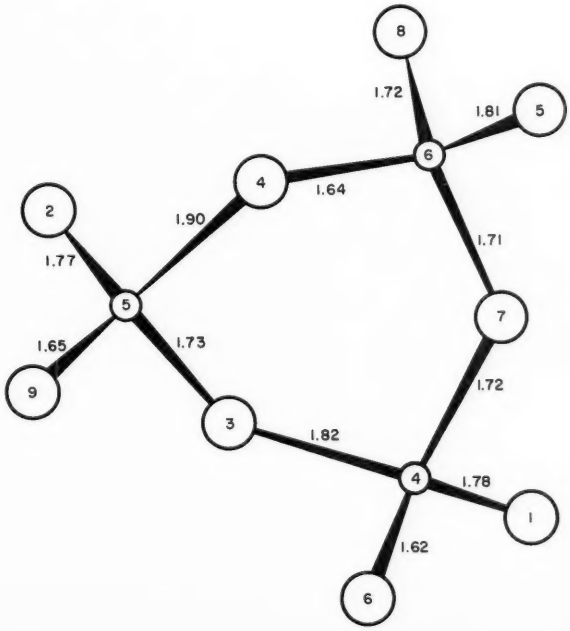

FIGURE 2. *[001] Projection of the* Ge_3O_9 *ring.*
The numbers identify atoms in table 1. Bond distances are in Å.

TABLE 2. *Comparison of observed and calculated structure factors* S(hk0)=*1.97*, S(hk1)=*2.68*, S(hk2)=*3.09*, S(hk3)=*3.25*, S(hk4)=*4.44*

h	k	l	Fo	sFc	h	k	l	Fo	sFc	h	k	l	Fo	sFc
0	15	0	97	88	3	5	1	55	68	2	8	2	124	121
1	4	0	104	107	3	6	1	178	170	-2	0	2	74	81
1	-5	0	111	108	-3	-6	1	190	184	-2	10	2	124	120
1	7	0	55	58	3	-7	1	51	73	3	0	2	136	133
1	-8	0	53	50	-3	7	1	43	46	3	-1	2	103	95
1	10	0	94	94	-3	-9	1	156	153	3	-2	2	62	60
1	-11	0	92	95	3	9	1	165	155	3	2	2	72	54
2	5	0	60	49	-3	9	1	176	173	3	4	2	55	39
2	-7	0	60	57	-3	12	1	168	160	3	5	2	53	53
2	8	0	169	171	4	0	1	34	36	3	-6	2	107	109
-2	10	0	169	176	4	-1	1	33	38	3	6	2	84	88
2	11	0	46	49	4	1	1	147	146	3	-7	2	99	98
-2	13	0	42	50	4	-2	1	82	94	-3	9	2	90	95
2	14	0	53	56	-4	-4	1	75	80	4	0	2	115	105
-2	16	0	54	56	4	4	1	72	81	4	1	2	73	68
3	0	0	123	113	-4	5	1	145	150	4	-2	2	223	224
3	3	0	116	111	4	7	1	92	80	4	4	2	164	148
3	6	0	132	138	-4	7	1	82	83	4	6	2	60	56
3	-9	0	134	134	4	9	1	50	58	-4	-7	2	72	74
3	9	0	80	85	5	0	1	92	83	5	0	2	62	66
3	12	0	82	77	5	2	1	139	130	5	-1	2	61	66
4	4	0	208	230	5	-3	1	56	59	5	1	2	156	146
4	7	0	85	75	5	3	1	33	37	5	2	2	73	72
4	10	0	120	115	5	5	1	108	106	5	-2	2	60	57
4	13	0	43	50	-5	-5	1	114	104	5	5	2	72	76
5	5	0	155	156	5	8	1	103	94	5	7	2	76	79
5	11	0	100	97	-5	-8	1	86	87	6	-1	2	150	150
5	-16	0	87	90	-5	13	1	111	95	6	1	2	37	47
6	6	0	189	194	6	3	1	193	188	6	-3	2	104	106
6	9	0	90	84	7	1	1	175	171	6	3	2	66	67
7	4	0	81	87	-7	-4	1	77	76	6	-5	2	96	83
7	10	0	64	65	7	7	1	134	125	6	5	2	109	110
8	8	0	79	68	-7	-7	1	134	125	6	6	2	157	150
9	0	0	108	107	7	-9	1	69	83	-6	6	2	215	234
9	3	0	79	85	8	1	1	56	55	7	0	2	74	77
9	6	0	93	90	8	-5	1	59	66	7	-2	2	63	64
9	9	0	93	80	8	5	1	103	91	7	-3	2	107	101
10	7	0	54	60	-8	8	1	72	66	7	3	2	73	67
10	10	0	50	52	9	0	1	140	128	7	4	2	69	70
12	0	0	185	179	9	-1	1	41	60	8	1	2	51	59
12	3	0	79	75	9	-2	1	56	60	8	2	2	118	121
12	6	0	113	93	-9	-6	1	84	89	8	-4	2	167	170
12	9	0	51	50	9	6	1	89	74	8	-5	2	67	61
12	-18	0	86	82	9	-7	1	62	78	9	0	2	108	93
13	4	0	49	54	10	1	1	81	81	9	-1	2	51	53
14	-7	0	36	45	10	3	1	42	48	9	3	2	66	67
14	-10	0	116	105	11	-1	1	90	87	9	-3	2	68	65
15	3	0	52	65	-12	-3	1	103	98	9	-10	2	72	65
0	3	1	274	286	-12	9	1	170	157	10	1	2	50	50
0	4	1	92	89	13	-3	1	51	52	-10	-1	2	92	82
0	5	1	35	42	0	2	2	36	33	10	-2	2	135	125
0	9	1	109	130		3	2	114	109	10	-3	2	62	64
1	2	1	85	80		4	2	37	40	10	-5	2	51	60
1	3	1	29	31		5	2	188	190	10	-6	2	51	56
1	4	1	127	128		6	2	229	233	10	-9	2	54	63
-1	5	1	129	125		9	2	76	71	-10	10	2	93	89
1	7	1	164	160		11	2	94	103	-11	1	2	82	77
-1	-7	1	171	166	1	1	2	62	63	11	1	2	69	74
-1	8	1	171	169	1	3	2	99	97	11	-1	2	77	66
1	13	1	79	94	1	4	2	83	75	11	2	2	64	56
2	1	1	105	100	-1	4	2	107	99	11	-5	2	105	107
2	-1	1	206	216	1	5	2	86	85	12	0	2	119	116
2	2	1	97	94	-1	5	2	79	83	12	-1	2	87	73
-2	3	1	107	94	1	6	2	104	98	-12	3	2	89	79
-2	-3	1	72	66	-1	7	2	106	96	12	-3	2	78	65
2	3	1	70	64	1	9	2	54	65	12	-6	2	149	143
-2	-5	1	130	127	1	10	2	65	77	12	-7	2	71	80
2	5	1	146	143	2	0	2	40	34	12	-9	2	89	77
2	6	1	37	44	2	-1	2	79	78	0	2	2	38	42
-2	7	1	141	136	2	2	2	198	214		3	3	145	147
-2	8	1	40	43	2	4	2	66	61		5	3	89	95
2	11	1	47	55	2	5	2	47	57		6	3	63	60
3	0	1	239	253	-2	6	2	54	58		8	3	88	90
3	2	1	68	66	2	7	2	78	80	1	1	3	97	108
3	4	1	39	57	-2	7	2	45	39	1	3	3	148	145

TABLE 2. *Comparison of observed and calculated structure factors* S(hk0 = *1.97*, S(hk1) = *2.68*, S(hk2) = *3.09*, S(hk3) = *3.25*, S(hk4) = *4.44* – Continued

h	k	l	Fo	sFc	h	k	l	Fo	sFc	h	k	l	Fo	sFc
1	4	3	93	87	8	−1	3	82	80	4	−3	4	90	80
1	7	3	82	76	8	−2	3	79	82	4	4	4	64	68
−1	8	3	82	82	8	−4	3	41	47	5	1	4	131	128
2	0	3	17	26	9	0	3	93	87	5	−2	4	35	35
2	−1	3	112	107	9	−1	3	122	121	5	4	4	74	74
2	1	3	186	172	9	3	3	49	61	5	−4	4	90	80
2	2	3	53	51	9	−3	3	100	105	5	5	4	73	69
2	5	3	93	90	9	−9	3	78	82	7	1	4	67	55
2	7	3	157	144	10	1	3	77	67	7	3	4	68	64
2	−7	3	79	79	10	3	3	98	98	7	4	4	45	58
−2	7	3	96	89	10	−3	3	109	105	7	−5	4	65	61
−2	9	3	141	143	10	−5	3	85	77	7	−8	4	67	73
3	0	3	99	93	11	−1	3	80	63	8	1	4	93	76
3	−1	3	170	175	11	−4	3	41	48	8	−1	4	67	58
3	2	3	127	115	11	−5	3	75	67	8	−4	4	52	65
3	3	3	108	106	11	−7	3	86	71	9	−1	4	72	68
3	5	3	103	104	12	−3	3	62	70	9	−6	4	49	54
3	−7	3	167	159	12	−4	3	86	93	9	−7	4	86	90
−3	8	3	105	105	0	2	4	57	54	10	−2	4	44	52
−3	9	3	80	74		3	4	83	81	10	−3	4	74	65
3	−9	3	98	97		5	4	158	153	10	−5	4	73	71
4	1	3	125	123		6	4	54	64	10	−6	4	95	85
4	−2	3	51	43	3	0	4	67	69					
4	−3	3	160	145	4	0	4	86	83					
4	4	3	33	42	6	0	4	42	54					
4	9	3	121	108	7	0	4	83	75					
5	−1	3	122	123	9	0	4	68	69					
5	−2	3	124	117	1	1	4	107	95					
5	−4	3	91	93	1	3	4	97	94					
5	5	3	80	77	1	4	4	90	79					
−6	2	3	57	55	1	6	4	95	85					
6	2	3	76	81	−1	7	4	84	81					
6	−3	3	103	106	1	7	4	91	73					
6	−4	3	50	53	−1	8	4	80	72					
6	5	3	64	61	2	1	4	98	97					
7	1	3	83	78	2	2	4	59	66					
7	−2	3	76	71	3	2	4	45	53					
7	3	3	112	98	3	6	4	45	53					
7	−3	3	164	151	3	−6	4	59	66					
8	1	3	130	119	4	1	4	99	83					

hedral coordination are given in table 3(A). The germanium-oxygen distances range from 1.617 ± 0.044 to 1.895 ± 0.048 Å,[2] with an average value of 1.74_0 Å. This agrees well with the average value of 1.74_0 Å recorded for $Na_4Ge_9O_{20}$ (Ingri and Lundgren [5]) and with individual independent values of 1.737 ± 0.003 Å and 1.741 ± 0.002 Å obtained by Smith and Isaacs [6] from a study of the α-quartz form of germanium dioxide. The O-Ge-O angles vary from $94.0 \pm 3.1°$ to $124.9 \pm 2.1°$ with an average value of 109.3°.

A GeO_6 group is shown in figure 3, [001] projection. Bond distances and angles for the three independent germanium atoms in sixfold coordination are presented in table 3(B). The mean Ge-O distance is 1.88 Å. This is in agreement with the value of 1.89 Å given by Ondik and Smith [7] for octahedrally coordinated germanium. It is apparent that both tetrahedra and octahedra are somewhat irregular.

[2] Standard deviation.

Germanium-germanium distances are listed in table 3(C). The average value of 3.15_3 Å is in good agreement with the value of 3.153_4 Å obtained by Smith and Isaacs [6].

The oxygen polyhedron about the barium ion is shown in figure 4 [001] projection. Barium is coordinated to ten oxygen atoms with bond lengths ranging from 2.663 ± 0.029 Å to 3.277 ± 0.087 Å. Bond distances and standard deviations are listed in table 4. The barium ions lie in channels in the germanate network as shown in figure 1.

5. Relation to Benitoite

The structural relationship between $BaGe[Ge_3O_9]$ and $BaTiSi_3O_9$ proposed by Robbins and Levin [1] is essentially correct. In figure 1, the dashed outline of the $BaTiSi_3O_9$ cell [3] is shown on the [001] projection of the germanate cell. Within the dashed lines, Ge(3) in six-fold coordination corresponds to titanium

TABLE 3. *Germanium-oxygen bond lengths and angles* [a]

A. Tetrahedrally coordinated germanium

Distances			*Angles*		
	Å	σ, Å			σ
Ge(4)–O(1)	1.783	0.039	O(1)–Ge(4)–O(3)	113.9°	1.8°
O(3)	1.823	.040	O(1) O(6)	123.3	1.6
O(6)	1.617	.044	O(1) O(7)	94.0	3.1
O(7)	1.719	.088	O(3) O(6)	96.3	2.1
			O(3) O(7)	105.4	2.6
			O(6) O(7)	123.8	3.2
Ge(5)–O(2)	1.770	.048	O(2)–Ge(5)–O(3)	97.0	2.0
O(3)	1.734	.033	O(2) O(4)	109.8	2.2
O(4)	1.895	.048	O(2) O(9)	124.9	2.1
O(9)	1.653	.053	O(3) O(4)	106.5	1.9
			O(3) O(9)	109.6	2.6
			O(4) O(9)	107.5	2.3
Ge(6)–O(4)	1.642	.049	O(4)–Ge(6)–O(5)	108.6	2.8
O(5)	1.805	.069	O(4) O(7)	108.0	3.5
O(7)	1.714	.060	O(4) O(8)	100.0	2.2
O(8)	1.720	.042	O(5) O(7)	101.5	3.3
			O(5) O(8)	121.9	2.7
Average	1.740		O(7) O(8)	116.2	3.1
			Average	109.3	
			Ge(4)–O(7)–Ge(6)	129.5	5.4
			Ge(4)–O(3)–Ge(5)	122.5	2.3
			Ge(5)–O(4)–Ge(6)	124.1	2.1
O(1)–O(3)	3.022	.056			
O(1)–O(6)	2.993	.059			
O(1)–O(7)	2.562	.080			
O(3)–O(6)	2.566	.047			
O(3)–O(7)	2.818	.107			
O(6)–O(7)	2.943	.097			
O(2)–O(3)	2.625	.050			
O(2)–O(4)	3.000	.071			
O(2)–O(9)	2.882	.069			
O(3)–O(4)	2.910	.052			
O(3)–O(9)	2.768	.056			
O(4)–O(9)	2.865	.068			
O(4)–O(5)	2.801	.091			
O(4)–O(7)	2.715	.081			
O(4)–O(8)	2.576	.068			
O(5)–O(7)	2.726	.100			
O(5)–O(8)	3.082	.074			
O(7)–O(8)	2.916	.070			

B. Octahedrally coordinated germanium

Distances			*Angles*		
	Å	σ, Å			σ
Ge(1)–O(1)	1.848	0.036	O(1)–Ge(1)–O(6)	88.0°	1.5°
O(6)	2.018	.039	O(1) O(1)^{i}	93.2	1.6
			O(6) O(6)^{i}	85.5	1.8
			O(1) O(6)^{i}	93.1	1.7
Ge(2)–O(2)	1.861	.063	O(2)–Ge(2)–O(2)^{i}	94.1	2.5
O(9)	1.957	.051	O(9) O(9)^{i}	84.8	2.4
			O(2)^{i} O(9)	94.0	2.0
			O(2)^{i} O(9)^{i}	86.9	2.3
Ge(3)–O(5)	1.717	.058	O(5)–Ge(3)–O(5)^{i}	91.2	2.8
O(8)	1.858	.056	O(8) O(8)^{i}	90.3	2.2
			O(8)^{i} O(5)	89.4	2.3
Average	1.877		O(8) O(5)^{i}	89.4	2.8
O(1)–O(6)	2.688	.059			
O(1)–O(1)^{i}	2.687	.039			
O(6)–O(6)^{i}	2.740	.068			
O(1)–O(6)^{i}	2.810	.052			
O(2)–O(2)^{i}	2.725	.087			
O(9)–O(9)^{i}	2.640	.089			
O(2)^{i}–O(9)	2.793	.080			
O(2)^{i}–O(9)^{i}	2.626	.069			
O(5)–O(5)^{i}	2.455	.066			
O(8)–O(8)^{i}	2.634	.080			
O(8)^{i}–O(5)	2.516	.084			
O(8)–O(5)^{i}	2.516	.074			

C. Distances between germanium atoms

	Å	σ, Å
Ge(1)–Ge(4)	3.167	0.017
Ge(1)–Ge(4)	3.194	.017
Ge(2)–Ge(5)	3.151	.019
Ge(2)–Ge(5)	3.159	.019
Ge(3)–Ge(6)	3.143	.015
Ge(3)–Ge(6)	3.210	.015
Ge(4)–Ge(5)	3.119	.011
Ge(4)–Ge(6)	3.106	.012
Ge(5)–Ge(6)	3.127	.014
Average	3.153	

[a] The standard deviations are derived from the diagonal terms of the least-squares matrix.

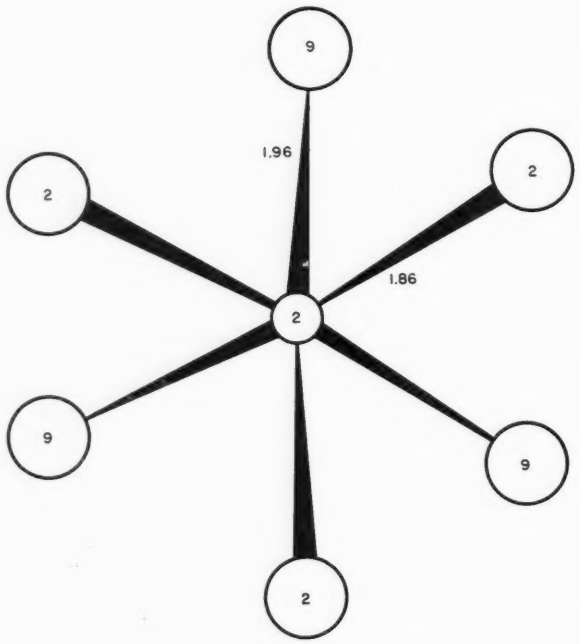

FIGURE 3. *[001] Projection of a GeO_6 group.*
The numbering is consistent with that of table 1. Bond distances are in Å.

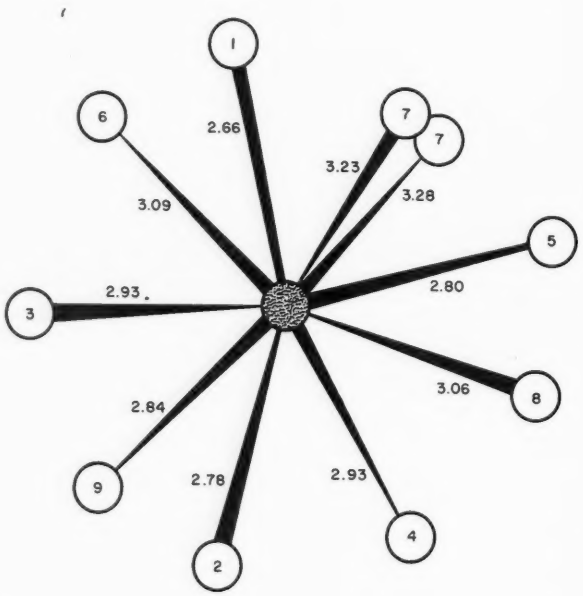

FIGURE 4. *Nearest neighbor barium ion coordination, [001] projection.*
The numbering is consistant with that of table 1. One O(7) atom is shown displaced slightly in *x* and *y*. Bond distances are in Å.

TABLE 4. *Bond distances of the barium coordination polyhedron*[a]

	Å	σÅ
Ba–O(1)	2.663	0.029
O(6)	3.088	.035
O(3)	2.929	.043
O(9)	2.836	.063
O(2)	2.780	.053
O(4)	2.927	.032
O(8)	3.063	.047
O(5)	2.802	.079
O(7)	3.277	.087
O(7)	3.227	.087

[a] The standard deviations are derived from the diagonal terms of the least-squares matrix.

TABLE 5. *Crystal data for* $BaGe[Ge_3O_9]$ *and* $BaTiSi_3O_9$

Compound	a, Å	c, Å	Space group	Calc. density, g cm^{-3}	Z
$BaGe[Ge_3O_9]$	11.61 ± 0.02	4.74 ± 0.01	P3	5.12	3
$BaTiSi_3O_9$ [a]	6.60 ± 0.01	9.71 ± 0.01	$P\bar{6}c2$	3.73	2

[a] Data from Zachariasen [3].

in the silicate compound and the rings to Si_3O_9 groups. In the silicate cell, the origin is on a threefold axis at the center of a ring. The Ba ion also lies on a threefold axis. In addition, $BaTiSi_3O_9$ has two sheets of rings in the length of the c axis ($c = 9.71$ Å, Zachariasen, [3] whereas $BaGe[Ge_3O_9]$ has one ($c = 4.74$ Å). For discussion, only the first sheet of the silicate structure will be considered.

With the substitution of three germanium atoms for three silicon atoms and one germanium atom for one titanium atom in the formula unit $BaTiSi_3O_9$ (to give $BaGe\ [Ge_3O_9]$) the following major structural changes are noted: (1) Unlike the silicon atoms and ring oxygens of Si_3O_9, germanium atoms and ring oxygens of the Ge_3O_9 group are not coplanar and the germanium ring does not have threefold symmetry. (2) While the titanium atom lies on a threefold axis at $z = 0$, three independent octahedrally coordinated germanium atoms lie on threefold axes at $z = -0.44_0$ Å, 0.02_9 Å and 0.48_5 Å.[3] (3) In benitoite, the barium ion is on a threefold axis surrounded by six oxygen atoms at a distance of 2.74 Å and six other oxygens at a distance of 3.4 Å. In the germanate cell, the barium ion is linked to 10 oxygen atoms at distances ranging from 2.66 Å to 3.28 Å, and no longer lies on a threefold axis. (4) SiO_4 tetrahedra share only corners with other polyhedra in benitoite. This is true of GeO_4 groups of the tetragermanate with the exception of Ge(6). The latter shares one edge with a barium polyhedron. (5) There are two sheets of rings within the c dimension of benitoite whereas $BaGe[Ge_3O_9]$ has one. Crystallographic data for the two compounds are presented in table 5.

[3] Origin chosen at $z = 0$ for Ba in both structures.

Computations were performed utilizing the x-ray 63 system of crystallographic programs developed at the University of Washington and the University of Maryland [8].

6. References

[1] C. R. Robbins and E. M. Levin, Tetragermanates of strontium, lead and barium of formula type AB_4O_9, J. Res. NBS **65A** (Phys. and Chem.) No. 2, 127–131 (1961).

[2] G. Eulenberger, A. Wittmann and H. Nowotny, Über wasserfreie germanate mit zweiwertigen metallion, Monatsh **93,** 123–128 (1962).

[3] W. H. Zachariasen, The crystal structure of benitoite, $BaTiSi_3O_9$, Z. Krist. **74,** 139–146 (1930).

[4] L. H. Thomas and K. Umeda, Atomic scattering factors calculated from the TFD atomic model, J. Chem. Phys. **26,** 293–303 (1957).

[5] N. Ingri and G. Lundgren, The crystal structure of $Na_4Ge_9O_{20}$, Acta Chem. Scand. **17,** 617–633 (1963).

[6] G. S. Smith and P. B. Isaacs, The crystal structure of quartz-like GeO_2, Acta Cryst. **17,** 842–846 (1964).

[7] H. Ondik and D. Smith, Interatomic distances in inorganic compounds, International Tables for X-ray Crystallography Vol. **III,** 257–274 (1962).

[8] University of Maryland, Computer Science Center, Technical Report TR–64–6 (1964).

(Paper 70A5–411)

JOURNAL OF RESEARCH of the National Bureau of Standards—A. Physics and Chemistry
Vol. 70A, No. 5, September–October 1966

A Rotating Cylinder Method for Measuring Normal Spectral Emittance of Ceramic Oxide Specimens From 1200 to 1600 °K

Howard E. Clark and Dwight G. Moore

Institute for Basic Standards, National Bureau of Standards, Washington, D.C. 20234

(June 10, 1966)

Equipment was designed and constructed for measuring the spectral emittance of polycrystalline ceramic oxide specimens in the wavelength region 1 to 15 μ and at temperatures of 1200, 1400, and 1600 °K. Specimens consisted of small hollow cylinders that were rotated at 100 rpm in a furnace cavity equipped with a water-cooled viewing port. Emittances were determined by comparing the radiance of the specimen to that of a blackbody at the same temperature.

A series of six measurements (two measurements each on three specimens) was made on commercially pure specimens of alumina, thoria, magnesia, and zirconia. All four materials showed similar behavior in that the emittances were low in the shorter wavelength regions and high at the longer wavelengths. The temperature coefficients of spectral emittance were positive for all four materials, but varied with the material; those for thoria were appreciably higher than the other three. In all cases coefficients were greater at short wavelengths than at long.

Error sources were investigated, and the measurement uncertainties associated with each source were evaluated. It was concluded that at 1200 °K the true values of emittance at 2 μ for the particular specimens measured might be as much as 0.032 lower or 0.012 higher than the reported values. The data were in good agreement with reflectance measurements of the same material and with recently reported absorption coefficients.

Key Words: Alumina, ceramic oxides, emittance, error sources, magnesia, measurement uncertainties, spectral emittance, thermal radiation, thoria, zirconia.

Contents

	Page
1. Introduction	394
2. Rotating specimen method	394
2.1 Selection of method	394
2.2 Rotational speed of specimens	395
3. Equipment	395
3.1 Specimen furnace	395
3.2 Blackbody furnaces	396
a. Details of construction	396
b. Temperature gradients in blackbody furnaces	397
3.3 Temperature control systems	398
3.4 Spectrophotometer and transfer optics	399
3.5 Calibration for linearity of response	400
4. Measurement procedure	400
5. Discussion of errors	402
5.1 Transfer optics	402
a. Atmospheric absorption	402
b. Preferential mirror absorption	402
5.2 Extraneous transmitted and reflected radiation	402
a. Nonopacity of specimen wall	402
b. Furnace radiation reflected into specimen beam	402
5.3 Errors from temperature uncertainties	403
5.4 Random error of measurement	405
5.5 Estimated accuracy	405
6. Measurements on polycrystalline oxide specimens	405
6.1 Description of specimens	405
6.2 Results and discussion	406
a. Spectral emittance data	406
b. Statistical scatter of data	406
c. Lack of stability of zirconia specimens	409
d. Effect of temperature on emittance	410
e. Comments on use of data for heat transfer computations	411
f. Correlation of data for alumina with reported absorption coefficients	413
7. Summary	414
8. References	414
9. Appendix A: Analysis of error caused by nonisothermal blackbody furnace	415

1. Introduction

Knowledge of the spectral emittance [1] of ceramic oxides at high temperatures is important, not only because of the many potential space applications for materials of this type, but also to obtain an improved understanding of the thermal emission mechanism in solids. Several investigators have made spectral emittance measurements on oxide materials; however, wide variations in the data are evident, especially in the shorter wavelength regions.

The lack of better agreement may be due, at least in part, to certain measurement problems that exist when determining the emittance of ceramic specimens. Three of the more important of these problems are

(A) *Temperature gradients in specimens.* Sizable temperature gradients are generated when a stationary ceramic oxide specimen is heated to a high temperature in such a way that it is free to radiate from an exposed surface. These gradients, which result from the low thermal conductivity of the material, create serious measurement problems. The radiation emitted from a ceramic oxide specimen originates not only from the outermost surface layer, as it does for metals, but also from volume elements at appreciable distances below the surface. Hence, when a gradient is present it becomes virtually impossible to assign a unique temperature to the source of the emitted radiation, and without a knowledge of this temperature, a reliable emittance measurement becomes impossible.

(B) *Extraneous reflected radiation.* Polycrystalline ceramic specimens are known to reflect thermal radiation diffusely rather than specularly. This means that any thermal radiation striking the viewed area of the specimen, regardless of the angle of incidence, will be diffusely reflected with some of it entering the specimen beam to give high values of emittance. Thus, unless elaborate precautions are taken to exclude this diffusely reflected radiation, for instance from furnace walls, measurements can be high by sizable amounts. This source of error becomes especially critical with ceramic specimens in the shorter wavelength regions where reflectance often exceeds 0.90.

(C) *Extraneous transmitted radiation.* Many single crystal oxides, such as sapphire, have a very high transmittance for radiation in the near infrared. However, when the same oxides are finely ground and then bonded by high temperature sintering, the material becomes less transparent because of internal scattering effects (multiple internal reflections at interfaces) and in this way it is sometimes possible to prepare polycrystalline specimens that will be substantially opaque to radiation in the near infrared at thicknesses as low as ¼ in. If the specimen to be measured is not opaque, then serious errors will result due to radiation from the furnace enclosure passing through the specimen and entering the specimen beam.

A rotating specimen method was chosen for the investigation described herein, since this approach minimizes temperature gradients in specimens. The present report begins by describing the earlier applications of this method. Subsequent sections include a description of the equipment and the measurement procedure, a detailed discussion of errors, and, finally, the results of spectral measurements for polycrystalline specimens of alumina, thoria, magnesia, and zirconia at 1200, 1400, and 1600 °K.

The investigation was conducted at the National Bureau of Standards. However, it was carried forward under the sponsorship and with the financial assistance of the National Aeronautics and Space Administration.

2. Rotating Specimen Method

2.1. Selection of Method

A review of earlier methods used to measure the emittance of nonmetals indicated that one of the best approaches for reducing temperature gradients in a ceramic specimen to workable levels is to move the heated specimen past a water-cooled viewing port. In this way, a freshly heated surface of the material is continuously arriving at the port for measurement. If the movement is sufficiently rapid, a thermal equilibrium is approached in which temperature gradients in the specimen approach minimal values.

The moving specimen concept was first introduced by Féry in 1902 [1].[2] In his measurements, and also in those made by Michaud [2] and Pattison [3], cylindrical specimens were rotated while being heated in a gas flame. The ratio of the radiant flux from the surface to that from a hole placed axially at the center of the specimen was then taken as the emittance. No viewing port was used. In other measurements, specimens were rotated in a furnace cavity that was equipped with a water-cooled viewing port. McMahon [4], Slemp and Wade [5], and Olsen and Katz [6], all used a semicircular disk-shaped specimen that was rotated in front of a viewing port so that blackbody radiation from the furnace struck the detector for one-half the cycle, and the detector saw radiation from the specimen for the remaining one-half cycle. Both McMahon [4] and Olsen and Katz [6] arranged for the periodic insertion of a water-cooled shutter behind the specimen so that it was possible, at least in theory, to determine the transmittance of the specimen material. Folweiler [7] described a rotating cylinder apparatus, which incorporated solid cylindrical specimens with a "V"

[1] As used in this paper, emittance is the ratio of energy radiated by a specimen per unit time and per unit area to that from a blackbody at the same temperature and under the same conditions. The conditions refer to the geometric and spectral distribution of the radiated energy.

[2] Figures in brackets indicate the literature references on page 414.

groove positioned around the circumference to serve as a reference blackbody. The specimens were heated in a furnace with silicon carbide heating elements. A water-cooled viewing port was used.

In measurements made by Clayton [8] a horizontal disk-shaped specimen was rotated in a carbon-resistance furnace that was equipped with separate water-cooled viewing ports for detecting radiation from both the specimen and the furnace enclosure. The specimen sighting tube could be moved to two positions. In the first position, the region behind the viewed portion was the hot furnace enclosure, and in the second, it was a water-cooled baffle. Here, again, the aim was to measure both emittance and transmittance.

A careful consideration of the possible errors and of the expected experimental difficulties inherent in each of these methods resulted in the selection for the present measurements of a rotating-cylinder approach with a separate blackbody. Briefly stated, the method consisted of rotating a hollow cylindrical specimen, approximately 1 in in diameter by 1-in high with $^3/_{16}$-in thick walls, in a wire-wound furnace equipped with a water-cooled viewing port. Spectral emittance measurements were then made with a double-beam spectrophotometer by comparing the radiance of the rotating specimen to that of a blackbody at the same temperature.

An earlier description of the measurement method has been published [9]. However, only preliminary data at one temperature (1200 °K) where given at that time. Also, there was no systematic analysis of errors, since this phase of the investigation had not been completed at the time of the earlier publication.

2.2. Rotational Speed of Specimens

A theoretical analysis of periodic heat flow in a specimen rotating before a viewing port, performed as a first phase of the study, has been published by Peavy and Eubanks [10]. The analysis showed that at low rotational speeds the surface temperature of a specimen at the center of the viewing port opening will be substantially lower than the temperature of the thermocouple in the specimen cavity. However, this difference will decrease with increasing speed. The speed at which the difference will become negligibly small will depend on system geometry, thermal properties of the specimen material, and a derived average heat flux for the portion of the cycle during which a point on the specimen is being heated by the furnace.

This analytical treatment may be used to compute the rotational speed required to reduce radial temperature gradients in the specimen to acceptable levels. However, since reliable thermal property data are not presently available for the specimen materials, such computations can be of only limited value. Therefore, in the present work, the minimum permissible speed of rotation was determined experimentally by first rotating a specimen at a very low speed and measuring its emittance at 1.4 μ.[3] As the speed was increased, the indicated emittance at 1.4 μ continued to rise until a point was reached where further increases in speed caused no further increase in the measured emittance. For the materials studied in this report, the maximum value of emittance was reached at about 50 rpm. However, as an added insurance against possible errors, actual emittance measurements were mad at 100 rpm.

3. Equipment

3.1. Specimen Furnace

Figure 1 is a schematic drawing of the specimen furnace. The high-temperature alumina core surrounding the specimen was wound with 0.032-in-diam platinum-40 percent rhodium wire. The winding was continuous to the edges of the rectangular opening that was cut into the core to permit entrance of the viewing port. A booster winding of the same wire positioned on the outer alumina core, as indicated in the figure, was used to compensate for the large heat losses at the center.

The water-cooled viewing port was machined from copper, and its inner surface was curved to the same radius as the specimen. A shield of platinum foil, 0.002-in thick, surrounded the outer surfaces of the port, including the edges that faced the specimen. This helped to thermally isolate the viewing port from the furnace interior. The inner surfaces of the viewing port and the portion of the platinum shield nearest the specimen were blackened to minimize the possibility of errors from reflected radiation. The opening at the inner end of the port was $^1/_8$-in wide by $^1/_2$-in high.

The specimens were prepared so as to be cylindrical to ±0.002 in. The alumina support tube (fig. 1) was surface ground to this same tolerance. The spindle was driven by a $^1/_8$ HP motor that was coupled to a gear reducer. With the arrangement used, the rotation of the specimen could be adjusted to any speed in the range 1 to 300 rpm.

The design of the furnace shell was such that the furnace could be operated in an inert atmosphere, as well as in air. Glass-metal seals were used for power leads and "O"-ring seals were used for the shell ends, as well as for a sodium chloride viewing windows. The thrust bearings were designed to provide a reasonably gas-tight seal at the point where the spindle shaft entered the shell. Although this controlled-atmosphere feature had been incorporated into the design, all measurements included in this report were made in air with no windows. Also, although the furnace was capable of being operated at 1800 °K, no measurements were made at this temperature, because of temperature control difficulties (see sec. 3.3).

[3] Difference in temperature between specimen and blackbody has the greatest effect on emittance at wavelengths below the energy peak of blackbody radiation. The selected setting of 1.4 μ is well below this peak for the selected test temperatures.

223-178 O-66-2

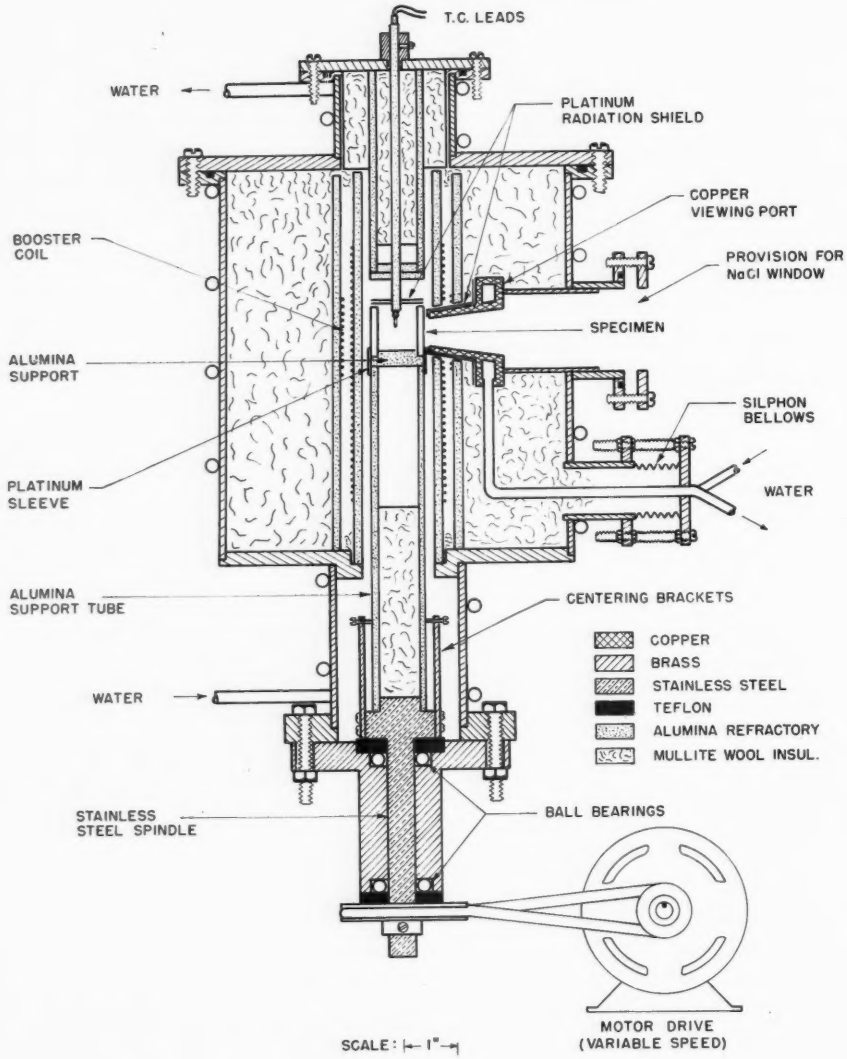

FIGURE 1. *Specimen furnace.*

Axial temperature gradients in the specimens were reduced to low values by adjusting the power to the booster coil. The gradients were measured by sighting a micro-optical pyrometer on a rotating specimen through the viewing port. With the settings used, no temperature difference from top to bottom was observed for any of the specimens at 1200 °K. At 1400 °K, the top may have been as much as 2 °K higher than the bottom, while at 1600 °K, the top was as much as 6 °K higher. The precision to which the pyrometer could be read was about 2 °K. The specimen thermocouple was located in the center of the specimen cavity and was shielded from furnace radiation as shown in figure 1.

3.2. Blackbody Furnaces

a. Details of Construction

Figure 2 is a schematic of the blackbody furnace. Two of these were required in the measurement system, and both were made to be as nearly identical as possible. The inner cavity of the furnaces was formed of fused alumina bonded with 20 percent by weight of a calcium aluminate cement. This mixture, which sets hydraulically, was mixed with 17.5 percent by weight of water and vibrated into a greased plaster mold. The mold was made by using an alumina core as a pattern; a brass mandrel was

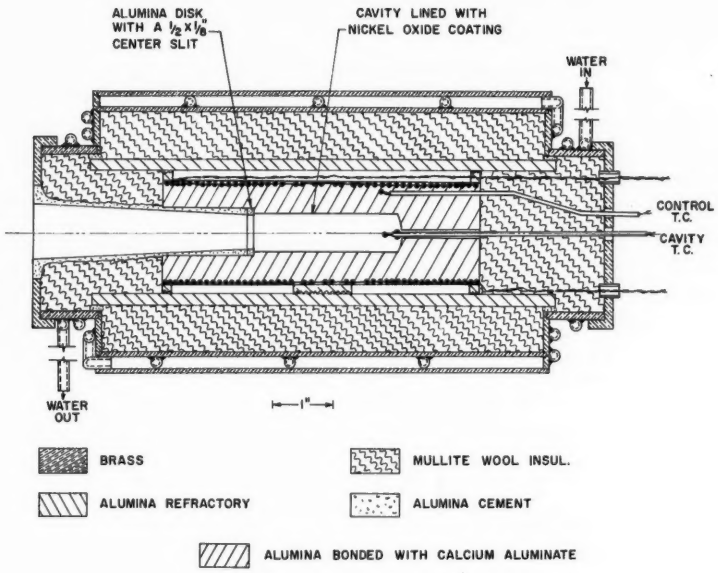

FIGURE 2. *Blackbody furnace.*

positioned at the center of the mold to form the outline of the cavity. After allowing 20 hr for curing, the core was removed from the mold, dried in an oven for 24 hr, and then heated to 1925 °K for 1 hr. It was later wound with 0.032-in-diam platinum-40 percent rhodium resistance wire.

An alumina disk with a ½-in by ⅛-in center slit was placed over the front end of the cavity to reduce heat losses by radiation. The viewing port was formed with mullite wool, over which was placed a thin layer of alumina cement. The shaping of the port was facilitated by use of a tapered aluminum mandrel that was machined especially for the purpose.

All furnace thermocouples (including the one for the specimen furnace) were made of 0.020-in-diam Pt:Pt-10 percent Rh wire that had been calibrated by the Temperature Physics Laboratory at the National Bureau of Standards. Two-hole alumina tubing was used to insulate the leads. This tubing was inserted into an alumina sleeve that was cemented into the core so that when the thermocouple was inserted, it would be nearly flush with the side wall of the cavity. With this arrangement, the spectrophotometer did not "see" the thermocouple bead, but rather was "looking" at the back of the cavity, which was largely isothermal. Of course, no important deviation from blackbody conditions would result from the presence of the thermocouple at the center of the cavity if the cavity was isothermal and if there was no separation between the alumina sleeving and the thermocouple tubing. However, a small clearance was present, and this clearance showed up as a tiny dark crescent when looking into the heated cavity. The presence of a dark area of this type was undesirable, in that it would tend to generate low flux readings.

The alumina core material has a low emittance in the wavelength region 1 to 5 μ. Inasmuch as the cavity emittance depends, in part, on the emittance of the walls, it was desirable to line the cavity with a coating that would have a high emittance at the short, as well as the long wavelengths. The coating developed for this purpose consisted of black nickel oxide (Ni_2O_3) bonded with 7.5 percent by weight of Florida kaolin. This coating was prepared as a coating slip and applied at a thickness of about 0.005 in to the inner wall surfaces of the cavity by a dipping operation. The core was then heated to 1850 °K for 1 hr, to bond the coating to the alumina. The spectral emittance of a cylindrical specimen of the core material coated in this way was found to be above 0.875 at all wavelengths from 1 to 15 μ when measured at 1200 °K. Hence, the lowest possible cavity emittance at any wavelength from 1 to 15 μ was 0.990 when computed by an expression derived by Gouffé [11]. This expression assumes that the walls are diffusely reflecting and that the cavity is isothermal. The expression has been shown to predict slightly low values of emittance for cavities with large depth-to-diameter ratios [12].

b. Temperature Gradients in Blackbody Furnaces

Several furnace designs were tested early in the study in an attempt to minimize temperature differences within the cavity. To test for gradients, a Pt: Pt-10 percent Rh thermocouple made with 0.010-in-diam wire was inserted into the viewing port and moved

from front to back with the hot junction within 1/8 in of the interior wall. A record was made of the response at each position. In almost all cases, the indicated wall temperature near the center of the cavity was higher than at either end. In some instances, power was shunted from the central region of the furnace windings, while in other tests, varying numbers of turns were omitted from the heater coil. The final configuration was that shown in figure 2. No shunts were used and four loops were omitted in the central region. With this arrangement, temperature probing revealed that the cavity walls near the back were colder than those in the center by the amounts indicated below.[4]

Approximate cavity temperature	Temperature difference
°K	°K
1200	18
1400	14
1600	8

The presence of these gradients was a potential source of error in the measurements because of (a) uncertainty in determining the temperature to assign to the "blackbody" radiation, and (b) deviations from the Planck distribution of energy caused by the nonisothermal conditions. Naturally, it would be desirable if the spectral distribution of radiated energy, $E(\lambda)$, was proportional to the Planck function, $W(\lambda,T)$; i.e., $E(\lambda)=\epsilon_{cav}W(\lambda,T)$. It was not immediately evident, however, that any single temperature could be assigned to the nonisothermal cavity. Temperatures that might be considered are the temperature of a thermocouple placed in the center of the cavity, the temperature of the back wall of the cavity, or the temperature indicated by an optical pyrometer sighted on the mouth of the cavity. This latter temperature was selected, since it represented the temperature of a perfect blackbody whose radiance at 0.65 μ was the same as that of the nonisothermal laboratory furnace. A theoretical analysis is presented in appendix A to show that when a radiance match is achieved at 0.65 μ then the spectral distribution of radiated energy can be approximated by a Planck function over the 1 to 15 μ range with no more than a 0.5 percent error.

The procedure used for positioning the furnace thermocouple so that its response would agree with the temperature measured with a calibrated optical pyrometer was as follows:

(1) The furnace was first heated to the desired operating temperature and allowed to stabilize.

(2) A micro-optical pyrometer was then sighted at the front opening of the furnace and the "optical" temperature of the furnace cavity was determined.

(3) The furnace thermocouple was next moved to a position where its response indicated the same temperature as that measured with the optical pyrometer. This position was always within 1 in of the rear wall of the cavity.

(4) Finally, a mark was placed on the thermocouple tubing at the back of the furnace shell so that the positioning of the junction could be duplicated in subsequent determinations at the same test temperature. This positioning was checked periodically to be certain that no changes in the temperature behavior of the furnace had occurred.

The calibration procedure as outlined needed to be applied to only one blackbody furnace. The position of the thermocouple in the second blackbody furnace could then be adjusted by noting the shape of the spectral curve that compared the energy from these two furnaces (100 percent line, see sec. 4). At long wavelengths, small temperature differences between the furnaces lead to negligible differences in energy content of the two beams, but at short wavelengths they had a pronounced effect. Thus, if the 100 percent curve was higher at 1 μ than at, say, 9 μ, it indicated that furnace No. 2 was at a higher temperature than the reference blackbody (No. 1). The thermocouple in No. 1 was then moved to a position where it indicated a lower temperature. The automatic control equipment would then lower the temperature of No. 2 until it matched that of No. 1 and a new spectral curve was determined. This procedure was repeated until a flat 100 percent line was obtained. When this condition was achieved, the furnace No. 1 was at the same effective temperature as No. 2 in that it was supplying an equivalent flux to the spectrophotometer.

3.3. Temperature Control System

A differential thermocouple control system similar to that described by Harrison et al. [13], was used to maintain temperature differences of less than 1 °K between blackbody No. 1 and either the specimen furnace or blackbody No. 2. The No. 1 furnace was controlled, in turn, by a separate temperature controller, which maintained its temperature to ± 0.5 °K. A double-pole, double-throw switch was used for switching the differential thermocouple controller from blackbody No. 2 to the specimen furnace.

The differential thermocouple controller was actuated by the difference in signal between the thermocouple in blackbody furnace No. 1 and the thermocouple in either blackbody No. 2 or the specimen furnace. This signal was amplified by a d-c amplifier and fed to a center-zero recorder-controller. The output of the recorder-controller, which was proportional to the temperature difference between the two furnaces, was fed to a current-actuating mechanism that provided three types of current control. One type was proportional to the input signal, a second to the first

[4] Large uncertainties existed in temperature measurements made near the front of the cavity, because of excessive heat losses by conduction along the thermocouple leads and the protection tubing.

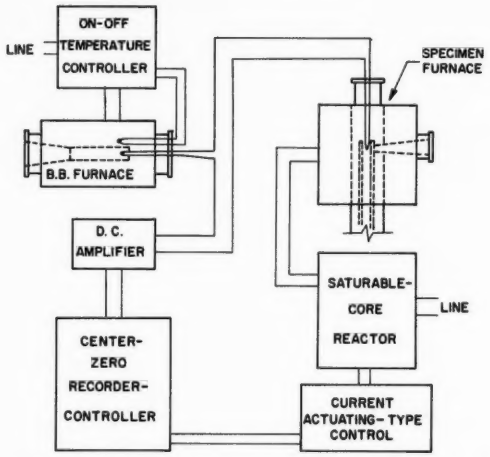

FIGURE 3. *Block diagram of temperature control equipment*
Controller is actuated by signal from differential thermocouple.

time derivative of the input signal, and a third selected the frequency at which the first correction was repeated. The output from this current actuating device was fed to the coil of a saturable-core reactor, which then varied the power input to either blackbody No. 2 or the specimen furnace, so as to bring the temperature into agreement with the reference blackbody (No. 1).

A block diagram of the temperature control equipment is shown in figure 3. The system gave almost trouble-free operation at 1200, 1400, and 1600 °K. However, at 1800 °K, it became largely inoperative because of excessive noise in the thermocouple signal. This may have originated from electrical leakage through the alumina core material, whose electrical conductivity becomes appreciable at these very high temperatures. For this reason, no measurements at 1800 °K were possible, even though all of the furnaces could be operated at this temperature.

3.4. Spectrophotometer and Transfer Optics

A double-beam infrared spectrophotometer with a sodium chloride prism was used for obtaining the radiance comparisons. This instrument, which utilizes a chopper operating at 10 Hz, was modified to operate from 1 to 15 μ rather than in the intended 2 to 16-μ range. A second modification consisted of reducing the angle of the attenuator-comb in the reference beam from blackbody No. 1, so that the maximum opening of the comb did not exceed the height of the furnace apertures. This required only a small reduction in the comb angle.

The double-beam optical system of the instrument was used for all measurements. When operating in this mode, the spectrophotometer achieves a null balance through use of the aforementioned mechanically-driven attenuator, or comb, in the reference

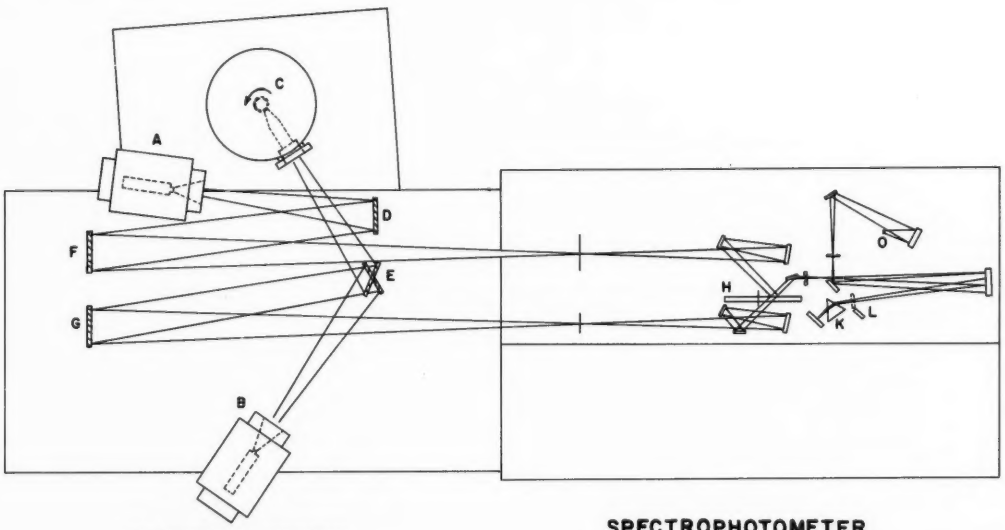

FIGURE 4. *Arrangement of equipment showing optical paths of the two beams.*

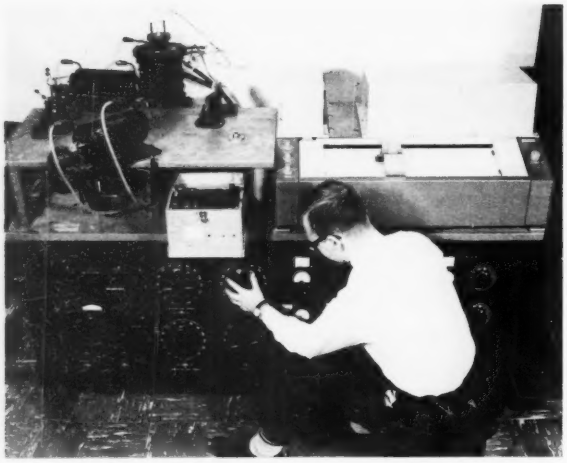

FIGURE 5. *Equipment in operation.*

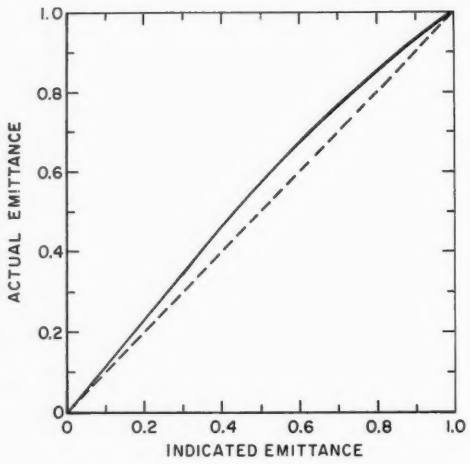

FIGURE 6. *Calibration curve (solid curve) for correcting for lack of instrument linearity.*
Dashed line shows type of behavior desired of an instrument (linear response).

beam. A recorder pen, coupled mechanically to the comb, permits the ratio of the radiances of the two beams to be continuously recorded with respect to wavelength. In all measurements reported herein, the instrument was set to scan the 1- to 15-μ range in 16 min.

Prior to using the instrument, the source optics were removed and replaced with the transfer optics shown schematically in figure 4. The off-axis angle of the two spherical mirrors was approximately 5°.

Figure 5 is a photograph of the equipment in operation.

3.5. Calibration for Linearity of Response

The response of the modified instrument to known attenuations of flux in the specimen beam was determined through use of sectored-disk attenuators. To conduct this test both blackbodies were first adjusted to some temperature in the range 1200 to 1600 °K. A sectored-disk attenuator was then inserted into the specimen beam and rotated at high speed (greater than 500 rpm). Six disks were used with measured transmission factors of 75.1, 50.1, 25.3, 12.7, and 5.1 percent, respectively. The resulting spectral curves, which were found to be reproducible to within the precision of measurement, showed that the instrument response was always lower than the actual beam attenuation. This lowering was the same at all wavelengths. Wide variations in disk speed above 500 rpm had no effect on the instrument response, which showed that resonance coupling between the chopper and attenuator was not affecting the results.

Since no method could be devised to restore linearity to the modified instrument, a correction curve (fig. 6) was prepared. This curve was then used to correct the spectral emittances that were obtained by the procedure outlined in section 4. The dashed line in figure 6 shows the type of behavior expected from an instrument with a completely linear response.

4. Measurement Procedure

In making a determination, a specimen was first placed on the top of the refractory pedestal, carefully centered, and then fixed in position with high-temperature alumina cement. This centering and mounting operation was performed outside the furnace with the aid of a specially prepared jig. After the mounting had been completed, the pedestal was inserted into the furnace from the bottom and carefully positioned radially by a screw adjustment of the bottom flange, so that the specimen rotated at an average distance of 0.010 in from the inner face of the viewing port. The separation distance was measured optically by a telescope with a calibrated reticle. The telescope was sighted through the top of the furnace tube while the furnace was at approximately 1400 °K. Specimen wobble did not exceed ± 0.005 in.

After positioning of the specimen was completed, the top insulation was replaced, the motor drive was started, and the specimen was brought to a rotational speed of 100 rpm. The controller on blackbody No. 1 was then adjusted to 1600 °K and the differential thermocouple controller actuated to bring blackbody No. 2 to the same temperature. As soon as the temperatures had equilibrated, the flux from blackbody No. 2 was compared to that from blackbody No. 1 by scanning from 1 to 15 μ. The resulting curve, a representative section of which is shown in figure 7, was termed the 100 percent line. Next, the beam from blackbody No. 2 was blocked, and a second curve was obtained on the same chart paper. This is the zero line shown in figure 7.

After the zero line had been obtained, the automatic control was switched to the specimen furnace, the movable mirror (see fig. 4) was shifted to the specimen

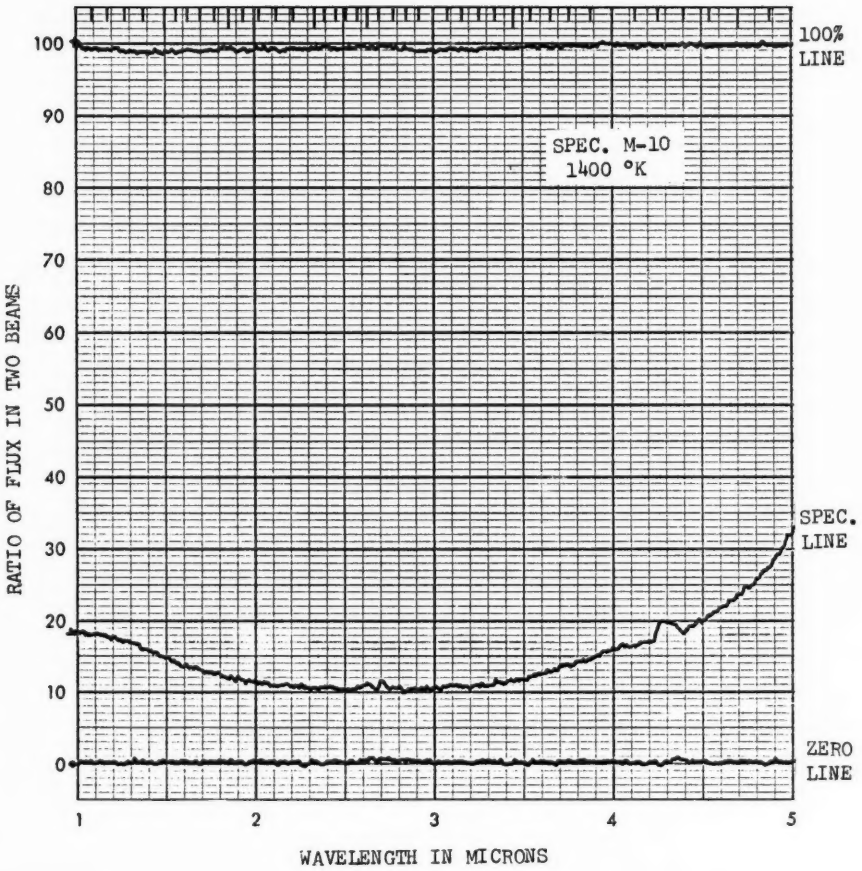

FIGURE 7. *Section of recorder chart showing segments of a "100 percent Line," "Specimen Line," and "Zero Line."*

position, and after an equilibrium condition had been attained a specimen curve was plotted, again on the same chart paper.

Curves such as those shown, in part, in figure 7 represent raw data for one determination at one temperature. To transform these data to an actual or true spectral emittance curve for the specimen, two operations were performed:

(1) The height of the specimen curve at preselected wavelengths was obtained as a ratio of the respective heights of the zero and 100 percent lines. Stated mathematically, if Z_λ is the height of the zero line, S_λ the height of the specimen curve, and H_λ the height of the 100 percent line, then $\epsilon_{\lambda i}$, the uncorrected or "indicated" emittance, is

$$\epsilon_{\lambda i}=\frac{S_\lambda - Z_\lambda}{H_\lambda - Z_\lambda}. \qquad (1)$$

Values for $\epsilon_{\lambda i}$ were, in most cases, obtained at intervals of 0.5 μ.

(2) The values for $\epsilon_{\lambda i}$ were next converted to true or actual emittances, ϵ_λ through use of the calibration curve shown in figure 6. These values were then plotted against wavelength to obtain the curves shown in later sections of the report.

In all data reported herein, measurements on each specimen were made first at 1600 °K, next at 1400 °K, and finally at 1200 °K; all three measurements being made during a single working day. Three specimens of each type were measured, and two completely independent determinations were made on each specimen. These duplicate determinations on the same specimen were always made on different working days, and in each case, the specimen had been removed from the furnace between the first and second series of measurements.

5. Discussion of Errors

5.1. Transfer Optics

An important consideration in the design of any double beam system is the requirement of complete optical equivalence of the two beams. Failure to meet this requirement would cause inflections in the spectral curves due to differential absorption by the atmosphere or by the mirrors in the system. In the present study the use of the two blackbodies to obtain a 100 percent line provided a convenient means to check for these effects.

a. Atmospheric Absorption

In most double-beam infrared spectrophotometers, no irregularities are observed when scanning through the absorption bands for carbon dioxide and water vapor, since the flux attenuation is the same for both beams. However, the flux available for measurement drops off drastically at the major absorption bands. In the present measurements, no appreciable inflection in the curve was observed at the strong water absorption band at 2.7 μ, since at this wavelength there was apparently sufficient energy in the beams to allow the instrument to compensate for the sudden change in flux. At longer wavelengths, however, there was considerably less energy in the beams, and whenever the instrument scanned through the strong absorption band for carbon dioxide at 4.2 μ, a small discontinuity in the curve was observed. However, since this represented a deficiency of the instrument rather than an abrupt change in specimen emittance, a smooth curve was drawn through the minor inflection at 4.2 μ. Any error resulting from this procedure would be extremely small and would apply to this one wavelength only.

b. Preferential Mirror Absorption

A thin protective layer of silicon oxide was present on the aluminum front surface mirrors procured for the transfer optics in the present equipment. Coating layers of this type normally consist of mixtures of such compounds as SiO, SiO_2, and Si_2O_3, all of which have absorption bands in the 8- to 10-μ region [14].

The presence of the silicon oxide layer on the mirrors would have no appreciable effect on the measurements if (a) the same number of mirrors were in both optical paths, (b) the coating thicknesses were the same on all mirrors, and (c) the respective beams struck the mirrors at the same angle for the determination of both the 100 percent and specimen curves. Unfortunately, this last requirement was not fulfilled since the beam from blackbody No. 1 strikes the plane mirror D (see fig. 4) at an angle of incidence of 9° while the beams from blackbody No. 2 and from the specimen strike the mirror E at angles of 19° and 32°, respectively. These differences in angle caused different attenuations in the respective beams at the wavelengths where the silicon oxide layer is highly absorbing but not at other wavelengths.

Because of this differential absorption effect, all 100 percent lines and specimen curves showed a small dip in the 8 to 10 μ region. The emittance curves included in this report have been smoothed out over the 8- to 10-μ region. Since this smoothing operation is equivalent to taking no data points in this region, the emittances indicated on the curves at both 8.5 μ and at 9 μ have greater uncertainty than those at other wavelengths.

5.2 Extraneous Transmitted and Reflected Radiation

In the paragraphs which follow, an attempt is made to place an upper limit on the magnitude of the errors that can arise due to extraneous radiation, i.e., energy which contributes to the radiance of the specimen beam but does not originate at the specimen.

a. Nonopacity of Specimen Wall

As mentioned in the introduction, many polycrystalline ceramic oxide specimens are partially transparent to radiation in the visible and the near infrared. Hence, when measuring emittance, if the specimen wall is not sufficiently thick to be opaque, energy from within the specimen cavity will pass through the specimen wall and enter the specimen beam. Since with the present measurement method this energy will approximate blackbody radiation, high emittance readings will result unless the wall thickness is sufficient to provide the required opacity.

Earlier work had suggested that a wall thickness of $^3/_{16}$ in would be adequate for the particular materials selected for study [9]. However, to be certain that the $^3/_{16}$-in thickness was sufficient in all cases, specimens with $^5/_{16}$-in walls were also measured. If the emittances were the same for both, then it would be almost positive evidence that the transmittance through the $^3/_{16}$-in wall was too small to cause an error.

Tests of this type were made for each material. The agreement between specimens with $^3/_{16}$-in and $^5/_{16}$-in-thick walls was, in each case, within the precision of measurement; hence, it was concluded that there was no measurable error from wall transmission when the specimens with $^3/_{16}$-in-thick walls were used.

b. Furnace Radiation Reflected Into Specimen Beam

The purpose of the water-cooled viewing port in the specimen furnace is to reduce extraneous flux, both emitted and reflected, from entering the specimen beam. Emitted flux is reduced to an insignificant level by water-cooling the walls of the port. To diminish reflected flux, however, the specimen must rotate in close proximity to the inner face of the port; otherwise, as illustrated in figure 8, flux from the furnace walls will strike the face of the specimen and be diffusely reflected into the specimen beam thereby giving high values of emittance.

It was recognized early in the investigation that large errors could result if sizeable separations were permitted between specimen and viewing port [15]. A theoretical computation of errors caused by various

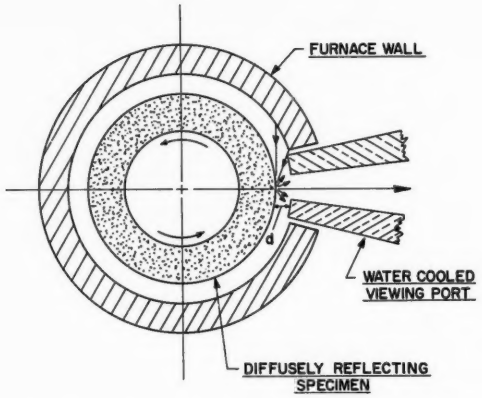

FIGURE 8. *Illustration of how flux from furnace walls may be diffusely reflected into specimen beam.*

separations was not feasible because of uncertainties in (a) the local furnace wall temperatures, and (b) the optical properties of the specimens. Thus an attempt was made to arrive at their magnitude experimentally.

The experiment consisted of determining the indicated emittance of various specimens at carefully measured distances of separation. To accomplish this, a screw adjustment was incorporated on the brass flange at the bottom of the specimen furnace. By turning this screw, the rotating pedestal could be moved in known increments toward or away from the viewing port. A microscope with a calibrated reticle was used to measure the distance of separation to ± 0.001 in.

To evaluate the effect of separation distance, the specimen was first brought to a temperature near 1400 °K with the microscope mounted above the top furnace opening. Next, the specimen was moved forward so that the average separation between the surface of the specimen and the viewing port was 0.010 in. In all of these particular tests, specimen wobble was less than ± 0.002 in. After completing the distance measurement, the microscope was moved out of position, the top cover reinserted, the furnace temperature allowed to stablize, and a spectral curve determined. Then, by adjusting the calibrated screw, the specimen was moved back from the viewing port in known increments. After each step, the emittance was determined at certain selected wavelengths. Finally, when the limit of travel of the adjusting screw had been reached, the microscope was again used to verify the final separation distance.

The first measurements of this kind were made with a polished platinum specimen. As might be predicted, no change occurred with separation distance, since all wall radiation that struck the viewed area of the specimen was specularly reflected away from the viewing port and did not enter the specimen beam.

When the same platinum specimen was grit-blasted, however, its surface became a partially diffuse reflector and the measured emittance was no longer insensitive to separation distance. This is illustrated by the solid curves in figure 9. At each of the four wavelengths, the rate of change of measured emittance with distance decreased as the distance approached zero. In fact, the shape of the curves suggests that if all measurements had been made with a separation of 0.01 in, which is as small as was practical with the present system, the measured values would be high by no more than about 0.005 in emittance.

Platinum, like other metals, is substantially opaque to radiation in the 1- to 15μ region. This means that the reflection occurs at or very near the surface. In the case of polycrystalline ceramics, however, reflection occurs largely by internal scattering. Flux striking the surface can penetrate to appreciable distances and then reemerge, after multiple internal reflections, at a point on the surface that may be appreciably separated from the point where it entered. This particular reflection behavior is believed to be responsible for the type of results obtained with the ceramic oxide specimens. The data for an alumina specimen plotted as dashed lines in figure 9 are typical. It will be noted that the rate of change of measured emittance with distance is largely unchanged as the specimen approaches the viewing port. This behavior at least implies that even if a zero separation was possible, radiation from the furnace walls would still be penetrating the surface at some distance from the viewing port and then reemerging at the port to enter the specimen beam. However, when emittances as low as 0.04 (Alumina, 2 μ, 1200 °K) were measured, it seems unlikely that they could be high by more than 0.02, notwithstanding any compensating errors. Various attempts were made either to eliminate or precisely evaluate the magnitude of this error, but none were successful.

5.3. Errors From Temperature Uncertainties

The comparison method of measuring emittance requires that the specimen and blackbody furnaces all be maintained at the same temperature. If this condition is not fulfilled, an error is introduced that is dependent upon (a) the magnitude of the temperature difference, (b) the wavelength, and (c) the test temperature. Since the thermocouples were prepared from wires taken from the same spools and were checked periodically, and since the controller maintained the thermocouples at the same temperature to within better than 1.0 °K, no sizeable error from temperature difference would be expected unless the thermocouples failed to indicate the "true" temperatures of the specimen and the reference blackbody.

With a specimen speed of 100 rpm, the analysis described in section 2 indicated that since radial gradients are small, the specimen thermocouple should be in close agreement with the specimen temperature and, hence, no important error should result from this source.

As mentioned in section 3.2.a, temperature gradients existed in the blackbody furnaces. However,

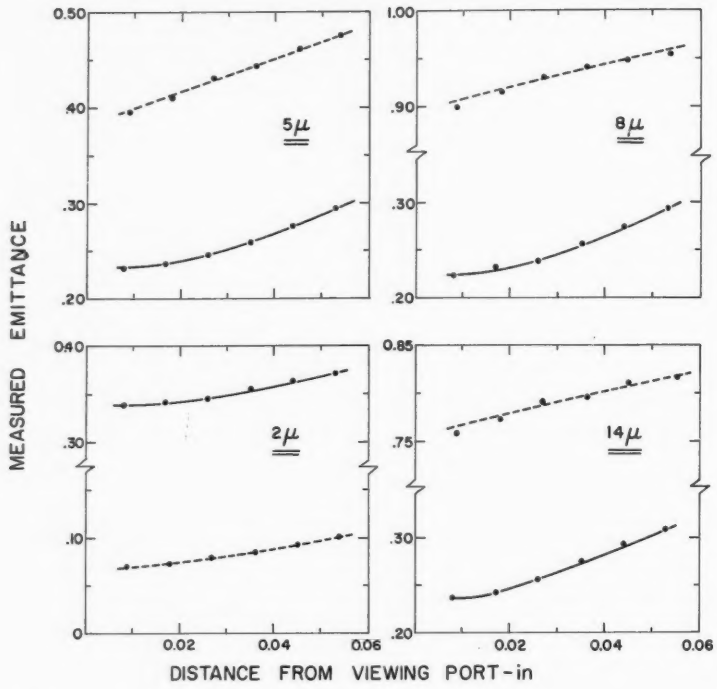

FIGURE 9. *Effect of distance of specimen from viewing port on measured emittance of grit-blasted platinum specimen (solid lines) and a polycrystalline alumina specimen (dashed lines).*

as shown in appendix A, when the thermocouple is located so that its response agrees with an optical pyrometer sighted on the cavity, the distribution of radiated flux at 1 μ differs from a Planck distribution by less than ½ percent at 1200 °K. The size of this error decreases with both increasing temperature and wavelength. If the true emittance of the specimen was 0.10, then an error of the magnitude discussed above would change the measured emittance by only 0.0005, a completely negligible quantity.

From the foregoing discussion it follows that any uncertainty in temperature measurements will depend primarily upon the accuracy and precision of the optical pyrometer used for positioning the thermocouple. Since the instrument had been carefully calibrated and periodically checked by the National Bureau of Standards Temperature Physics Section, it is unlikely that the combined uncertainty due to inaccuracy of the pyrometer and imprecision introduced by the operator would exceed ±5 °K.

At wavelength λ, temperature T, and uncertainty dT, a sample whose true emittance was ϵ_t would appear to have an emittance ϵ_m given by

$$\epsilon_m = \frac{\epsilon_t W(\lambda, T)}{W(\lambda, T+dT)} = \frac{\epsilon_t W(\lambda, T)}{W(\lambda, T)+dW} \tag{2}$$

where $W(\lambda, T)$ is the Planck function. Dividing both numerator and denominator by $W(\lambda, T)$ one obtains

$$\epsilon_m = \epsilon_t \frac{1}{1+\frac{dW}{W}} = \epsilon_t \frac{1}{1+F\frac{dT}{T}} \tag{3}$$

where the factor $F = F(\lambda\ T)$ relating $\frac{dW}{W}$ to $\frac{dT}{T}$ is a tabulated function [16].

For the purpose of estimating errors it is more useful to have the true emittance in terms of a measured value. Thus eq (3) is written

$$\epsilon_t = \epsilon_m \left(1+F\frac{dT}{T}\right) \tag{4}$$

If the uncertainty in temperature is ±5 °K at $T=1200$ °K and $\lambda=2$ μ, then $F=6.2$ and

$$\epsilon_t = \epsilon_m \pm 0.026\epsilon_m.$$

Thus, a sample whose measured emittance was 0.050 would be in error by no more than $\epsilon_t - \epsilon_m = \pm 0.026 \times 0.050 = \pm 0.0013$. Similarly, if the measured emittance was 0.30 at 2 μ and 1200 °K, the error would be $\epsilon_t - \epsilon_m = \pm 0.0078$. The function F is a monotonically decreasing function of the product λT; emittance, on

the other hand, generally increases. The net result is that errors of this type are not greatly influenced by changes in either wavelength or temperature.

The effect of a temperature gradient along the axis of the specimen may be treated in much the same way. As pointed out in section 3.1 this gradient amounts to little more than 5 °K so that some sort of "average" temperature T' may be assigned to the specimen. When this is done, it then becomes possible to approximate the flux from the specimen, $N(\lambda)$, by $\epsilon_t W(\lambda,T')$ with very little error. Only if the thermocouple bead was located at the extreme top or bottom of the specimen cavity, would its temperature differ from T' by even 3 °K. Since the bead is carefully positioned in the center of the viewed area, it is reasonable to assume, on the basis of the previous discussion, that any errors from temperature differences which may exist along the axis of the specimen are negligible.

5.4. Random Error of Measurement

When expressed in terms of emittance, the pooled estimate, $\bar{S}_w$, of the standard deviation due to random error of measurement at $\lambda = 2\ \mu$ was 0.00427. ($\bar{S}_w$ is the root mean square value for the S_w's tabulated in table 3). This estimate is based on two completely independent measurements at each of three temperatures on three polycrystalline ceramic oxide specimens of three different materials.[5] In effect, this standard deviation is an index to the reproducibility of the measurement, and takes into consideration such factors as the ability to mount the specimen on its pedestal with a minimum amount of wobble, the ability to mount each specimen at the same distance from the viewing port, and the ability to return the blackbody thermocouples to the proper position each time the temperature is changed. It also considers the reproducibility of the spectrophotometer, the precision with which the data are read from the charts and corrected for linearity, the day-to-day variations in moisture content of the air and numerous other variables which could affect the reproducibility of the measurements; and finally, its value is influenced by the stability of the specimens, i.e., their ability to resist changes caused by the high temperatures (see sec. 6.2c).

More important, however, is the fact that pooled estimates of the standard deviation due to measurement error, like the one above, may be used to establish a confidence interval for the true averages corresponding to the measured emittances given in table 2. Thus, using the standard statistical formulas, one may conclude with 95 percent confidence that the values listed in this table at 2 μ are within

$$\Delta = t \cdot \frac{\bar{S}_w}{\sqrt{np}} = 2.052\ \frac{0.00427}{\sqrt{6}} = 0.00358 \approx 0.004 \quad (5)$$

of the true average values (for these three specimens) that would be obtained if an infinite number of measurements were made. In the foregoing expression, $\bar{S}_w$ is the pooled estimate of the standard deviation due to random measurement errors, and the value of $t_{0.975}$ was obtained from reference [17] for the case of $9 \times 3 = 27$ deg of freedom.

5.5. Estimated Accuracy

An estimate of the accuracy of measurements made with the rotating-cylinder equipment on nonmetals can be obtained by considering both types of error; i.e., those that cause a bias and those that cause random errors. Let us now assume one of the worst conditions from the accuracy standpoint; i.e., data at 2 μ taken at 1200 °K. Error from extraneous radiation would certainly not exceed +0.02 in emittance. Temperature uncertainties would contribute ±0.008 as a maximum while random error of measurement will be on the order of ±0.004 (see sec. 5.4). Thus, the true values of emittance at 2 μ and 1200 °K for the particular specimens measured might be as much as 0.032 lower or 0.012 higher than those listed in table 2.

The uncertainty in the listed values could, of course, be decreased to ±0.012 if the data were corrected for the extraneous radiation that entered the specimen beam. However, as mentioned earlier, the uncertainties as to the exact magnitude of this error were too great to justify this procedure.

6. Measurements on Polycrystalline Oxide Specimens

6.1. Description of Specimens

The ceramic oxide specimens were obtained commercially. They consisted of hollow cylinders 1 1/16-in high and 1 1/32-in o.d. with a wall thickness of 3/16-in, although wall thickness of 5/16-in were also furnished. All specimens were cylindrical to ±0.002 in. The outer surfaces were smooth but not polished.

The sintering treatment for all specimens was 27 hr at 1865 °K. Chemical analyses of the raw materials, as provided by the manufacturer, are shown in table 1.

The measured porosity of the alumina specimens was about 30 percent; of the thoria 13 percent; of the magnesia 30 percent, and of the zirconia 20 percent. All are given as percentage by volume. Grain sizes were not measured.

No attempts were made to characterize the surface finish of the specimens since it was found that roughening the initially smooth surface of an alumina specimen by grit blasting had no measurable effect on emittance in the 1 to 15 μ range. This observation is in agreement with the recent results of Gannon and Linder [18] as well as those reported by Cox [19]. Also, it agrees with the predictions made recently by Richmond as a result of a theoretical analysis of the possible effects of surface roughness on the thermal radiation properties of nonmetals [20].

[5] The values of S_w for zirconia are abnormally high because of the extreme structural instability of this material (see sec. 6.2c). For this reason the zirconia data were omitted from this particular analysis.

TABLE 1. *Vendor's chemical analysis of specimen materials in percentage by weight*

	Alumina [a]	Thoria [b]	Magnesia	Zirconia
Al_2O_3	99.+		0.1	0.15
ZrO_2+HfO_2				94.2
ThO_2		99.+		
SiO_2	0.10	0.05	0.4	0.60
TiO_2				0.30
CaO	0.07	trace	0.1	4.50
MgO		0.02	99.2	0.07
Fe_2O_3	0.40		0.1	0.10

[a] Also, 0.02 percent Na_2O.
[b] Also, trace amounts of the oxides of phosphorus, iron, and the rare earths as well as a minor amount of alkali oxides which was expressed in the analysis as 0.10 percent of combined Na, K, and Li.

6.2. Results and Discussion

a. Spectral Emittance Data

Results of measurements on the four oxide materials are given in table 2 and in figures 10, 11, 12, and 13. In each case the values listed or plotted are the averages of six determinations, two each on three specimens, taken at 0.5 μ intervals over the 1 to 15 μ range. The small dip in the magnesia curve (fig. 12) at 6.4 μ was observed for all specimens at all three temperatures.

b. Statistical Scatter of Data

The statistical scatter of the data at 1200, 1400, and 1600 °K is listed in tables 3 and 4. The sample estimate of the standard deviation due to error of measurement, S_w (i.e., due to differences within specimens), was computed from the expression given below [21].

$$S_w=\sqrt{\frac{\sum_1^n (x-\bar{x}_1)^2+\sum_1^n (x-\bar{x}_2)^2 \ . \ . \ .+\sum_1^n (x-\bar{x}_p)^2}{(n-1)p}} \tag{6}$$

where x is an individual measurement, $\bar{x}_1$ is the average of n measurements on one specimen, and p is the number of specimens. For data in this report, $n=2$, $p=3$, and S_w corresponds to $(n-1)p=3$ deg of freedom.

A sample estimate of the overall standard deviation due to differences in specimens and random errors of measurement $S_{\bar{x}}$ was also computed. The expression used for this computation was

$$S_{\bar{x}}=\sqrt{\frac{\sum_1^p (\bar{x}-\bar{\bar{x}})^2}{p-1}} \tag{7}$$

where $\bar{\bar{x}}$ is the overall average of the $n\times p$ measurements, n each on p specimens. $S_{\bar{x}}$ corresponds to $p-1=2$ deg of freedom. One could, if it were desired, use the values of $S_{\bar{x}}$ given in table 4 to set up a confidence interval for the true mean of the entire population of specimens similar to those described

TABLE 2. *Normal spectral emittance of ceramic oxide specimens*

Wavelength	Emittance [a]											
	Alumina			Thoria			Magnesia			Zirconia		
	1200	1400	1600	1200	1400	1600	1200	1400	1600	1200	1400	1600
μ												
1.0	0.060	0.073	0.097	0.259	0.347	0.418	0.182	0.201	0.227	0.163	0.207	0.297
1.5	.046	.063	.088	.235	.330	.407	.131	.162	.196	.148	.192	.269
2.0	.042	.061	.085	.223	.319	.399	.095	.124	.151	.129	.172	.247
2.5	.045	.065	.089	.216	.314	.398	.088	.114	.141	.131	.172	.243
3.0	.058	.075	.097	.214	.311	.395	.088	.114	.144	.137	.177	.244
3.5	.080	.106	.125	.215	.314	.396	.102	.133	.160	.150	.188	.250
4.0	.141	.169	.177	.223	.318	.400	.149	.181	.205	.187	.222	.262
4.5	.248	.287	.316	.238	.330	.406	.191	.229	.260	.266	.308	.356
5.0	.389	.431	.459	.297	.366	.429	.336	.368	.388	.416	.448	.482
5.5	.530	.572	.595	.359	.416	.471	.502	.526	.546	.537	.572	.585
6.0	.653	.696	.715	.416	.473	.521	.593	.623	.640	.626	.654	.676
6.5	.789	.821	.832	.491	.544	.586	.613	.659	.687	.713	.744	.760
7.0	.892	.910	.912	.575	.624	.662	.692	.732	.755	.791	.818	.826
7.5	.945	.956	.955	.667	.714	.747	.777	.809	.827	.855	.872	.876
8.0	.968	.975	.973	.757	.793	.817	.840	.855	.878	.892	.902	.906
8.5 [b]	.939	.947	.944	.802	.825	.838	.852	.871	.879	.876	.885	.882
9.0 [b]	.965	.973	.967	.878	.893	.894	.911	.926	.929	.913	.920	.919
9.5	.978	.985	.981	.918	.929	.928	.947	.958	.959	.935	.942	.940
10.0	.984	.989	.986	.934	.942	.939	.966	.972	.970	.949	.954	.952
10.5	.982	.987	.986	.939	.946	.946	.976	.978	.978	.957	.960	.957
11.0	.958	.972	.971	.941	.949	.949	.975	.981	.977	.961	.965	.962
11.5	.885	.909	.921	.947	.954	.953	.976	.981	.977	.964	.968	.965
12.0	.836	.860	.873	.954	.960	.957	.983	.982	.980	.970	.973	.968
12.5	.833	.848	.856	.959	.963	.962	.983	.985	.982	.974	.977	.969
13.0	.833	.849	.852	.962	.967	.964	.979	.983	.979	.972	.973	.967
13.5	.833	.848	.852	.964	.970	.966	.951	.962	.962	.975	.962	.955
14.0	.828	.841	.846	.967	.971	.966	.875	.899	.910	.935	.938	.935
14.5	.814	.830	.833	.965	.966	.964	.809	.830	.842	.893	.902	.900
15.0	.799	.813	.813	.958	.955	.948	.793	.804	.805	.844	.852	.850

[a] Average of two readings each on three specimens.
[b] Emittance values low because of error from preferential mirror absorption (sect. 5.1).

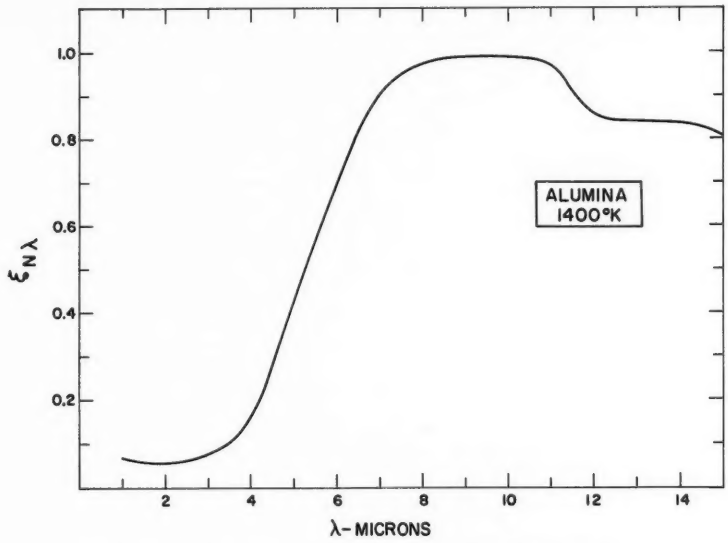

FIGURE 10. *Normal spectral emittance of commercially pure alumina.*
Curve represents average from six determinations; two each on three specimens.

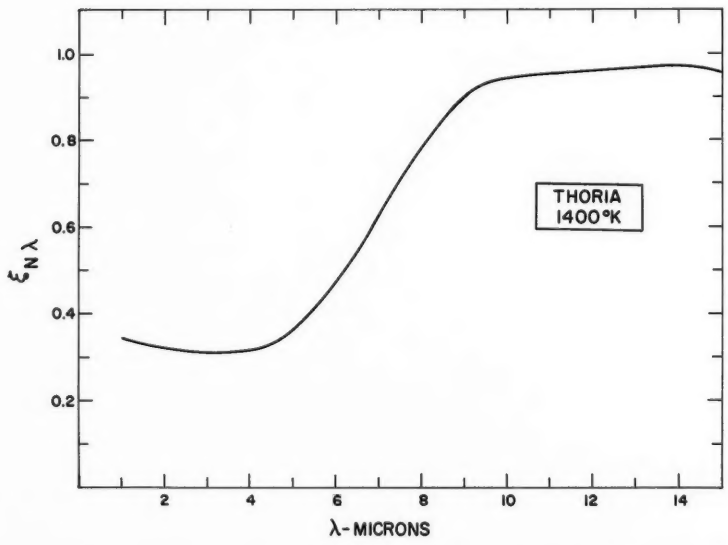

FIGURE 11. *Normal spectral emittance of commercially pure thoria.*
Curve represents average from six determinations; two each on three specimens.

in this report. Also, it is interesting to note that the two standard deviations are related in the following way

$$S_{\bar{x}}^2 = \frac{S_w^2 + nS_b^2}{n} \tag{8}$$

where S_b is the sample estimate of the standard deviation due to differences between specimens.

As shown in table 3, the values of S_w fall in the range 0.001 to 0.021 and are largely independent of temperature. Their magnitude, however, is a function of wavelength, the values being appreciably larger at the short wavelengths than at the long. The values of $S_{\bar{x}}$, on the other hand, are less well behaved due to the manner in which they depend upon differences between specimens. For example, the average value of $S_{\bar{x}}$ is about 0.008 in the wavelength region 1 to 6 μ

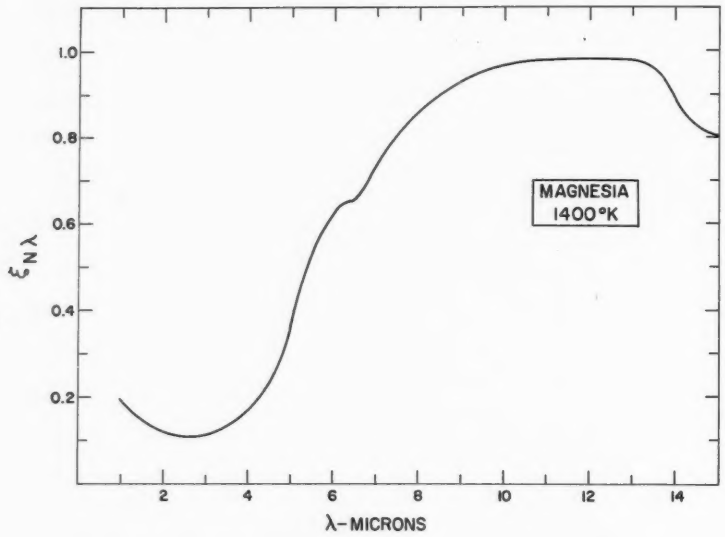

FIGURE 12. *Normal spectral emittance of commercially pure magnesia.*
Curve represents average from six determinations; two each on three specimens.

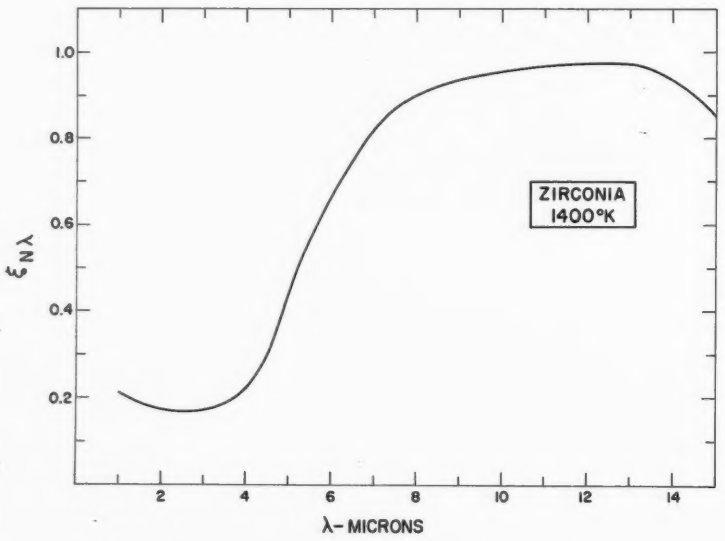

FIGURE 13. *Normal spectral emittance of commercially pure, lime-stabilized zirconia.*
Curve represents average from six determinations; two each on three specimens.

for the alumina, magnesia, and zirconia specimens, but for thoria the average is approximately 0.041 over this same region. Visual examination of the thoria specimens revealed that one of the three (T–10) was darker in color than the other two. This was the same specimen that yielded high emittance in the short wavelength regions. For example, at 2 μ the average emittances from the two determinations on the three thoria specimens were as follows:

Spec. No.	Ave. $\epsilon_{n\lambda}$ at 2 μ		
	1200 °K	1400 °K	1600 °K
T–10	0.276	0.367	0.437
T–11	.201	.299	.382
T–12	.193	.292	.377

TABLE 3. *Standard deviations due to error in measurement*

Sample estimate, S_w, of standard deviation due to error in measurement [a]

Wavelength	Alumina			Thoria			Magnesia			Zirconia		
μ	1200	1400	1600	1200	1400	1600	1200	1400	1600	1200	1400	1600
1	0.00376	0.00163	0.00464	0.00582	0.00862	0.00367	0.00141	0.00091	0.00408	0.00780	0.00523	0.00410
2	.00058	.00372	.00212	.00570	.00404	.00706	.00314	.00319	.00520	.01511	.01185	.00700
3	.00684	.01470	.01390	.00493	.00464	.01173	.00346	.00684	.00890	.01674	.01380	.00889
4	.00689	.00801	.00954	.00777	.00919	.01358	.00671	.01021	.01390	.02071	.01652	.01266
5	.00793	.00696	.00793	.00927	.01099	.01389	.00757	.00933	.01507	.01618	.01363	.00881
6	.00850	.00478	.00635	.01002	.01179	.01488	.00814	.00458	.00751	.01081	.01034	.00498
7	.00153	.00289	.00507	.00389	.01797	.00751	.00332	.00615	.00809	.00835	.00523	.00493
8	.00091	.00220	.00396	.00534	.00456	.00346	.00297	.00370	.00464	.00292	.00168	.00394
9	.00220	.00235	.00449	.00351	.00379	.00416	.00349	.00204	.00238	.00420	.00300	.00204
10	.00187	.00242	.00465	.00402	.00361	.00329	.00376	.00300	.00314	.00297	.00204	.00402
11	.00277	.00321	.00385	.00406	.00208	.00523	.00332	.00337	.00122	.00422	.00258	.00245
12	.00518	.00520	.00486	.00458	.00372	.00274	.00385	.00332	.00231	.00168	.00410	.00306
13	.00513	.00451	.00754	.00332	.00351	.00300	.00416	.00321	.00122	.00129	.00311	.00041
14	.00670	.00513	.00802	.00389	.00449	.00442	.00574	.00505	.00480	.00071	.00178	.00387
15	.00780	.00822	.00883	.00058	.00614	.00890	.00518	.00596	.01122	.00464	.00297	.00367

[a] Each entry corresponds to three degrees of freedom.

TABLE 4. *Overall standard deviation*

Standard deviation, $S_{\bar{x}}$, due to differences between specimens and random error of measurement [a]

Wavelength	Alumina			Thoria			Magnesia			Zirconia		
μ	1200	1400	1600	1200	1400	1600	1200	1400	1600	1200	1400	1600
1	0.00407	0.00721	0.01077	0.04497	0.03311	0.02943	0.00624	0.00673	0.00757	0.00465	0.00416	0.00679
2	.00486	.00764	.01258	.04612	.04102	.03362	.00300	.00687	.00660	.00553	.00525	.00939
3	.00597	.01169	.01473	.04418	.04526	.03597	.00400	.00776	.00889	.00676	.00633	.01225
4	.00541	.01125	.01136	.04571	.04592	.04024	.00530	.01025	.01159	.00912	.00725	.01334
5	.00937	.00854	.00975	.04258	.04217	.03892	.00624	.00889	.01002	.00879	.00606	.01190
6	.00705	.00701	.00752	.03744	.03783	.03646	.00407	.00541	.00695	.00621	.00797	.00855
7	.00597	.00247	.00626	.02948	.03248	.02980	.00391	.00379	.00486	.00318	.00551	.00525
8	.00650	.00475	.00633	.01779	.02019	.01473	.00419	.00650	.00333	.00306	.00362	.00161
9	.00375	.00401	.00626	.00275	.00729	.00404	.00401	.00377	.00318	.00150	.00176	.00050
10	.00568	.00379	.00425	.00293	.00355	.00325	.00377	.00189	.00300	.00236	.00257	.00132
11	.00527	.00425	.00548	.00321	.00180	.00200	.00375	.00306	.00202	.00100	.00153	.00000
12	.00454	.00522	.00625	.00444	.00153	.00229	.00506	.00325	.00351	.00029	.00229	.00058
13	.00605	.00725	.00737	.00275	.00328	.00257	.00404	.00247	.00278	.00318	.00126	.00293
14	.00825	.00759	.00804	.00586	.00225	.00202	.00506	.00701	.00506	.00058	.00321	.00328
15	.00813	.00978	.00709	.00391	.00501	.00306	.00501	.00477	.00666	.00350	.00104	.00450

[a] Each entry corresponds to two degrees of freedom.

At 10 μ and beyond all three thoria specimens were in excellent agreement as indicated by the $S_{\bar{x}}$ values plotted in figure 14. This observation suggests that minor variations in composition can have appreciable effects on the emittance at low wavelengths without causing any significant changes in the longer wavelength region.

c. Lack of Stability of Zirconia Specimens

The first shipment of zirconia specimens showed poor reproducibility of the emittance curves for repeated determinations on the same specimen. Since the degree of reproducibility seemed to be associated with the time of testing at 1600 °K, a series of hourly measurements was made on a zirconia specimen maintained at that temperature. The emittances were found to progressively increase at the short wavelengths and progressively decrease at the longer wavelengths. The observed changes after 4½ hr at 1600 °K are shown in figure 15. X-ray diffraction patterns made before and after the 1600 °K treatment showed that the zirconia had become partially destabilized. Before testing the crystal structure was primarily cubic; however, after 5 hr at 1600 °K, the percentage of the monoclinic form had increased by a factor of about three. Thus, although calcium oxide had been added to the zirconia to "stabilize" it as a cubic solid-solution crystal [22], the degree of stabilization actually achieved was inadequate. A later shipment of zirconia showed less significant changes in emittance after a similar test at 1600 °K. The data reported in the tables were obtained with zirconia specimens from the latter shipment.

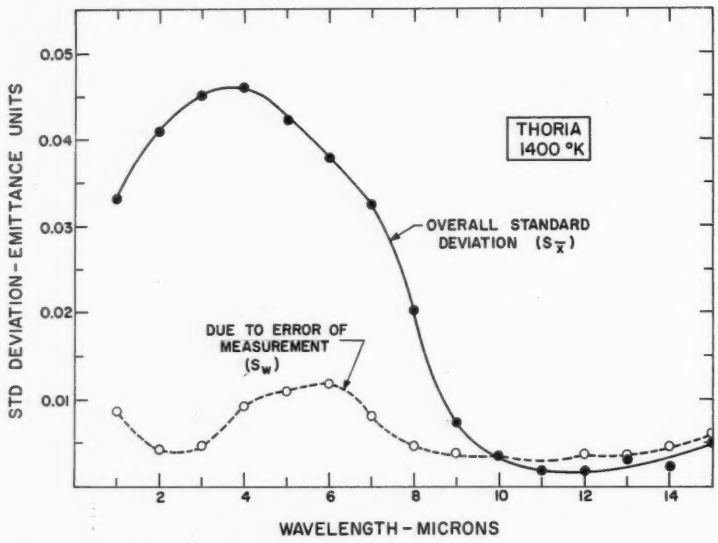

FIGURE 14. *Standard deviation due to error of measurement (S_w) and overall standard deviation ($S_{\bar{x}}$) for the six thoria determinations.*

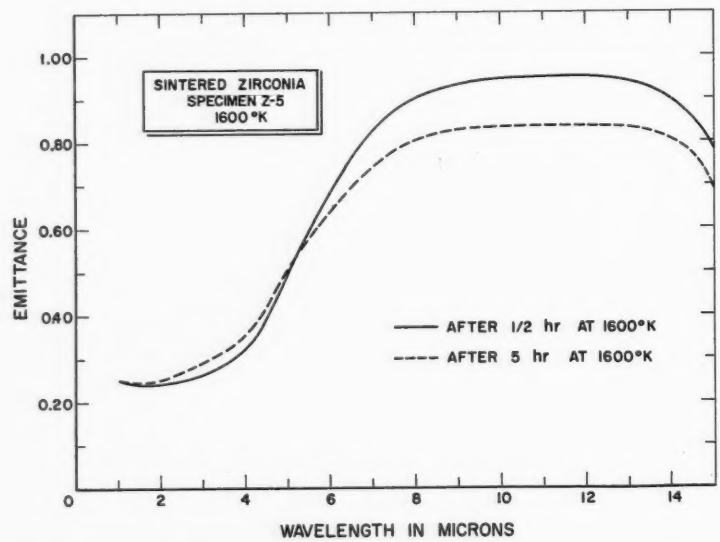

FIGURE 15. *Effect of 5 hr heating at 1600 °K on emittance of poorly stabilized zirconia specimens (first lot).*
Later shipment did not show this behavior.

d. Effect of Temperature on Emittance

Inspection of table 2 shows that the emittance of all four materials increases with increasing temperature. As shown in table 5 the magnitude of the increase is much less at the longer wavelengths, where the emittances are high, than at shorter wavelengths where the emittances are low. In fact, in a few cases at the long wavelengths no measurable change was observed, and for three cases in table 5 a small negative coefficient is reported, although these negative values are not believed to be real.

TABLE 5. *Average increases in emittance per 100 °K over 1200 to 1600 °K temperature range*

Wavelength in microns	Average increase in ϵ_λ per 100 °K [a]			
	Alumina	Thoria	Magnesia	Zirconia
1	0.009	0.040	0.011	0.034
2	.011	.044	.014	.030
3	.010	.045	.014	.027
4	.009	.044	.014	.019
5	.018	.033	.013	.017
6	.016	.026	.012	.012
7	.005	.022	.016	.009
8	.001	.015	.010	.004
9	0	.004	.005	.002
10	0	.001	.001	.001
11	.003	.002	.001	0
12	.009	.001	−.001	−.001
13	.005	0	0	−.001
14	.004	0	.009	0
15	.004	−.002	.003	.002

[a] Computed by subtracting emittance at 1200 °K from emittance at 1600 °K and dividing by four.

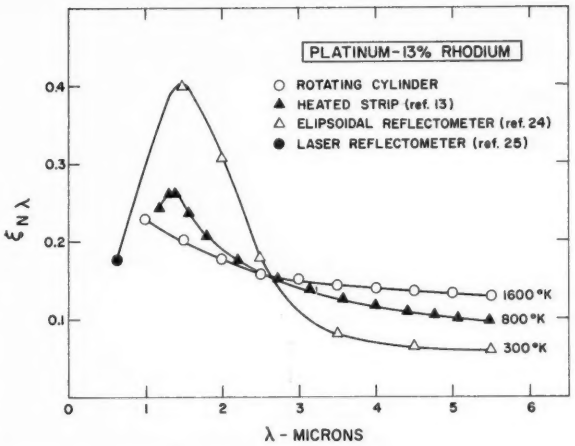

FIGURE 16. *Emittances of a platinum-13 percent rhodium alloy at three temperatures.*

Determinations by all three methods were made in air on specimens that had been heated for 1 hr at 1850 °K prior to measurement.

Some metals have been shown to have a negative temperature coefficient of spectral emittance in the very short wavelength regions and a positive coefficient at the longer wavelengths [23]. This means that a "crossover" or "x-point" exists in the emittance curves, and at the wavelength of this "x-point" the spectral emittance is independent of temperature. Comparison of the rotating-cylinder data for a platinum-13 percent rhodium alloy with other types of measurements made in the same laboratory by other methods [13, 24, 25] strongly suggests that an "x-point" exists for this alloy also. This comparison is shown in figure 16.

No such crossover points were observed for the oxide specimens in the particular wavelength and temperature ranges investigated. At the long wavelengths the temperature dependence approaches zero but since the emittances in this region are already above 0.90, it would obviously be impossible for the emittances to increase by any appreciable extent with temperature.

Figures 17 and 18 compare the changes in emittance with temperature obtained by the rotating-cylinder with those reported by other investigators [7, 26, 27, and 28]. The agreement between the reported values is better at 10.0 μ than at 2.0 μ. At both wavelengths, however, the trend is toward positive coefficients.

For this relatively narrow temperature range the data points obtained from the present measurements are roughly linear with temperature. This relationship can not be expected to apply in general. In fact, it does not even extend downward to room temperature as indicated by the curves plotted in figure 19. The room-temperature (300 °K) points were computed from reflectance measurements made with an ellipsoidal reflectometer that measures absolute reflectance of specimens irrespective of whether they are specular, diffuse, or only partially diffuse in their reflection behavior [24]. The specimens were prepared with the same materials and processing used for the cylinders. Since the measurements were made under near-normal illumination and hemispherical viewing, the reflectances can, in accordance with Kirchhoff's law, be converted to spectral normal emittance by subtracting the reflectances from unity. The fact that the points computed from the room-temperature reflectances fall reasonably well in line with the rotating-cylinder points tends to lend credence to both sets of data.

e. Comments on Use of Data for Heat Transfer Computations

In the past many heat transfer computations have been made with the assumption that the spectral emittance does not change greatly with temperature. The present results indicate that this is not a safe assumption for the polycrystalline oxide materials. Thoria, for example, shows almost a fourfold increase in emittance at 2 μ when the temperature is raised from 300 to 1600 °K. Many more data of this type on temperature dependence are needed before completely reliable heat transfer analyses will be possible. Temperature dependence data for both metals and nonmetals below room temperature are practically nonexistent and emittance data suitable for computing temperature coefficients are notably absent. The reflectance approach has been suggested as a means of obtaining these data because of its potentially greater accuracy [13, 24]. Much can be said for this approach at low temperatures, but at high temperatures difficulties can be expected because of noise in the signal caused by the high background of radiant flux that is emitted from the specimen. Therefore, it seems likely that at temperatures above about 1200 °K, direct measurements of emittance will continue to provide the most reliable data.

The emittances presented in the tables and figures of this report are for specimens of the compositions and structures outlined in section 6.1. Specimens prepared by different processing from materials of different purity, or from materials with different types of impurities, would be expected to show somewhat

223-178 O-66-3

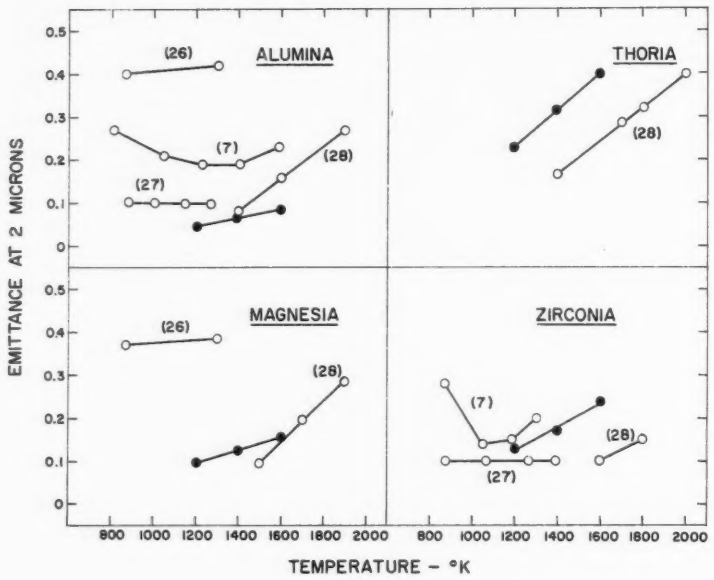

FIGURE 17. *Comparison of reported effects of temperature on normal spectral emittance at 2 μ.*
Source of data is given by reference number in brackets.

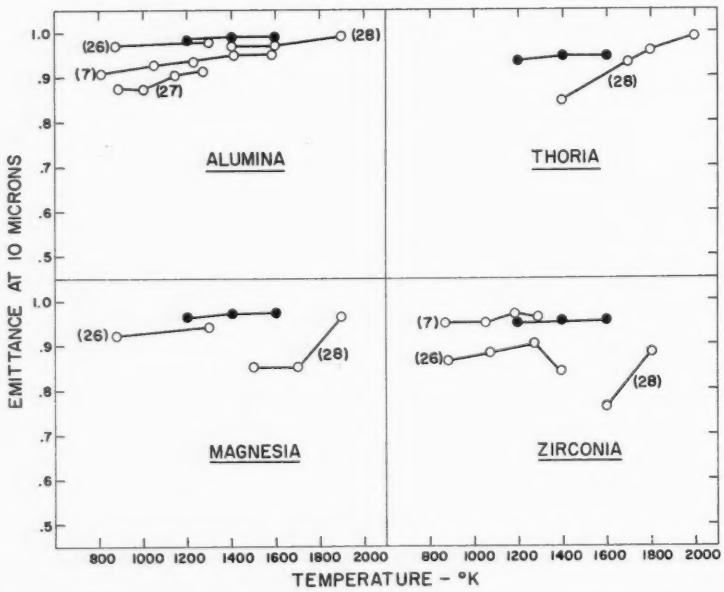

FIGURE 18. *Comparison of reported effects of temperature on normal spectral emittance at 10 μ.*
Source of data is given by reference number in brackets.

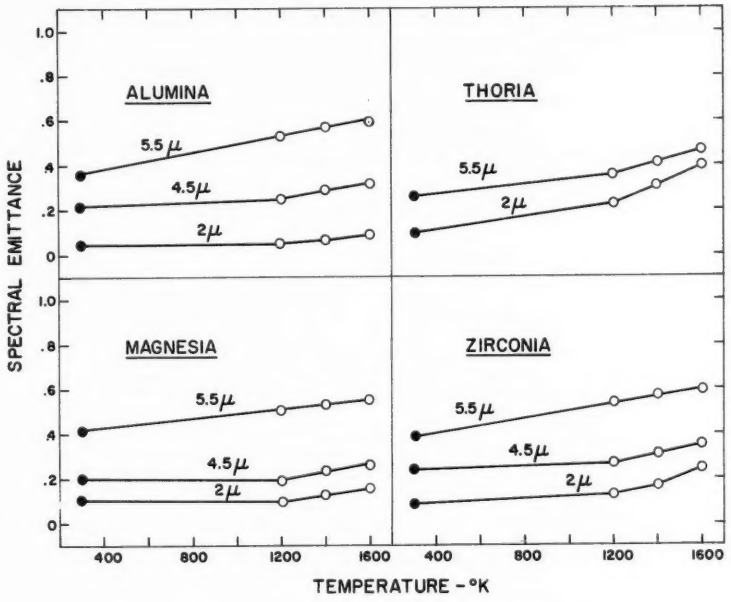

FIGURE 19. *Temperature dependence of normal spectral emittance.*
Open circles are rotating specimen data; closed circles were computed from reflectance data measured with ellipsoidal mirror reflectometer (reference 24).

different emittances, especially in the short wavelength region. For this reason, the emittances as reported herein should not be taken as the emittance of all alumina, thoria, magnesia, or zirconia materials. The only method that will define the thermal radiation properties of any given engineering material is actual measurement by a reliable technique.

Temperature gradients will normally exist in oxide parts used in engineering applications inasmuch as these parts are usually heated in such a way that one or more of the surfaces is free to radiate to ambient. Emittances measured for a specimen with no temperature gradients could of course be used for heat transfer calculations for such parts if the gradients were small. In those cases where the gradients are large, however, the emittances determined for isothermal specimens should be used with caution because of the sizable changes of $\epsilon_{n\lambda}$ with temperature that occur in some wavelength regions (table 3).

f. Correlation of Data for Alumina With Reported Absorption Coefficients

The changes observed in normal spectral emittance, $\epsilon_{n\lambda}$, with both wavelength and temperature undoubtedly reflect changes that are occurring in the optical properties of the materials. Recently Gryvnak and Burch [29] measured the absorption coefficient of single crystal alumina (sapphire) from room-temperature to the melting point. Figure 20 is copied from their data. It will be noted that the absorption coefficient of sapphire increases with increasing tem-

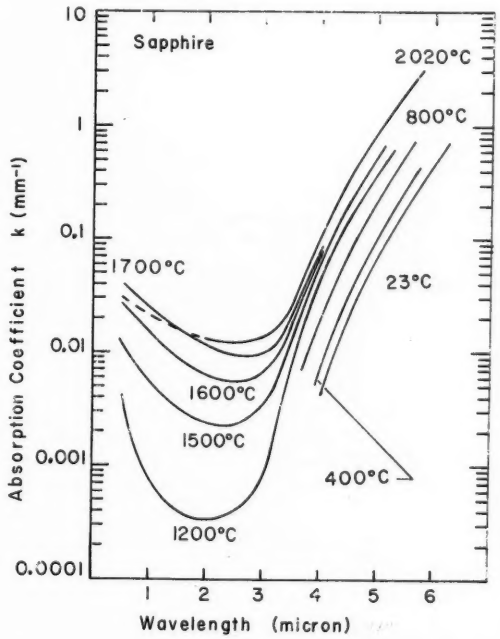

FIGURE 20. *Absorption coefficient-wavelength curves for single crystal alumina as reported by Gryvnak and Burch (reference 29).*

perature and that the temperature dependence is greater at the shorter than at the longer wavelengths. The temperature dependence of emittance shows a somewhat similar behavior (table 3). This similarity is to be expected since, from a reflectance analogy, as absorption within the material increases the amount of the incident energy that emerges from the surface as reflected energy decreases. Therefore, the reflectance will decrease with increasing absorption coefficient, and the emittance will increase.

Figure 20 shows a dip in the absorption coefficient-wavelength curves in the range 1 to 3 μ. As shown in figure 10, a slight dip was also found when $\epsilon_{n\lambda}$, for the polycrystalline alumina, was plotted against wavelength. This dip, however, was not as pronounced for alumina as it was for magnesia (fig. 12), and zirconia (fig. 13).

7. Summary

Equipment is described for measurement of the normal spectral emittance of polycrystalline ceramics in the temperature range 1200–1600 °K. Specimens consisted of hollow cylinders that were rotated at 100 rpm in a furnace enclosure before a water-cooled viewing port.

Various sources of error were investigated. The major source was determined to be furnace radiation that was reflected and/or scattered by the specimen into the specimen beam. At 2 μ and 1200 °K, this effect could cause measured values of emittance to be as much as +0.02 higher than the true value. Temperature uncertainties would contribute ±0.008 as a maximum while the random error of measurement will be on the order of ±0.004. Thus, the true values of emittance at 2 μ and 1200 °K for the particular specimens measured might be as much as 0.032 lower or 0.012 higher than the reported values.

Measurements were made on commercially pure, polycrystalline specimens of alumina, thoria, magnesia, and zirconia. All showed similar behavior in that the emittance was low in the shorter wavelength regions and high at the longer wavelengths. Over the temperature range investigated the temperature coefficients of spectral emittance were positive for all four materials. The coefficients, however, varied with the material, those for thoria being much higher than for the other three. In all cases coefficients were greater at short wavelengths than at long.

The data were shown to be consistent with those obtained by several other measurement methods and in the case of alumina, the data were consistent with recently reported absorption coefficients for sapphire. Temperature coefficients appeared plausible on the basis of room-temperature reflectance measurements made on the same materials.

The authors gratefully acknowledge the assistance of A. G. Eubanks, who contributed to the solution of some of the early design and construction problems; of J. C. Richmond, for many helpful suggestions on method and procedure; of Francis J. Kelly, who prepared the computer programs for obtaining the standard deviations; and of Dr. David Hogben for guidance in preparing the statistical analysis.

8. References

[1]. Féry, C., Ann. Phys. Paris **27**, 443 (1902).
[2]. Michaud, M., Silicates Ind. **19**, 248 (1954).
[3]. Pattison, J. R., Trans. Brit. Cer. Soc. **54**, 698 (1955).
[4]. McMahon, H. O., J. Am. Cer. Soc. **34** (3), 91 (1950).
[5]. Slemp, W. S. and Wade, W. R., Sym. on Measurement of Thermal Radiation Properties of Solids, Dayton, Ohio, NASA SP-31, 433 (1963) (available from U.S Govt. Printing Office, Washington, D.C., 20402, $3.50).
[6]. Olson, O. H. and Katz, S., First Sym. Surface Effects on Spacecraft Materials, Palo Alto, Calif., 164 (1959).
[7]. Folweiler, R. C., Thermal Radiation Characteristics of Transparent, Semi-transparent, and Translucent Materials under Non-Isothermal Conditions, ASD-TDR-62-719 (April, 1964).
[8]. Clayton, W. A., Sym. on Measurement of Thermal Radiation Properties of Solids, Dayton, Ohio, NASA SP-31, 445 (1963), (Available from U.S. Govt. Printing Office, Washington, D.C., 20402, $3.50).
[9]. Clark, H. E. and Moore, D. G., Equipment for Measuring Thermal Emittance of Ceramic Oxides to 1800 °K, Sym. on Thermal Radiation of Solids, San Francisco, Calif., NASA SP-55, 241 (1965). (Available from U.S. Govt. Printing Office, Washington, D.C., 20402 $3.50.)
[10]. Peavy, B. A. and Eubanks, A. G., Sym. on Measurement of Thermal Radiation Properties of Solids, Dayton, Ohio, NASA SP-31, 553, (1963). (Available from U.S. Govt. Printing Office, Washington, D.C. 20402, $3.50.)
[11]. Gouffé, A., Rev. d'Opt. **24**, 1 (1945).
[12]. Sanders, C. L. and Stevens, B. A., Rev. d'Opt. **33**, 179 (1954).
[13]. Harrison, W. N., Richmond, J. C., Shorten, F. J., and Joseph, H. M., Standardization of Thermal Emittance Measurements, WADC TR-59-510, Pt. IV (Nov. 1963).
[14]. Hass, George and Salzberg, Calvin D., J. Opt. Soc. Am. **44**, 181 (1954).
[15]. Clark, H. E., On Avoiding Errors From Stray Radiation in Measuring the Spectral Emittance of Diffusely Reflecting Specimens, J. Appl. Opt. **4**, 1356 (1965).
[16]. Richmond, J. C., Radiative Transfer from Solid Materials, 142, ed. H. Blau & H. Fischer (MacMillan Co., New York, 1962).
[17]. Natrella, M. G., Experimental statistics, National Bureau of Standards Handbook 91, Table A-4 (1963). (Available from USGPO, Wash., D.C. 20402, $4.25.)
[18]. Gannon, R. E. and Linder, B., J. Am. Cer. Soc. **47**, 592 (1964).
[19]. Cox, R. L., Fundamentals of Thermal Radiation in Ceramic Materials, Sym. on Thermal Radiation of Solids, San Francisco, Calif., NASA SP-55, **83** (1965). (Available USGPO, Wash., D.C. 20402, $2.75.)
[20]. Richmond, J. C., Effect of Surface Roughness on Emittance of Non-metals, J. Opt. Soc. Am. **56**, 253 (1966).
[21]. Eisenhart, C., Realistic Evaluation of the Precision and Accuracy of Instrument Calibration Systems, J. Res. NBS **67C** (Engr. and Inst.) No. 2, 161 (1963).
[22]. Weber, B. C., Garrett, H. J., Mauer, F. A., and Schwartz, M. A., J. Am. Cerm. Soc. **39**, 197 (1956).
[23]. Emslie, A. G., A Review of Some Problem Areas in the Theory of Thermal Radiation of Solids, Sym. on Thermal Rad. of Solids, San Francisco, Calif., NASA SP-55, p. 3 (1965). (Available from USGPO, Washington, D.C. 20402 $2.75.)
[24]. Dunn, S. T., Design and Analysis of an Ellipsoidal Mirror Reflectometer, Ph.D. Thesis, Okla. State Univ., May 1965. (Available from University Microfilms, Inc., Ann Arbor, Mich.)
[25]. DeWitt, D. P. and Richmond, J. C., Design and Calibration of a Laser Source Integrating Sphere Reflectometer. (Presented at Am. Inst. Astr. and Aeronautics Meeting in New York City on Jan. 27, 1965—to be published.)

[26]. Blau, H. H., Marsh, J. B., Jasperse, J. R., and Chaffee, E. Infrared Spectral Emittance Properties of Solid Materials. AFCRL TR-60-416 (Oct. 1960).
[27]. Schatz, E. A., Counts, C. R. and Burks, T. L., Coatings for Energy Utilization, Control, and Protective Functions, AFML ML TDR 64-146 (1964).
[28]. Ritzow, G., Ann. der Physik **19**, 769 (1934).
[29]. Gryvnak, D. A. and Burch, D. E., Optical and Infrared Properties of Al_2O_3 at Elevated Temperatures. J. Opt. Soc. Am. **55**, 625 (1965).

9. Appendix A. Analysis of Error Caused by Nonisothermal Blackbody Furnace

Consider a cylindrical blackbody furnace cavity, whose back wall is maintained at 1200 °K and whose sides are at 1225 °K. Further, assume that the cavity is constructed of an opaque material with an emittance ϵ_λ of 0.50 at all wavelengths. As a first approximation, the energy radiated along the axis of the cavity will consist of two components, an emitted component, $\epsilon_\lambda W(\lambda, T_b)$, and a reflected component, $\rho_\lambda W(\lambda, T_s)$, where $W(\lambda, T)$ is Planck's expression for the energy radiated by a blackbody at temperature T. T_b is the temperature of the back wall, and T_s is the temperature of the sides. Since the reflectance of the back wall will be $\rho_\lambda = 1 - \epsilon_\lambda$, its reflectance will be 0.50. One can then write for the energy distribution of radiant flux, W_λ

$$W_\lambda = 0.50\, W(\lambda, T_b) + 0.50\, W(\lambda, T_s) = 0.50\, W(\lambda, 1200\ °K) + 0.50\, W(\lambda, 1225\ °K) \quad \text{(A1)}$$

When an optical pyrometer is sighted on the furnace opening, as was done in the present measurements, the indicated temperature, T', at $\lambda = 0.65\ \mu$ is assumed to be that of a perfect blackbody. Thus, one can write:

$$W(0.65\ \mu, T') = 0.50 W(0.65\ \mu, 1200\ °K) + 0.50 W(0.65\ \mu, 1225\ °K). \quad \text{(A2)}$$

The error E_λ introduced by assuming that the nonisothermal furnace can be approximated by a perfect blackbody at the optical temperature T' is

$$E_\lambda\ (\%) = \frac{W_\lambda - W(\lambda, T')}{W_\lambda} \times 100. \quad \text{(A3)}$$

A computer program, prepared to calculate T' and E_λ at 0.25 μ intervals over the range 1 to 15 μ, showed a maximum error of only 0.44 percent. This occurred at a wavelength of 1.25 μ. At 10 μ the error is only 0.14 percent.

The blackbody furnaces used in this investigation had gradients less severe than those assumed in the calculation, and the emittance of the actual cavity walls is significantly higher than 0.50. Thus, the energy radiated along the axis of the laboratory furnaces should even more closely approximate blackbody radiation. At higher temperatures, 1400 and 1600 °K, the Planck Function $W(\lambda, T)$ is less sensitive to temperature differences, and the measured gradients are smaller, so that the errors will be even less significant than at 1200 °K.

(Paper 70A5-412)

JOURNAL OF RESEARCH of the National Bureau of Standards—A. Physics and Chemistry
Vol. 70A, No. 5, September–October 1966

Electron Absorption Spectrum of Cobalt (II)-Doped Trisphenanthrolinezinc Nitrate Dihydrate

Curt W. Reimann

Institute for Materials Research, National Bureau of Standards, Washington, D.C. 20234

(May 10, 1966)

The electron absorption spectrum of cobalt(II)-doped trisphenanthrolinezinc nitrate dihydrate has been observed at room temperature and at 77 °K. Broad bands appear at 10,750 and 22,000 cm^{-1} which are assigned to the $^4T_{1g}(F) \leftarrow\rightarrow {}^4T_{2g}(F)$ and the $^4T_{1g}(F) \leftarrow\rightarrow {}^4T_{1g}(P)$ transitions respectively. A broad weak band occurs near 19,000 cm^{-1} but at 77 °K this band is resolved into a series of narrower bands. These bands are assigned to ^2G transitions. The relationship between the spectrum of cobalt(II) trisphenanthrolinezinc nitrate dihydrate and the solution spectra of cobalt(II) in ammonia and ethylenediamine is discussed.

Key Words: Trisphenanthroline cobalt(II) nitrate dihydrate, trisphenanthrolinezinc nitrate dihydrate, electron absorption spectrum.

1. Introduction

Several spectroscopic studies of single crystals of octahedrally coordinated cobalt(II) have appeared recently [1–4].[1] Cobalt(II) spectra are particularly interesting in that they are characterized by narrow spin-forbidden bands as well as by broad spin-allowed bands which are more typical of *d-d* transitions. In each of the previously reported spectra, however, the ligand field strength parameter, D*q*, was less than 1000. Such D*q* values are smaller than would be expected in octahedral cobalt(II) complexes of ammonia, ethylenediamine or 1, 10 phenanthroline. These complexes assume some importance since Liehr [5] has constructed a diagram of electron energy versus ligand field strength D*q* for the d^7 system which indicates that for D*q* greater than about 1100 the $^4A_{2g}(F)$ state lies higher than the $^4T_{1g}(P)$ state while at lower D*q* the reverse obtains. Ballhausen and Jorgensen [6] reported the spectra of cobalt(II) in ammonia and ethylenediamine solutions which quite clearly correspond to D*q* greater than 1000. These workers assigned weak broad bands near 19,000 cm^{-1} as $^4T_{1g}(F) \leftarrow\rightarrow {}^4A_{2g}(F)$ transitions and bands near 21,000 cm^{-1} as arising from $^4T_{1g}(F) \leftarrow\rightarrow {}^4T_{1g}(P)$ transitions thereby suggesting that the $^4A_{2g}(F)$ state lies lower than the $^4T_{1g}(P)$ state in each of their spectra.

Exploratory studies were carried out on alcohol solutions of cobalt (II) and 1, 10 phenanthroline and they revealed the following:

(1) The ligand field strength provided by 1, 10 phenanthroline as evidenced by spectral shifts was greater than that provided by either ammonia or ethylenediamine.

(2) a weak broad band near 19,000 cm^{-1} was present as it had been in ammonia and ethylenediamine solutions of cobalt (II).

In an attempt to bring new evidence to bear on possible assignments single crystals of cobalt(II)-doped trisphenanthrolinezinc nitrate dihydrate were grown and low-temperature spectra were investigated. In what follows the outcome of this investigation is described.

2. Experimental Procedure

Crystals of cobalt(II)-doped trisphenanthrolinezinc nitrate dihydrate were grown from ethyl alcohol solutions of zinc nitrate, cobalt(II) nitrate and phenanthroline in slight excess of the stoichiometrically required amount. Crystals of trisphenanthrolinezinc nitrate dihydrate are triclinic with two molecules per unit cell [7]. Polarized spectra were measured on a spectrophotometer (Cary 14) with Glan-Thompson polarizers. Spectra at 77 °K were taken with single crystals mounted on brass disks in thermal contact with the coolant which was contained in a simple Dewar. When viewed with polarized light crystals of cobalt(II)-doped trisphenanthrolinezinc nitrate dihydrate vary in color from bright orange to pale yellow.

3. Results

The absorption spectrum of cobalt(II)-doped trisphenanthrolinezinc nitrate dihydrate from 8,000 to 20,000 cm^{-1} is shown in figure 1. The features of this spectrum are identical with the alcohol-water solution spectrum of cobalt(II) nitrate and phenanthroline and very similar to the solution spectra of $Co(NH_3)_6^{++}$ and

[1] Figures in brackets indicate the literature references at the end of this paper.

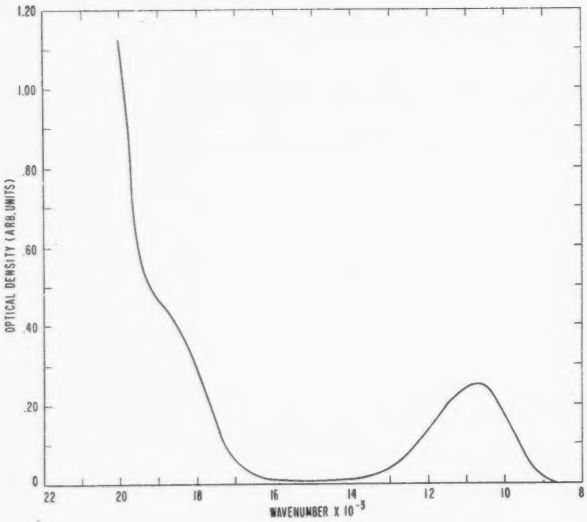

FIGURE 1. *Single crystal spectrum of cobalt* (II)*-doped trisphenanthrolinezinc nitrate dihydrate from 8000 to 20,000 cm*$^{-1}$

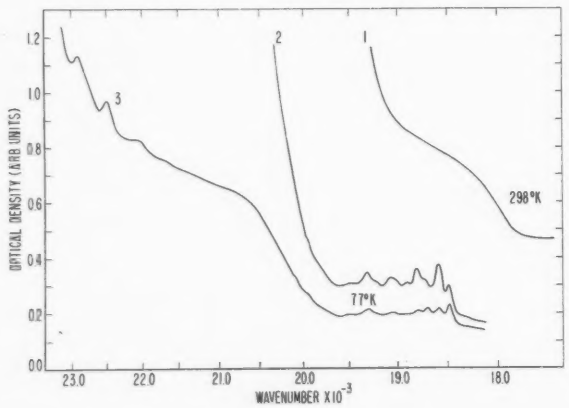

FIGURE 2. *Single crystal spectra of cobalt* (II)*-doped trisphenanthrolinezinc nitrate dihydrate near 19,000 cm*$^{-1}$.

Curve 1 shows the spectrum at room temperature while curves 2 and 3 are polarized spectra taken at 77 °K. Polarized spectra were taken along the direction in which the narrow band system was best resolved (curve 2) and perpendicular to this direction.

$Co(en)_3^{++}$ reported by Ballhausen and Jorgensen. For purposes of calculating D_q and B for $Co(phen)_3^{++}$ and comparing the results with those obtained by Ballhausen and Jorgensen for $Co(NH_3)_6^{++}$ and $Co(en)_3^{++}$ spectral data were obtained from solutions of cobalt(II) nitrate and phenanthroline. To obtain the best values for the band energies samples were prepared from carefully degassed solutions. Absorption bands were observed in these solutions at 10,750 cm^{-1}, 22,000 cm^{-1} and a broad weak band occurred at about 19,000 cm^{-1}.

At 77 °K the absorption bands in cobalt(II) doped trisphenanthrolinezinc nitrate dihydrate narrowed slightly and relatively sharp bands appeared in the region from 18,450 cm to 23,000 cm^{-1} (fig. 2). The narrow bands from 18,450 cm to 19,800 cm^{-1} were polarized and most clearly resolved along the direction in which the crystal appeared orange.

4. Discussion

Cobalt (II), a d^7 system, has free ion states ^4F, ^4P, ^2P, ^2D, ^2G, ^2H, and ^2F. In an octahedral crystalline field the lowest free ion state, ^4F, splits into two orbital triplets, $^4T_{1g}$ and $^4T_{2g}$, and an orbital singlet, $^4A_{2g}$, while the next lowest free ion state, ^4P, remains unsplit ($^4T_{1g}$). Transitions from the ground state, $^4T_{1g}(F)$, to $^4T_{2g}(F)$, $^4A_{2g}(F)$ and $^4T_{1g}(P)$ lead to broad banded absorptions in the visible and near infrared spectral regions. Typically, the spectrum of cobalt (II) in an octahedral environment consists of a broad band in the near infrared ($^4T_{1g}(F) \leftrightarrow {}^4T_{2g}(F)$), a broad and less intense band in the visible ($^4T_{1g}(F) \leftrightarrow {}^4A_{2g}(F)$) and another broad band in the visible ($^4T_{1g}(F) \leftrightarrow {}^4T_{1g}(P)$). In single crystals, particularly at low temperatures, much less intense and narrower bands appear in the spectrum of cobalt (II). These bands are usually assigned to spin-forbidden transitions to doublet states. The spectrum of cobalt (II) doped trisphenanthrolinezinc nitrate dihydrate will now be considered in terms of the simple octahedral picture.

The band at 10,750 cm^{-1} is assigned to the $^4T_{1g}(F) \leftrightarrow {}^4T_{2g}(F)$ transition and the broad absorption located at 22,000 cm^{-1} is assigned as the $^4T_{1g}(F) \leftrightarrow {}^4T_{1g}(P)$ transition. The assignment of the $^4T_{1g}(P)$ and the $^4T_{2g}(F)$ levels permits the calculation of D_q and B by the method of Tanabe and Sugano [8]. D_q is the crystal field strength parameter and B is the interelectronic repulsion parameter. From the computed values of D_q and B the energy of the $^4A_{2g}$ level is found to be about 22,800 cm^{-1} above the $^4T_{1g}(F)$ ground state. From the assignments of the $^4T_{1g}(P)$ and $^4T_{2g}(F)$ states in $Co(NH_3)_6^{++}$ and $Co(en)_3^{++}$ made by Ballhausen and Jorgensen the D_q and B values can be computed and these values utilized, in turn, to calculate the $^4A_{2g}(F)$ levels. The calculated D_q, B, and $^4A_{2g}(F)$ levels for $Co(phen)_3^{++}$, $Co(NH_3)_6^{++}$ and $Co(en)_3^{++}$ are presented in Table 1.

TABLE 1

	D_q	B	$^4A_{2g}$
$Co(phen)_3^{++}$	1206	837	22813
$Co(NH_3)_6^{++}$	1023	889	19228
$Co(en)_3^{++}$	1102	875	20818

In addition to the assignment of the $^4T_{1g}(P)$ and $^4T_{2g}(F)$ states Ballhausen and Jorgensen attributed weak absorption near 19,000 cm^{-1} in their spectra to the $^4T_{1g}(F) \longleftrightarrow {}^4A_{2g}(F)$ transition. It is clear, however, that such an assignment in $Co(phen)_3^{++}$ is less tenable not only because the absorption near 19,000 cm^{-1} is resolvable at low temperatures into a series of sharp bands but also because the computed separation of the $^4A_{2g}(F)$ level from the ground state is 22,800 cm^{-1}. Our interpretation of the spectrum of $Co(phen)_3^{++}$ is based upon the evidence that the absorption near 19,000 cm^{-1} can be assigned as transitions to other states within the cobalt (II) manifold. In terms of this interpretation the $^4T_{1g}(F) \longleftrightarrow {}^4A_{2g}(F)$ band lies above 20,000 cm^{-1} but must remain unspecified because of the more intense $^4T_{1g}(F) \longleftrightarrow {}^4T_{1g}(P)$ and charge transfer bands which occur in this region.

The narrow bands observed near 19,000 cm^{-1} are analogous to those reported by Ferguson and by Ferguson, Wood, and Knox who assigned the bands to transitions to doublet levels. Liehr has constructed an energy level versus ligand field strength, D_q, diagram for the d^7 electronic system in octahedral symmetry. Ferguson, Wood, and Knox have computed the energies of the doublet states for cobalt(II) in $KCOF_3$, $CoCl_2$, $CoBr_2$, and $CoWO_4$ utilizing the D_q and B values obtained from their observed spectra. Briefly, these workers show that in the free ion the ^2G states lie lowest of the doublet states with ^2P and ^2H levels occurring some 4,000 cm^{-1} above ^2G. ^2F and ^2D lie still higher. In an octahedral crystalline field the ^2G states split into six levels four of which are relatively insensitive to the strength of the ligand field. The energies of the other two states arising from ^2G show a rather strong dependence upon the ligand field strength. One of these states increases while the other decreases in energy with increasing ligand field strength. The energies of states arising from ^2H, ^2P, ^2D, and ^2F of the free ion increase moderately rapidly with increasing ligand field strength. This analysis shows that transitions to four ^2G states would be expected to give rise to transitions in a spectral region which is free of transitions to other doublet states. More specifically, one would expect that transition to the four intermediate ^2G states would give rise to absorption in the 15,000 to 20,000 cm^{-1} region and that the lowest and highest of this set of ^2G states would be separated by about 1000 cm^{-1}. In the spectrum of cobalt(II) doped trisphenanthrolinezinc nitrate dihydrate narrow bands are observed from 18,450 cm^{-1} to 19,500 cm^{-1} and these are assigned to transitions to the ^2G states.

Figure 2 shows, however, that nine peaks are resolved between 18,450 and 19,500 cm^{-1}. The number of observed bands cannot be accounted for on the basis of symmetry lower than octahedral since reduction in symmetry could produce only two additional bands. Moreover, the occurrence of too many bands cannot be accounted for on the basis of transitions from a thermally populated excited state. The latter conclusion follows from the fact that the minimum separation between observed bands is about 100 cm^{-1} and no bands were observed to diminish as the temperature was reduced from 77 to 20 °K. The occurrence of more peaks than the number of ^2G levels is undoubtedly associated with the fact that the bands in question are strictly forbidden in octahedral symmetry and arise via a coupling to antisymmetric vibrations. That is, the electronic transitions must be accompanied by a simultaneous change of one quantum in an antisymmetric mode. In principle progressions of symmetric vibrational modes can be superimposed on the perturbing antisymmetric mode to greatly complicate the appearance of an electronic absorption band. It appears therefore that the vibrational structure which was so evident in the cobalt(II) crystal spectra of Ferguson and Ferguson, Wood, and Knox also arises in the spectrum of cobalt(II)-doped trisphenanthrolinezinc nitrate dihydrate.

While no conclusions regarding the bands near 19,000 cm^{-1} in $Co(NH_3)_6^{++}$ and in $Co(en)_3^{++}$ should be drawn without low temperature spectra of the corresponding crystalline materials it appears likely that these bands are analogous to those which we have assigned to ^2G transitions. The closeness in the Dq and B values in these materials and the insensitivity of the energy of the intermediate ^2G levels to small changes in Dq, support this notion.

The author thanks Harry C. Allen, Jr., Deputy Director of the Institute for Materials Research for suggesting that this investigation be carried out.

5. References

[1] J. Ferguson, D. L. Wood, and K. Knox, J. Chem. Phys. **39,** 881 (1963).
[2] J. Ferguson, J. Chem. Phys. **32,** 533 (1960).
[3] R. Pappalardo, D. L. Wood and R. C. Linares, Jr., J. Chem. Phys. **35,** 2041 (1961).
[4] W. Low, Phys. Rev. **109,** 256 (1958).
[5] A. D. Liehr, J. Phys. Chem. **67,** 1314 (1963).
[6] C. J. Ballhausen and C. K. Jorgensen, Acta Chem. Scand. **9,** 397 (1955).
[7] G. F. Kokoszka, C. W. Reimann, H. C. Allen, Jr., and G. Gordon (in preparation).
[8] Y. Tanabe and S. Sugano, J. Chem. Soc. Japan **9,** 753 (1954).

(Paper 70A5–413)

(Paper 70A5–413)

JOURNAL OF RESEARCH of the National Bureau of Standards—A. Physics and Chemistry
Vol. 70A, No. 5, September–October 1966

Procedures for Homogeneous Anionic Polymerization

Lewis J. Fetters*

Institute for Materials Research, National Bureau of Standards, Washington, D.C. 20234

(May 11, 1966)

This report is a review of the procedures and equipment used in the preparation of polymers of predictable molecular weights and narrow molecular weight distributions. The monomers considered in detail are styrene, α-methylstyrene, isoprene, and butadiene.

Key Words: Homogeneous anionic polymerization, monodisperse, polystyrene, poly-α-methylstyrene, polyisoprene, and polybutadiene.

1. Introduction

Organometallic actuated addition polymerizations of unsaturated compounds (vinyl, diene, etc.) in hydrocarbon and ether media have received considerable attention. Many of these polymerizations are unusual in that spontaneous termination is avoidable through the judicious choice of experimental conditions; a feature first fully appreciated by Szwarc [1, 2].[1] Of considerable experimental value is the fact that the deactivation of these "living" polymercarbanions may be accomplished at the leisure of the experimenter by the selective addition of a reagent suited to meet a particular need. This retention of chain-end activity is a feature that facilitates investigations of the thermodynamics of polymerization processes, simplifies studies of polymerization kinetics, and permits synthesis of novel macromolecules.

These systems can therefore consist of active chains which will continue to incorporate monomer until monomer depletion is accomplished. Hence, if each center of propagation is afforded equal opportunity of growth, the resulting product will possess a homogeneous molecular weight [3]. As a result, many studies of homogeneous anionic polymerization have had as a foremost goal the synthesis of polymers of predictable molecular weight and predeterminable molecular weight distributions. Obviously, this goal can only be attained in the absence of any constituent capable of reacting with these carbanions, e.g., acids, alcohols, or the usual atmospheric components.

The general case of a termination-free system received treatment by Flory [3], who showed that the growth of a fixed number of active chains leads to molecular weight distributions approaching monodispersity, i.e., the Poisson distribution. These molecular weight distributions may be represented by the Poisson function,

$$W(K, \overline{X}_{n_0}) = [K(\overline{X}_{n_0} - 1)^{K-1} \exp(1 - \overline{X}_{n_0})]/[\overline{X}_{n_0}(K-1)!]$$

$$K = 1,2,3,4, \ldots$$

where $W(K, \overline{X}_{n_0})$ denotes the weight fraction of K-mers residing in a mixture of chains of number average chain length X_{n_0}. For these systems, the weight-to-number average chain length ratio is given as:

$$\overline{X}_{w_0}/\overline{X}_{n_0} = 1 + 1/\overline{X}_{n_0} - 1/\overline{X}^2_{n_0}.$$

Such distributions have not been achieved, or even approached, until quite recently with monomers such as styrene [4–15], α-methylstyrene [16, 17], isoprene [18–21], and butadiene [21–24]. This was due principally to various factors which combined to veil the true possibilities of these systems. These factors included the presence of impurities or solvents which could terminate or transfer with the growing chains, a slow initiation reaction, a depropagation step (equilibrium polymerization) or the presence of interchange reactions between polymer chains. The latter two phenomena are encountered in the polymerization of cyclic siloxanes [25, 26].

Hence, the fulfillment of the following conditions is necessary if precise control over molecular weight and molecular weight distribution is to be achieved: (a) rigorous exclusion of substances capable of causing termination or transfer; (b) uniformity of reaction conditions with regard to temperature and concentration of reactants; (c) a high ratio of the apparent initiation to propagation rates; and (d) the absence of depropagation steps and bond interchange reactions. In view of increasing interest in the study of bulk and solution properties of polymers with narrow distributions of molecular weights, as well as those of precisely constructed copolymers and "star" macro-

* National Academy of Sciences-National Research Council Postdoctoral Resident Research Associate.

[1] Figures in brackets indicate the literature references at the end of this paper.

molecules, the purpose of this communication is to review the techniques by which the preparation of these polymers may be achieved. Results from various laboratories have indicated that the high-vacuum technique provides the most reliable method for the successful attainment of these goals. As will be discussed later, among those who have realized the potential of these techniques have been Bywater and Worsfold, Wenger, Szwarc, Rempp, and Morton.

The monomers considered herein are styrene, α-methylstyrene, isoprene, and butadiene. The polymerization initiators described are the isomers of butyllithium. These monofunctional initiators provide several advantages over the electron transfer initiators, e.g., sodium biphenyl or sodium naphthalene. Addition of an electron transfer initiator to an ether solution of monomer results in the formation of an ion-radical [1, 2] which eventually undergoes a combination reaction with the resultant generation of a polymeric species possessing a carbanion at each end. In preparing the difunctional species, the accidental deactivation of a fraction of the carbanions will result in a bimodal molecular weight distribution [5, 7, 16], i.e., the material will possess a portion that will have one-half the molecular weight of the remaining polymer.

For the case of the polymerization of styrene in an ether such as tetrahydrofuran (THF), complications arise as a consequence of the rapidity of the propagation reaction [27, 28]. In order to maintain homogeneous reaction conditions, it is necessary to add monomer very slowly, either by distillation or dropwise addition, to a rapidly agitated solution. The presence of trace impurities in the monomer will cause a broadening of the molecular weight distribution because of continuous termination of chain ends throughout the duration of the polymerization. This assumes a constant rate of replenishment of any impurity. Szwarc has shown [29] that when an anion deactivator is present in the monomer at concentrations sufficient to annihilate the entire initial polymercarbanion population by the time the monomer supply is exhausted, the resultant sample will possess the "most probable" molecular weight distribution.

The monofunctional organolithium-initiated polymerization of styrene and other monomers in hydrocarbon media offers several distinct advantages over reactions carried out in tetrahydrofuran. The slow propagation rates [30] permit the addition of the monomer to the solvent-initiator solution in a batchwise fashion. Hence, any impurities will react on mixing with the initiator. If a fraction of the total initiator is destroyed, the molecular weight distribution will not be broadened, although an increase in the molecular weight will occur. The effect on the distribution of a slow termination reaction, comparable in speed to the comsumption of monomer, has received consideration by Coleman et al., [31]. Fortunately, for certain monomers the occurrence of such reactions is avoidable through the proper selection of solvent and by the application of the procedures to be outlined shortly.

2. Experimental Techniques

2.1. High Vacuum Apparatus

A high vacuum apparatus, figure 1, permits the attainment of the rigorous experimental conditions necessary to prevent the termination of a reaction by the presence of contaminants. Therefore, all monomer and solvent purifications and polymerizations are carried out on the vacuum line, or in sealed evacuated vessels. The vacuum apparatus is composed of an oil pump (1) working in concert with a mercury diffusion pump (2). In a leak-free system pressures in the range of 10^{-5} to 10^{-6} mm Hg are obtainable. A liquid nitrogen trap (3) is used to condense any condensable gases so that the pressure registered on the McLeod gage (4) is exclusively that of noncondensable species. The nitrogen trap also prevents the passing of mercury vapor from the diffusion pump into the main manifold (5).

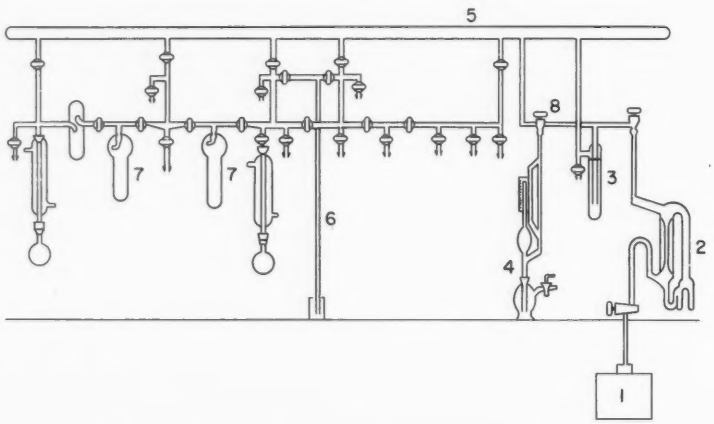

FIGURE 1. *High vacuum apparatus.*

The pressure release (6) is a tube over 76 cm in length with one end connected to the vacuum apparatus and the other end submerged in a mercury pool. When substances with low boiling points, e.g., butadiene, ethylene oxide, etc., are used in vacuum systems there exists the possibility that pressure may build up to the point of fracturing the apparatus or blowing temporarily attached pieces of equipment off the line. The purpose of the pressure release is to relieve such pressure in the apparatus and still maintain an airtight system. Furthermore, the fall of the mercury column provides a visual indication of the onset of such a pressure increase.

a. The Main Manifold

A manifold of this type consists of a 4 to 6 cm diameter section of Pyrex glass tubing, clamped in place on a metal supporting frame. The vacuum stopcocks connecting the main manifold to the secondary one possess stopper bores of 6 to 10 mm. The stopcocks placed in the secondary manifold are those with 4 mm stopper bores. The connecting tubes of the secondary manifold are made of 12 mm diam heavy wall Pyrex tubing, since this is about the largest size of glass tubing that is practical in constructing a large and rigid piece of apparatus where proper annealing is impractical. Apiezon *N* hydrocarbon grease is recommended for use in the main manifold whereas silicon grease should be used in the secondary manifold stopcocks since this lubricant is highly resistant to the passage of ether and hydrocarbon vapors. After the application of grease to a stopcock, the system should be pumped for several hours in order to remove trace amounts of moisture from the freshly applied grease.

Graduated cylinders (7) are used to measure out approximate amounts of solvent or monomer prior to final collection. These pieces of equipment may either be permanently attached to the line or equipped with ground glass joints for temporary placement.

The entrance stopcock (8) of the McLeod gage to the vacuum line is located so as to register pressure on either side of the nitrogen trap. During the early stages of evacuation readings taken between the cold trap and the manifold will indicate a lower pressure than will measurements made directly from the manifold. This disparity is due to the removal of condensable gas in the nitrogen trap. Hence the readings referred to herein are those registered directly from the main manifold.

2.2. General High Vacuum Techniques and Equipment

All reactors and ampoules are constructed from Pyrex glassware. Prior to assembly of the equipment, the glassware should be cleaned with either cleaning solution or hydrofluoric acid, rinsed with a dilute solution of sodium hydroxide, washed with distilled water, and dried.

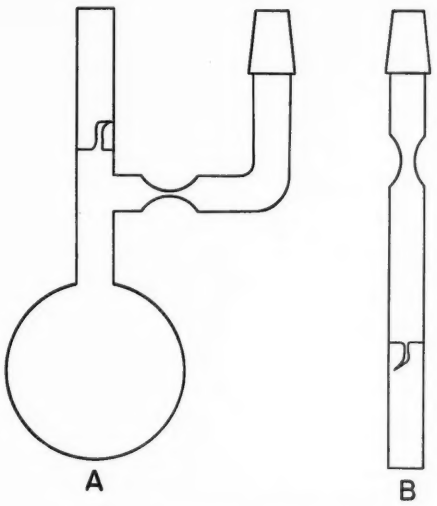

FIGURE 2. *Monomer-solvent ampoules.*

Figure 2 depicts typical monomer-solvent ampoules. The breakseals are usually those made from 12 mm diam tubing. A convenient size of ground glass joint is the 14/35 type.

After construction of the equipment, the glassware is evacuated on the vacuum line and tested with a Tesla coil for leaks. When it is ascertained that the apparatus is structurally sound, the glassware is heated, with a handtorch adjusted to give a soft blue flame, until the yellow sodium flame is given off from the glass surface. The glassware during this heating period is continuously being evacuated. Intermittent heating is continued until a pressure of $\sim 10^{-6}$ mm Hg is recorded on the McLeod gage. The purpose of this treatment is to remove the adsorbed gas and water film which are present on the surface of the glassware.

Rupturing the breakseals is accomplished with the aid of an iron nail enclosed in a glass envelope. The glass jacket is made from tubing of the appropriate diameter rounded off at one end. The nail is put in place with either glass wool or asbestos fibers to pack it solidly in place. A constriction is then placed above the nail and the tube sealed onto a manifold for eventual evacuation. After thorough evacuation is accomplished, the nail is sealed off and the end of the envelope rounded off.

a. Distillation and Degassing Procedures for Liquids in a Vacuum System

In the absence of appreciable amounts of noncondensable gases, transfer of volatile materials to a cooled zone is rapidly effected. However, in the

presence of even small amounts of noncondensable gases, the diffusion of condensable materials is impeded. It is therefore necessary to maintain the pressure below $\sim 10^{-3}$ mm Hg in order to carry out transfer of condensable materials at a practical rate. Thus, it is quite important to exhaustively degas all liquids prior to any subsequent operation, such as distillation, drying, and collection.

The removal of air is carried out as follows. The flask containing the liquid to be degassed is connected to the vacuum line and cooled until frozen. An appropriate cooling bath such as liquid nitrogen or a dry-ice-alcohol mixture is used, depending on the freezing point of the liquid being degassed.

When the substance is frozen, the flask is evacuated by opening the stopcock between it and the vacuum line. After approximately 5 min, the flask is isolated from the vacuum line and the frozen material warmed to room temperature. To expedite melting, the flask may be submerged in an alcohol bath. The freezing and thawing cycle is repeated until the pressure registered on the McLeod gage is of the order of 10^{-5} mm Hg with the material in the frozen state. The material is then considered degassed and is ready for subsequent treatment. A supplementary discussion on the distillation and collection of liquid hydrocarbons can be found elsewhere [32].

b. Preparation of Sodium Mirrors

For use as a drying agent for *trace* quantities of moisture, a thin sodium mirror is advantageous. This mode of drying is not to be confused with the usual ritual of drying organic liquids with large lumps of sodium, which in the usual course of events all too soon accumulate a coating of oxide and hydroxide. These mirrors are readily prepared on a high vacuum line as follows. Approximately ⅛ to ¼ g of dry sodium metal (not kept under mineral oil) is placed in a flask, which may be of any size up to 1 to 2 liters capacity, and connected to the vacuum line. The flask is evacuated until a pressure of 10^{-4} mm Hg or less is obtained.

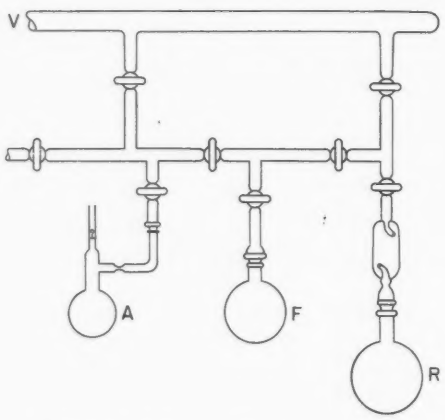

FIGURE 3. *Solvent purification apparatus.*

While still being evacuated, a small area at the bottom of the flask is gently and intermittently heated with a small, soft flame from a hand torch until the metal begins to melt. The metal will then vaporize to form the mirror. Excess heating may cause the flask to crack. Once the mirror is formed, evacuation is continued until the flask has cooled to room temperature. Then the liquid to be dried is distilled onto the sodium film. Once the liquid is in contact with the mirror, it should receive further degassing in order to remove any hydrogen formed by the reaction of moisture with sodium. Exposure to two or three mirrors is usually sufficient to ensure dryness.

c. Preparation of Sodium-Potassium Alloy

The alloy of sodium and potassium is prepared in a flask (R) as noted in figure 3. Approximately equal parts by weight of the two alkali metals are used in the preparation. The use of this ratio ensures the existence of the alloy in the liquid state at room temperature. In this form it serves as a very efficient drying agent for hydrocarbon solvents. The total weight of the two metals need not exceed 1 g.

The sodium used in this preparation should be as free as possible from hydroxide. The mineral oil is removed from the potassium by rinsing the metal in dry benzene or toluene. The rinsed lumps must be covered by solvent at all times during handling and transfer.

Following the placing of the flask containing the two alkali metals, the covering solvent and a stirring bar on the vacuum line, the apparatus is then carefully evacuated and the covering solvent distilled off and allowed to collect in a second flask cooled by a dry-ice-alcohol mixture. After the attainment of a good vacuum ($\sim 10^{-5}$ mm Hg), the flask is gently heated with a soft flame from the gas torch until the liquid alloy is formed. The glass-enclosed stirring bar is held against the side of the flask until the alloy cools to room temperature. Extreme care must be exercised during the heating operation since a crack in the flask would result in spontaneous ignition of the alloy.

A consequence of this characteristic is that a flask containing the alloy should never be allowed to lose its vacuum unless the alloy is covered with solvent. In this condition, the flask can be removed from the vacuum line for the decomposition of the residual alloy. The flask should be placed in a hood and the alloy destroyed by the addition of cold (dry-ice temperature) isopropyl alcohol. The reaction must be monitored until the decomposition is complete.

d. Preparation of Organolithium Purge Ampoule

The final step in the purification of hydrocarbon solvents and of diene and vinyl monomers is exposure to an organolithium. Butyllithium is used except for styrene. Fluorenyllithium is used for this mono-

mer. A flask is constructed with a sidearm constriction, to which is added an ampoule of organolithium. The apparatus is placed on the vacuum line and evacuated. The solution of organolithium is added to the flask by rupturing the breakseal. The solvent is then distilled away. Exposure of either solvent or monomer to the organolithium ensures eradication of the final vestige of any polymerization terminating impurity.

3. Preparation of Materials

From a practical standpoint it is necessary to delineate what is meant by pure materials. We are concerned with the removal from the various reaction components of any material capable either of carbanion deactivation or of influencing the reaction pattern of the polymerization. The exclusion of this latter class of impurities, e.g., polar compounds, is of importance in the polymerization of dienes since the intrusion of even trace amounts of certain polar species can alter the microstructure of the polydienes.

3.1. Solvent Purification

a. Tetrahydrofuran

This ether is stored over finely ground calcium hydride and stirred for several days on the vacuum line (fig. 3). After degassing, the ether is distilled, with the aid of a dry-ice-alcohol bath, over a succession of sodium mirrors (F) until the ether produces no visible degradation of the mirror at room temperature. The ether is again degassed and subsequently distilled into a flask (R), usually of one liter capacity, containing approximately one-quarter gram of biphenyl or naphthalene and one-half to one gram of sodium or potassium. The addition of the ether to the alkali metal and the organic aromatic species soon results in the formation of a dark blue (biphenyl) or dark green (naphthalene) solution. The excess alkali metal is necessary to ensure complete conversion of the aromatic to the complex since any unreacted aromatic will sublime in subsequent distillations of the ether.

When naphthalene is used, a dark red color may eventually develop in the solution. This is due to the reaction between the alkali metal naphthalene and an isomer of dihydronaphthalene [33]. Either 1,2- or 1,4-dihydronaphthalene may be generated by the reaction of water with the alkali metal naphthalene complex. The 1,2-isomer will polymerize to give an insoluble low molecular weight product while the 1,4-form will react with the alkali metal naphthalene but will not polymerize [34].

Measured quantities of ether can be flash-distilled as needed into an appropriately evacuated, calibrated, and weighed ampoule (A). The collection ampoule may be given a thin sodium film in order to ensure dryness. Shielding the collected ether from any ultraviolet radiant-energy source, including sunlight, should be practiced as a precaution against peroxide formation and other deleterious side reactions. This can best be accomplished by storing the ampoules in the refrigerator. Other ethers (dioxane, methyltetrahydrofuran, ethyl ether, etc.) can be processed by this procedure.

b. Benzene

This solvent is stored over sulfuric acid, with stirring, for at least one week. The material is then placed on the vacuum line (fig. 3) and degassed. The liquid is then distilled to flask (R) which contains the alloy of sodium and potassium. Stirring is then commenced and continued for 24 hr. After degassing, portions are distilled to a sodium mirror (F). From flask (F), the benzene can then be distilled to a flask containing butyllithium. The residence time of the benzene with the butyllithium is usually of several hours duration. Then measured quantities are collected in ampoule (A), as needed, or distilled directly into a reactor.

c. Toluene

Toluene is processed in a fashion similar to that used for benzene. The only difference is the deletion of the exposure to sulfuric acid. In its stead, the solvent is exposed to lithium alluminum hydride prior to treatment on the alkali metal alloy.

d. *n*-Hexane

The purification process for *n*-hexane is identical to that of benzene.

3.2. Monomer Purification

a. Styrene

Styrene is purified in a vacuum apparatus as follows. A flask (A), figure 4, is prepared containing a slurry of finely ground calcium hydride in styrene. The mixture is then throroughly pumped and degassed.

The contents ($\sim$ 100 to 150 cm^3) are then agitated by a magnetic stirrer for several days with periodic degassing. During this period, the viscosity of the mixture will increase slightly, indicative of the formation of a small amount of low molecular weight polymer. At the end of this treatment the styrene is distilled through the manifold into a chain flask where the monomer is circulated through a sodium coated bulk (B) and condensed in flask (D) by a dry-ice-isopropanol mixture. The sodium-coated bulb is formed by placing approximately 0.1 g of sodium into the side arm of the flask and gently melting the alkali metal. The metal vapor will then condense on the upper portion of the chain flask. This mode of monomer purification was developed by Hall [8] and Meier [22].

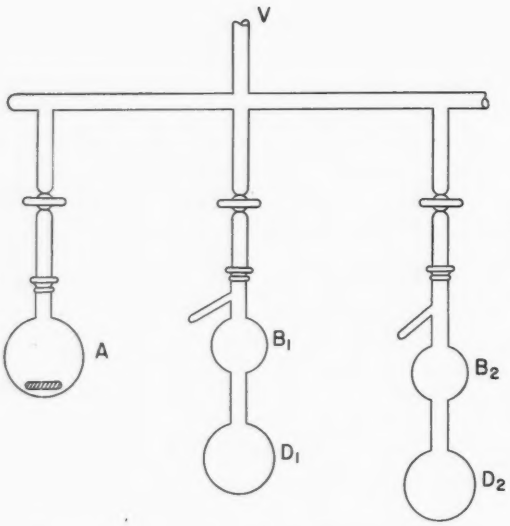

FIGURE 4. *Apparatus for the purification of styrene.*

The monomer is then distilled into several additional flasks prior to its final collection. Exposure to a minimum of three flasks is recommended. This procedure has proved to be adequate for reducing contaminants to low levels. However, if desired, the monomer may also be exposed to fluorenyllithium prior to final collection. Unlike butyllithium, this organolithium will not react with styrene [35]. Care must be exercised in the final collection step to ensure that residual fluorene does not sublime into the collection ampoule. This can be circumvented by distilling the monomer into a chain flask prior to the final collection.

b. α-Methylstyrene

This monomer can be purified by procedures similar to those used for styrene. Polymer formation during purification is negligible due to the low ceiling temperature of the monomer. Several separate exposures are sufficient to dry the monomer rigorously. After purification the monomer is collected and stored in a manner identical to styrene.

c. Isoprene

This diene lends itself to ready purification with the use of a high vacuum manifold as depicted in figure 5. The monomer is exposed in flask (R) to calcium hydride and stirred for 24 hr. The monomer is then degassed, with nitrogen used to freeze the monomer. The monomer is flash-distilled three times to flasks (F) which are coated with freshly sublimed sodium. The first distillation removes, as it does with the other monomers, any inhibitor. The monomer is then exposed to butyllithium at room temperature for 15 min or so. Finally, designated quantities of monomer are collected in ampoules (A), where final degassing is accomplished. The ampoules are sealed off, weighed, and stored at ~0 °C until used.

d. Butadiene

The section of the manifold used is fitted with a mercury column pressure release (P), as depicted in figure 5. The drying procedure is identical to that of isoprene. Due to the low boiling point (−4.4 °C) of butadiene, it is necessary to maintain the temperature at a low level with a dry-ice-alcohol bath.

3.3. Preparation of Organolithiums

a. *n*-Butyllithium

The apparatus used to prepare *n*-butyllithium is illustrated in figure 6. An amount of di-*n*-butylmercury sufficient to make up a one molar solution of organolithium is placed in a clean dry flask fitted with a standard-taper joint vacuum connection and a breakable seal. After the flask is degassed, dry *n*-hexane (50–75 ml) is distilled in, the contents are again degassed, and the flask is sealed off. This ampoule (S) is then sealed to the apparatus (R) as illustrated in figure 6. Lithium ribbon or wire with

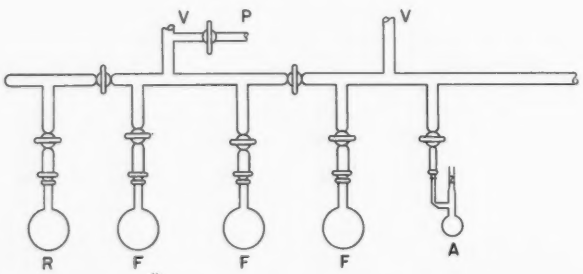

FIGURE 5. *Apparatus for the purification of diene monomers.*

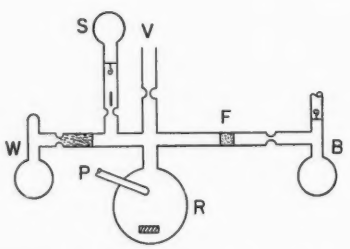

FIGURE 6. *Apparatus for the preparation of* n*-butyllithium.*

the petroleum coating intact is charged into (R), a reaction flask of about 300 cm^3 capacity, through (P) an open side arm; (P) is then sealed off. After pumping to high vacuum, 50 cm^3 or so of anhydrous hexane is distilled into (R) and degassed. After degassing, the apparatus is removed from the vacuum line and the contents of the flask (R) are stirred for several hours. The resultant solution of petrolatum in hexane is then decanted through a glass wool plug to (W). Clean hexane is then distilled back to (R) and the cycle repeated until the lithium surface is cleaned and all soluble residue removed from flask (R). Flask (W) is then removed by sealing off. The di-*n*-butylmercury-hexane mixture is then added to the lithium in (R) and stirring commenced at room temperature. At the end of the reaction period, usually of several week's duration, the *n*-butyllithium-hexane solution is transferred to (B) through a medium porosity fritted glass disk (F). (R) is rinsed several times by back-distillation in order to ensure a clean transfer. The content of (B) is divided into several ampoules having breakable seals. Analysis is made according to the method of Gilman [36, 37].

b. Isomers of Butyllithium

A vacuum modification of the method reported by Telalaeva and Kocheskov [38] is used for the preparation of the remaining isomers of butyllithium. The appropriate organo-chloride or bromide (*sec*-butyl, *iso*-butyl, or *t*-butyl) is placed under vacuum in a manner similar to that of the di-*n*-butylmercury. Reaction progress is accompanied by the formation of the lithium halide. After completion, the slurry is filtered and the solution collected in flask (B). This procedure has also been used by Hall [8] for the preparation of ethyllithium.

c. Fluorenyllithium

The preparation of fluorenyllithium for monomer purification is a modification of procedures presented elsewhere [39]. A reaction ampoule is constructed to which is attached a breakseal and a sidearm constriction. Attached to the sidearm constriction is an ampoule of *n*-butyllithium. The amount of fluorene added is always in slight excess (~ 5 mole %) of the added *n*-butyllithium. After thorough evacuation, about 75 cm^3 of dry benzene is distilled into the reactor and the reaction allowed to proceed until completion. Complete conversion of the *n*-butyllithium must be accomplished since any residual organolithium will react with styrene. After completion of the reaction, the fluorenyllithium is divided into ampoules for use.

d. Polyorganolithium "Seed" Preparation

It is now recognized [30, 40–48] that the reaction between organolithiums and unsaturated monomers is a relatively sluggish process in hydrocarbon media. It should be remembered that initiation is a one-step reaction whereas the growth of a chain involves a large number of consecutive addition steps. Hence, even if the individual initiation is somewhat slower than the individual propagation reaction, the actual formation of a chain may take considerably longer than the time required for complete initiation. However, if the initiation reaction is two or three orders of magnitude slower than propagation, then the two processes may become competitive.

The slowness of the initiation reaction results in a process in which the kinetics of initiation and propagation become rather complex [41–46]. The deciphering of the order of the initiation reaction in organolithium for these polymerizations has thus far proved to be highly troublesome. From a synthesis viewpoint, the simultaneous occurrence of the two reaction steps lead to relatively broad molecular weight distributions ($\overline{M}_w/\overline{M}_n$ 1.3–1.4) [49, 50]. This complex behavior results from, in part, the ability of the initiating organolithium to form associated species with itself [51] as well as with polymer-lithium [52]. Kinetic [30, 40–48, 53–55] and molecular weight measurements [47, 52–57] indicate that the various organolithium species participating in initiation and propagation form diverse associated species. The unambiguous assignment of the kinetic orders of the various processes and the elucidation of the association states of the various species and the nature of the reactive species, remain incomplete.[2]

The effect of slow initiation can be partially circumvented by using a two-stage polymerization method, i.e., a "seeding" technique. In this procedure, a small quantity of monomer and solvent are mixed in an ampoule with an appropriate amount of the initiating organolithium. The low molecular weight polyorganolithium is formed under conditions that are not practicable or convenient for the preparation of the high molecular weight polymer.

For the preparation of low molecular weight polystyryllithium, styrene (in benzene) is mixed with *n*-butyllithium and the reaction permitted to proceed at approximately 30 °C for 12 hr or so. It has been determined [30] that for complete conversion of *n*-butyllithium to polystyryllithium, the following must hold,

$$[M]_0[I]_0^{-4/3} \geqslant 504$$

where $[M]_0$ and $[I]_0$ are the initial monomer and organolithium concentrations, respectively. At the completion of the initiation reaction the value of $\overline{M}_n$, the number-average molecular weight, is

$$\overline{M}_n = \frac{\text{grams of monomer}}{\text{moles of initiator}}.$$

[2] For an interesting probe into this problem see T. L. Brown, J. Organometallic Chem. **5**, 191 (1966); Advance in Organometallic Chem. 3, Ed. by F. G. A. Stone and R. West, p. 365, Academic Press, New York, 1965.

223-178 O-66-4

This relation is valid since each of the monofunctional initiating organolithium molecules generates one polymer chain. The relatively broad distribution of the "seed" polystyryllithium is overshadowed by the great excess of additional polymerization where all growing chains have equal probability of growth.

It should be mentioned that polystyryllithium in benzene undergoes a slow isomerization reaction at elevated (~ 75 °C) temperatures [58]. This reaction was first noted by Szwarc [59] and co-workers for polystyrylsodium in tetrahydrofuran. Thus the "seed" preparation, as well as the polymerization reaction, should be accomplished at relatively mild temperatures.

The preparation of the polyisoprenyllithium "seed" can be carried out in a manner similar to that used for polystyryllithium. For this procedure *n*-hexane is used as the solvent. Complete conversion of *n*-butyllithium to polyisoprenyllithium can be accomplished as follows [42]. A solution of *n*-hexane and isoprene is made with an isoprene concentration of ~ 8 moles liter^{-1}. This is then mixed with an appropriate amount of *n*-butyllithium to yield a polymer with a number average molecular weight of $\sim 10{,}000$. The reaction is carried out at a temperature of 0 °C. This relatively mild temperature is used since the apparent energy of activation for initiation (~ 18 kg cal) has been found to be lower than for propagation (~ 22 kg cal) [40, 42]. These values lack their usual physical significance since they contain contributions from the heats of dissociation of the alkyllithium, polyisoprenyllithium, and the cross-associated species. Therefore, the initiation efficiency is found to increase at lower temperatures [42]. This is convenient from an experimental point of view, since it permits working at high monomer and initiator levels without fear of the exotherm becoming uncontrollable.

These conditions may also be applied for the formation of polybutadienyllithium. Evidence exists [40, 41] that the rate of initiation of butadiene is faster than that of isoprene under identical conditions. This, coupled with the fact that the apparent rate of propagation for butadiene is less than that of isoprene, greatly enhances the quantitative conversion of the *n*-butyllithium to polybutadienyllithium under the conditions outlined above.

It is of interest to record that the preparation of these low molecular weight polymeric-lithiums free from unreacted initiating organolithium, is facilitated by the substitution of *sec*-, *iso*-, or *t*-butyllithium for *n*-butyllithium. Kuntz [46] and Hsieh [41] have noted that these isomers are more efficient in initiating isoprene and butadiene than is *n*-butyllithium. Although no truly quantitative study of the relative apparent rates of initiation of these various isomers of butyllithium is currently available, the indication does exist that under the conditions outlined herein, replacement of *n*-butyllithium with one of the other isomers will result in a faster and more efficient "seed" preparation. The enhanced initiation rates appear to be due, in part, to the lower degrees of self-association exhibited by these isomers of butyllithium [60].

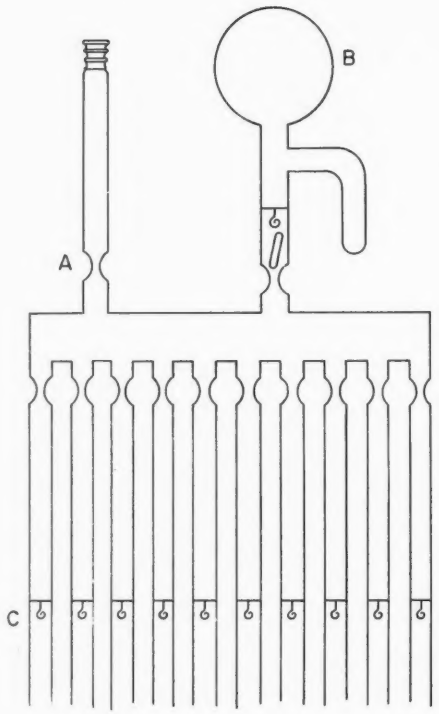

FIGURE 7. *Apparatus for subdivision of initiator solution.*

After completion of the "seed" preparation, the flask (B) containing the solution is sealed onto a manifold containing approximately 10 ampoules, as shown in figure 7. The manifold is then connected to the high-vacuum apparatus, evacuated, leak-tested, and flamed. After removal from the high-vacuum line by sealing the manifold off at the constriction (A), the breakseal of the "seed" solution is ruptured thus permitting the mixture to flow into the breakseal ampoules. Flask (B) is removed by sealing it off at the constriction which has been rinsed by refluxing solvent. The manifold is then inverted so that a uniform solution in all of the ampoules is achieved. The manifold is then allowed to stand for approximately 24 hr in order that each constriction has sufficient time to drain free of residual polymer. The refluxing of solvent onto the constrictions is not recommended since distillation of solvent among the ampoules will cause fluctuations in the lithium concentration. The same procedure is used for the dilution of the initiating organolithiums.

The determination of the lithium content is carried out as follows. The volume of solution in the 12 mm diamater sealed breakseal tubes is estimated by a comparison with a similar tube which is calibrated in 1 ml increments. A more accurate measure can be obtained, after use of the solution, by titration of the used

ampoule by means of a 10 ml micro-buret. After the volume of the sample is determined, the decomposed organolithium is titrated with either 0.01 *N* or 0.1 *N* hydrochloric acid to a phenolphthalein end point. For the polymeric-lithium, the titration is carried out in a neutralized solution (1/1 by volume) of methanol and water. This prevents the coagulated polymer from absorbing either indicator or lithium hydroxide. Two ampoules from each batch are titrated in this manner to determine the lithium content per cubic centimeter of solution. It is also recommended that the Gilman double titration procedure [36,37] be employed on occasion to ascertain the concentration of noninitiating lithium compounds in solution.

4. Polymerization Procedures

The procedures outlined in the following will apply, in the main, to all of the monomers covered herein. Where applicable, the necessary variations will be listed in the appropriate place. To perform an experiment, the various ampoules are sealed onto a reactor, figure 8, in such a manner that the separate components can be conveniently added to the reaction mixture while maintaining a closed system. A vacuum line (V) consisting of a standard-taper ground-glass joint at one end and a constriction at the other is also attached to the reactor vessel in a position that will evenly support the weight of the reactor. The vacuum line is the sole connection and, in many instances, the only support holding the reactor to the vacuum system. It is therefore imperative that the weight of the reactor and its components be well balanced. The respective ampoules pictured contain monomer (M), solvent (S), initiator (I), and terminator (T). A glass wool plug, previously washed with THF, is placed above the constriction of ampoule (S) to provide a filter for any sodium particles which might be carried from the mirror on which the solvent is stored. For most cases the terminator may consist of several drops of well-degassed water or methanol. Sampling ampoules (1) and (2) may be added to (R) if desired.

Once the reactor is assembled as shown in figure 8, it is connected to the high-vacuum apparatus by means of the ground-glass joint on the vacuum tube and evacuated. After several minutes, the reactor is tested with a Tesla coil for pinholes or cracks, especially in the area where the component parts are sealed on. If no pinholes are found, or after those that are found are sealed, the reactor is evacuated until a pressure of 10^{-6} mm Hg is obtained. All of the glass surfaces, except the ampoules containing the reaction ingredients, are flamed strongly with a yellow-blue flame from a hand torch. The reactor is continuously under evacuation during this procedure. After 1 hr or so the vacuum is again checked, and if a pressure of 10^{-6} mm Hg is obtained, the reactor is sealed off from the high-vacuum line at the constriction.

Prior to the addition of the reactants, the reactor is purged, on occasion, by an additional ampoule of dilute butyllithium. This solution is removed in ampoule (1).

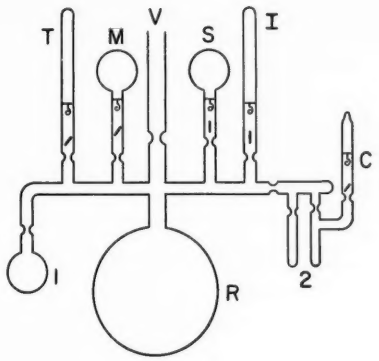

FIGURE 8. *Polymerization reactor.*

This procedure is used when very large reactors and small initiator charges are employed. However, care must be taken to thoroughly rinse the system free from any traces of the purge catalyst. Fluorenyllithium may also be used as a purge organolithium.

The solvent and initiator are introduced and the initiator ampoule is rinsed by refluxing solvent. The mixture is then allowed to come to the desired reaction temperature and the monomer is added. The monomer generally comprises from 10 to 20 percent by volume, with 5 to 20 g being a typical charge. All empty ampoules are then removed by sealing off at the respective constrictions. The exact volume of initiator used can then be determined by sealing the ruptured breakseal and titrating to the previously applied mark. If desired, samples may be removed at (2) in order to analyze for the active lithium content of the solution by means of the Gilman double titration. Ampoule (C) contains a THF solution of benzyl chloride, allyl bromide, or 1,2-dibromoethane used in this analysis.

For the styrene polymerization (in benzene or toluene), a procedure may be used which can circumvent the slow initiation reaction. Several workers [22,61] have investigated the effect of small quantities of tetrahydrofuran on the initiation and propagation reactions of styrene in benzene. It was noted that with small concentrations of the ether ([THF]=[BuLi]), the initiation reaction becomes very rapid, i.e., too fast to be measured by the optical methods usually used [30,61] in studies of this system. These characteristics are of value from a synthesis standpoint since it is possible now to prepare samples of monodisperse, low molecular weight (~ 1000) polystyrene [14,62]. The propagation reaction changes its rate in a rather complex fashion with variations in the THF concentration at a constant concentration of butyllithium. These results [22,61] have been tentatively explained on the basis of solvation of the active species

with the ether. It would appear that the changes in carbanion reactivity are due to the formation of peripherally solvated and solvent-separated ion-pairs. This change in reactivity is a further demonstration of the sensitivity and susceptibility of carbanions to subtle environmental changes.

The use of the ether in the concentration mentioned above eliminates the relatively long period of initiation but does not appreciably alter the rate of the propagation reaction [22,61]. This results in an easily controllable polymerization in benzene at moderate (~ 30 °C) temperatures. Also, this low ratio of ether to organolithium rules out the possibility of any extensive reaction between THF and the organolithium [8,63,64].

In this procedure the measured quantity of ether is added immediately after the addition of monomer. The solution will then turn bright red within several seconds. Only small amounts of ether are required, i.e., [THF]/[BuLi]=1 to 10. After thorough mixing, the polymerization is allowed to proceed at the desired temperature (0 to 30 °C). Depending upon temperature, initiator concentration, and ether concentration, complete conversion can be attained from 15 min to 8 hr.

Atactic polystyrene is prepared [65] under the conditions outlined above. It has been reported [66–68] that polystyrene resulting from organolithium-initiated polymerizations in nonpolar solvents (toluene) at low (-20 to -40 °C) temperatures contains a substantial fraction of crystallizable polymer. The presence of any polar material prevents stereoregularity. The crystallizable portion has been identified as isotactic material. It was shown [69] that the formation of the isotactic material was due entirely to the presence of lithium hydroxide, the formation of which was due to the presence of moisture in the reaction mixture. Polystyrene prepared under anhydrous conditions is predominately syndiotactic [69]. Elevation of the reaction temperature above 0 °C results in the production of atactic material.

In connection with this point, it has been reported [70] that the presence of lithium methoxide in the *n*-butyllithium-initiated polymerization of methyl methacrylate enhances the rate of propagation, increases slightly the amount of isotactic polymer, and facilitates the formation of high molecular weight material. The presence of lithium ethoxide or lithium butoxide increases the rate of initiation of isoprene [42,47]. A possible explanation for this is given by Brown [71]. Brown has shown that lithium ethoxide forms a soluble complex with ethyllithium, presumably through the unshared pair of electrons on the oxygen atom. It is therefore possible that these lithium salts can associate or complex with the normal organolithium ion-pair. Their presence may also promote the dissociation of the associated organolithium, as do traces of ethers. In any case, the infiltration of these lithium salts can alter the reactivity of an active organolithium and influence the mode of monomer addition. These findings emphasize the necessity of obtaining a stringently pure system and of maintaining a static reaction environment.

The polymerization of α-methylstyrene is carried out in tetrahydrofuran at -78 °C. This low temperature is necessary since the formation of high polymer is thermodynamically unfavorable at higher temperatures [72,73]. Mixing and initiation are carried out at room temperature. At this temperature, initiation will occur without the formation of high polymer. The *n*-butyllithium should be added to the monomer-ether solution in order to retard the reaction [63] between the ether and the organolithium. The reactor is then placed in a dry-ice-alcohol bath and the contents swirled for 10 min or so while the mixture is cooling. Complete conversion usually occurs in 24 hr [74].

The polymerization of dienes is readily accomplished in hexane at temperatures ranging from 0 to 30 °C. The use of THF to circumvent the "seed" preparation is avoided since the microstructure of these dienes is altered by trace amounts of polar compound [47, 56,57,75].

Polyisoprene prepared in pure hydrocarbon media is structurally a close counterpart to Hevea rubber. The cis-1,4 enchainment is enhanced if the organolithium concentration is of the order of 10^{-3} to 10^{-4} moles liter^{-1} and the reaction temperature remains in the vicinity of 0 °C [75]. Under these conditions, several days are necessary for the attainment of complete conversion. Polybutadiene microstructure appears to be moderately dependent on reaction temperature and initiator concentration [76,77]. Generally a polymer with 10 percent vinyl, 40 percent cis-1,4, and 50 percent trans-1,4 content is obtained.

On termination of the polydienyllithium species, a marked decrease in solution viscosity will occur. This is due to the association which the active chain ends undergo [30,47,53–57]. It is advisable to maintain the samples under vacuum at ~ 0 °C so as not to impair their structural integrity.

In conjunction with this point, it is pertinent to note that a small amount of branched material, in contradistinction to the claims of others [23,24], is formed during the polymerization of butadiene [22,56]. This appears to be due to the susceptibility of the vinyl group to attack by an organolithium. At high molecular weights ($\sim 10^6$), gel has been observed [56] to form. This behavior is parallel to the branching and gelation encountered in the sodium- or potassium-initiated polymerization of butadiene [78]. The formation of branched material is retarded by carrying out the polymerization at 0 °C. At this temperature, at least several days are necessary for complete conversion.

The measurement of viscosity is a convenient mode of determining the molecular weight of polymers prepared by these homogeneous anionic polymerization techniques. Values for K and α for several polymer-solvent pairs have been published; polystyrene [13,14], poly-α-methylstyrene [17], polyisoprene [20,] and polybutadiene [23,24].

The retention of chain end activity of these polyorganolithiums has many important ramifications from the standpoint of opportunities to synthesize polymers

of novel architecture, i.e., branched macromolecules. Morton [79] and Wenger [80,81] have synthesized tri- and tetra-functional "star" macromolecules from linear monodisperse polystyrene joined at one end through a common junction. Similar star species were created from polybutadiene [82]. Interesting viscosity studies have been performed on bulk and dilute constellations of these composite polymers. Trichloromethylsilane [82], silicon tetrachloride [79,82], 1,2,4-tri and 1,2,4,5-tetrachloromethylbenzene [14,80,81] have been utilized as coupling agents.[3] Branched polymers of the "comb" type have also been synthesized by coupling polystyryllithium to a partially chloromethylated polystyrene backbone [81] and by reacting acrylonitrile with poly-*p*-lithostyrene [83]. Yen [15] has used a tetrahydrofuran solution of α-phenylethylpotassium to prepare virtually monodisperse polystyrene and star species. Utilization of the polystyrylpotassium carbanion results in a more efficient preparation of a star macromolecule, ascribable, in part, to the absence of any metal-halogen interconversion. Szwarc [84] has also outlined several ingeneous procedures by which star- and comb-shaped polymers might be synthesized.

An additional consequence of these systems is that linear block copolymers can be prepared by the selected addition of monomer according to a preconceived plan. After the complete conversion of monomer A, monomer B is added to the solution and polymerization again ensues. In this fashion, precise control is afforded over the number, sequence, and length of the blocks. Polymers can thus be produced having blocks of elastomeric and nonelastomeric segments.

An example of this type of polymerization is the preparation of a polystyrene-polyisoprene-polystyrene block copolymer. A polymer with good elastomeric properties is obtained when the segment molecular weights are about 10,000–50,000–10,000. These elastomers exhibit the high gum tensile strength of at least 3500 psi at an elongation of 1100 percent. The elastomeric properties of this composite macromolecule arise from the agglomeration of the glassy polystyrene segments. Hence, these aggregates act as cross-links.

Since participation in the network by a chain is dependent upon the diene unit having polystyrene segments at each end, it is important that the initiation reaction be accomplished as rapidly as possible. It is particularly important that no butyllithium be present at the cessation of the first styrene polymerization. The residual butyllithium would eventually react with isoprene and subsequently form an elastomerically ineffective chain. The slow initiation step is eliminated by the addition of a tertriary amine or anisole in amounts equal to the concentration of butyllithium. Initiation is thus completed in several minutes. The presence of either of these two components does not alter, to any detectable degree, the diene microstructure [85].

After depletion of the styrene, the desired amount of isoprene is added and polymerization again ensues. In hydrocarbon media, the rate of reaction of isoprene with a styryllithium polycarbanion is rapid [86]. Hence no problem similar to the slow *n*-butyllithium-monomer reaction is encountered. Following the complete incorporation of the diene, the desired amount of styrene is then added. Since the reaction of a dienyllithium with styrene is a relatively slow process, the addition of a trace amount of tetrahydrofuran is desirable to expedite the crossover step. In this fashion it is possible to prepare a copolymer with virtually monodisperse segments of any degree of polymerization. Butadiene can, of course, be used in lieu of isoprene. Copolymers with polybutadiene as the interior segment have achieved commercial importance as thermoplastic elastomers.

Table 1 lists some block copolymers. Many of these copolymers were prepared so as to compare their dynamic mechanical properties and thermal stability with those of random copolymers and mechanical blends of similar composition.

The selective termination of these polycarbanions permits the introduction of specialized functional groups at the ends of the chains. When the polymers in question possess two active sites, it is possible to form bifunctional macromolecules which may then be applied to further synthetic work. The addition of carbon dioxide to a solution of polycarbanions generates, after hydrolysis, chains with carboxylic endgroups [97–100]. Carboxyl terminated polystyrene is obtained by reacting the carbanion ends with succinic or phthalic anhydride [101]. Reaction with ethylene oxide introduces hydroxylic endgroups [93,99,102]. The introduction of terminal double bonds is effected by the addition of allyl chloride or allyl bromide to an ether solution of polystyrylsodium [101]. Terminal primary amine endgroups can also be added. This procedure consists of reacting *p*-aminoethyl benzoate with polystyrylsodium carbanions [103]. Michlers ketone also reacts quantitatively with polystyrylsodium carbanions [104–105].

These polymeric species have been utilized in a variety of ways. For example, polybutadiene with two hydroxylic groups may be reacted with an appropriate coupling agent, e.g., a trifunctional isocyanate, to yield an elastomeric network. This procedure unveils possibilities for novel applications in casting and molding polymers. Solid rocket fuel binders are one example of cast elastomers.

Cyclohexadiene [106] may, under the appropriate conditions, be polymerized to yield monodisperse rubber. The polymerization of methyl methacrylate by organolithium compounds [107] is kinetically complex and yields polydisperse polymer. Much of this complexity is the result of reaction of the organolithium reagents with the carbonyl group. Monodisperse poly(methyl methacrylate) has been prepared in tetrahydrofuran at -75 °C by sodium biphenyl initiation [108]. The susceptibility of this monomer to electron transfer initiation was described earlier [109,110].

[3] The formation of star polymers with more than four chains per molecule has been reported. T. Altures, Jr., D. P. Wyman, V. R. Allen, and K. Meyersen, J. Polymer Sci. **3A**, 4131 (1965); J. Gervasi and A. B. Gosnell, J. Polymer Sci. **4A-1**, 1391 (1966).

TABLE 1. *Summary of block copolymers prepared in anionic polymerization*

Monomer A	Monomer B	Initiator	Solvent	Sequence	Ref.
Styrene	Isoprene	Na-naphthalene	THF	$B_yA_xB_y$ $A_xB_yA_x$ $A_x(B_yA_xB_y)_2$ $B_y(A_xB_yA_xB_y)_2$	2, 87
Styrene	Isoprene	Cs-naphthalene	THF	$B_yA_xB_y$	88
Styrene	Isoprene	*n*-butyllithium	Hexene and benzene	A_xB_y and B_yA_x	89
Styrene	Methyl-methacrylate	Na-naphthalene	THF	$B_yA_xB_y$	90
Styrene	Methyl-methacrylate	Phenylisopropyl-K	THF	A_xB_y	91
Styrene	Methyl-methacrylate	Na-naphthalene	Dimethoxyethane	$B_yA_xB_y$	92
Styrene	α-methylstyrene	Na-naphthalene	Dimethoxyethane	$B_yA_xB_y$ $A_xB_yA_x$	
Styrene	Ethylene oxide	Na-naphthalene	Dimethoxyethane	$B_yA_xB_y$	92
Styrene	Ethylene oxide	α-methylstyryl-Na	THF	$B_yA_xB_y$	93
Styrene	Octamethylcyclotetrasiloxane	Styryl-K K-naphthalene	THF	$B_yA_xB_y$	94
Isoprene	Octamethylcyclotetrasiloxane	Isoprenyl-K K-naphthalene	THF	$B_yA_xB_y$	94
Ethylene oxide	*n*-Butyl isocyanate*	Na-biphenyl	Toluene (1% THF)	$B_yA_xB_y$	85
Styrene	*n*-Butyl isocyanate	Na-biphenyl	Toluene (2% THF)	$B_yA_xB_y$	85
		n-butyllithium	Toluene (1% THF)	A_xB_y	
α-methylstyrene	*n*-Butyl isocyanate	Na-biphenyl	Toluene (10% THF)	$B_yA_xB_y$	
		n-butyllithium	Toluene (10% THF)	A_xB_y	
Isoprene	*n*-Butyl isocyanate	*n*-butyllithium	Toluene	A_xB_y	
Methyl-methacrylate	*n*-Butyl isocyanate	Na-biphenyl	Toluene (10% THF)	$B_yA_xB_y$	
		α-phenylethyl-K	Toluene (10% THF)	A_xB_y	
Acrylonitrile	*n*-Butyl isocyanate	Na-biphenyl	Toluene (10% THF)	$B_yA_xB_y$	
		α-phenylethyl-K	Toluene (10% THF)	A_xB_y	
Vinyl cyclohexane	Butadiene	*n*-butyllithium	Benzene	$A_xB_yA_x$	85
Styrene	Butadiene or Isoprene	*n*-butyllithium	Benzene	$A_xB_yA_x$	85
α-methylstyrene	Formaldehyde	Na-naphthalene	THF	$B_yA_xB_y$	95
Styrene	Formaldehyde	Na-naphthalene	THF	$B_yA_xB_y$	
Isoprene	Formaldehyde	Na-naphthalene	THF	$B_yA_xB_y$	
Butadiene	Formaldehyde	Na-naphthalene	THF	$B_yA_xB_y$	
2-Methyl-5-vinyl pyridine	Formaldehyde	Na-naphthalene	THF	$B_yA_xB_y$	

In the toulene-THF mixtures the amount of THF is expressed in volume percent.
*Poly-(*n*-butyl)isocyanate has been characterized as a rigid rod [96].

The presence of transfer reactions prohibits the preparation of monodisperse polymer from acrylonitrile or methacrylonitrile [111–114].

The guidance in years past of Dr. E. E. Bostick is gratefully recalled.

5. References

[1] M. Szwarc, Nature **178,** 1168 (1956).
[2] M. Szwarc, M. Levy, and R. Milkovich, J. Am. Chem. Soc. **78,** 2656 (1956).
[3] P. J. Flory, J. Am. Chem. Soc. **62,** 1561 (1940).
[4] R. Waack, A. Rembaum, J. D. Coombes, and M. Szwarc, J. Am. Chem. Soc. **79,** 2026 (1957).
[5] H. McCormick, J. Polymer Sci. **36,** 341 (1959).
[6] F. Wenger, Makromoleculare Chem. **36,** 200 (1960); **64,** 151 (1963).
[7] M. Morton, R. Milkovich, D. McIntyre, and L. J. Bradley, J. Polymer Sci. **1A,** 443 (1963).
[8] M. Morton, A. A. Rembaum, and J. L. Hall, J. Polymer Sci. **1A,** 461 (1963).
[9] T. Lyssy, Helv. Chim. Acta. **42,** 2245 (1959).
[10] H.-J. Cantow, Makromoleculare Chem. **30,** 169 (1959).
[11] G. Meyerhoff, Z. physik Chem. (Frankfurt) **23,** 100 (1960).
[12] F. M. Bower and H. W. McCormick, J. Polymer Sci. **1A,** 1749 (1963).
[13] J. M. G. Cowie, D. J. Worsfold, and S. Bywater, Trans. Faraday Soc. **57,** 705 (1961).
[14] T. Altares, D. P. Wyman and V. R. Allen, J. Polymer Sci. **2A,** 4533 (1964).
[15] S.-P. S. Yen, Makromoleculare Chem. **81,** 152 (1965).
[16] H. McCormick, J. Polymer Sci. **41,** 327 (1959); F. Wenger J. Am. Chem. Soc. **82,** 4281 (1960); Makromoleculare Chem. **37,** 143 (1960).
[17] A. F. Sirianni, D. J. Worsfold, and S. Bywater, Trans. Faraday Soc. **55,** 2124 (1959).
[18] M. Morton, E. E. Bostick, and R. G. Clarke, J. Polymer Sci. **1A,** 475 (1963).
[19] N. Calderon and K. W. Scott, J. Polymer Sci. **3A,** 551 (1965).
[20] W. H. Beattie and C. Booth, J. Appl. Polymer Sci. **7,** 507 (1963).
[21] S. E. Bresler, A. A. Korotkov, M. I. Mosevitsky, and I. Ya. Poddubnyi, Zhur. Tech. Fiz. **28,** 114 (1958).
[22] J. F. Meier, Ph.D. Dissertation, University of Akron, 1963.
[23] H. Hsieh, J. Polymer Sci. **3A,** 191 (1965).
[24] J. T. Gruver and G. Kraus, J. Polymer Sci. **2A,** 797 (1964); **3A,** 105 (1965).
[25] M. Morton and E. E. Bostick, J. Polymer Sci. **2A,** 523 (1964).
[26] W. T. Grubb and R. C. Osthoff, J. Am. Chem. Soc. **77,** 1405 (1955).
[27] C. Geacintov, J. Smid, and M. Szwarc, J. Am. Chem. Soc. **84,** 2508 (1962).
[28] D. N. Bhattacharyya, C. L. Lee, J. Smid, and M. Szwarc, Polymer **5,** 54 (1964).
[29] M. Szwarc and M. Litt, J. Phys. Chem. **62,** 568 (1958).
[30] D. J. Worsfold and S. Bywater, Can. J. Chem. **38,** 1891 (1960).
[31] B. D. Coleman, F. Gornick, and G. Weiss, J. Chem. Phys. **39,** 3233 (1963).
[32] B. J. Mair, D. J. Termini, C. B. Willingham, and F. D. Rossini, J. Res. NBS **37,** 229 (1946) RP1744.
[33] N. D. Scott and J. F. Walker, Ind. Eng. Chem. **32,** 312 (1940).
[34] L. A. Wall, L. J. Fetters and S. Straus, Polymer Preprints **6,** 930 (1965).

[35] R. K. Graham, D. L. Dunkelburger and W. E. Goode, J. Am. Chem. Soc. **82,** 400 (1960).
[36] H. Gilman and A. H. Haubein, J. Am. Chem. Soc. **66,** 1515 (1944).
[37] H. Gilman and F. K. Cartledge, J. Organometallic Chem. **2,** 447 (1964).
[38] T. V. Talalaeva and K. A. Kocheskov, Zhur. Obshchei Khim. **23,** 392 (1953); J. Gen. Chem. U.S.S.R. (Engl. trans.) **23,** 399 (1953).
[39] H. Gilman and R. D. Gorsich, J. Org. Chem. **23,** 550 (1958); A. G. Evans and N. H. Rees, J. Chem. Soc. 6039 (1963).
[40] M. Morton, E. E. Bostick, R. A. Livigni and L. J. Fetters, J. Polymer Sci. **1A,** 1735 (1963).
[41] H. Hsieh, J. Polymer Sci. **3A,** 163 (1965).
[42] G. L. Taylor, Ph.D. Dissertation, University of Akron, 1964.
[43] J. L. Hall, Ph.D. Dissertation, University of Akron, 1962.
[44] R. C. P. Cubbon and D. Margerison, Proc. Roy. Soc. **268A,** 260 (1962).
[45] G. C. East, P. F. Lynch, and D. Margerison, Polymer **4,** 139 (1963).
[46] I. Kuntz, J. Polymer Sci. **2A,** 2827 (1964).
[47] D. J. Worsfold and S. Bywater, Can. J. Chem. **42,** 2884 (1964).
[48] H. Hsieh, J. Polymer Sci. **3A,** 153, 173 (1965).
[49] L. Gold, J. Chem. Phys. **28,** 91 (1957).
[50] E. Bauer and M. Magat, J. Chim. Phys. **47,** 841 (1950).
[51] D. Margerison and J. P. Newport, Trans. Faraday Soc. **59,** 2058 (1963).
[52] L. J. Fetters, Ph.D. Dissertation, University of Akron, 1962.
[53] L. J. Fetters, J. Res. NBS **69A** (Phys. and Chem.) No. 2, 159 (1965).
[54] B. Francois, V. Sinn, and J. Parrod, J. Polymer Sci. **4C,** 375 (1964).
[55] H. Sinn, C. Lundborg, and O. T. Onsager, Makromoleculare Chem. **70,** 222 (1964).
[56] M. Morton and L. J. Fetters, J. Polymer Sci. **2A,** 3311 (1964).
[57] M. Morton, L. J. Fetters, and E. E. Bostick, J. Polymer Sci. **1C,** 311 (1963).
[58] S. Gadkary, Ph.D. Dissertation, University of Akron, 1963.
[59] G. Spach, M. Levy, and M. Szwarc, J. Chem. Soc. 355 (1962); M. Levy, M. Szwarc, S. Bywater, and D. J. Worsfold, Polymer **1,** 515 (1960).
[60] M. A. Weiner, G. Vogel, and R. West, Inorganic Chem. **1,** 654 (1962).
[61] S. Bywater and D. J. Worsfold, Can. J. Chem. **40,** 1564 (1962).
[62] L. J. Fetters, L. A. Wall, and S. Straus, unpublished results.
[63] A. A. Rembaum, S.-P. S. Yen, and N. Indictor, J. Polymer Sci. **56,** S17 (1962).
[64] L. J. Fetters, J. Polymer Sci. **2B,** 425 (1964).
[65] F. A. Bovey and G. V. D. Tiers, Advances in Polymer Sci. **3,** 139 (1963).
[66] R. J. Kern, Nature **187,** 410 (1960).
[67] D. Braun, W. Betz, and W. Kern, Makromoleculare Chem. **42,** 89 (1960).
[68] R. J. Kern, Polymer Preprints **4,** No. 2, 324 (1963).
[69] D. J. Worsfold and S. Bywater, Makromolekulare Chem. **65,** 245 (1963).
[70] D. M. Wiles and S. Bywater, J. Phys. Chem. **68,** 1983 (1964).
[71] T. L. Brown, J. A. Ladd, and G. N. Newman, J. Organometallic Chem. **3,** 1 (1965).
[72] H. McCormick, J. Polymer Sci. **25,** 488 (1957).
[73] D. J. Worsfold and S. Bywater, J. Polymer Sci. **26,** 299 (1957).
[74] D. J. Worsfold and S. Bywater, Can. J. Chem. **36,** 1141 (1958).
[75] R. S. Stearns and L. E. Forman, J. Polymer Sci. **41,** 381 (1959).
[76] I. Kuntz and A. Gerber, J. Polymer Sci. **42,** 299 (1960).
[77] H. Hsieh, J. Polymer Sci. **3A,** 181 (1965).
[78] I. Ya. Poddubnyi and E. G. Erenburg, Vysokomol. Soed. **2,** 1625 (1960); Rubber Chem. Tech. **34,** 975 (1961).
[79] M. Morton, T. E. Helminiak, S. D. Gadkary, and F. Bueche, J. Polymer Sci. **57,** 471 (1962).
[80] T. A. Orofino and F. Wenger, J. Phys. Chem. **67,** 566 (1963).
[81] F. Wenger and S.-P. S. Yen, Polymer Preprints **3,** [1] 162 (1962).
[82] R. P. Zelinski and C. F. Wofford, J. Polymer Sci. **3A,** 93 (1965).
[83] M. B. Huglin, Polymer **5,** 135 (1964).
[84] M. Szwarc, Makromoleculare Chem. **35,** 132 (1960).
[85] L. J. Fetters, unpublished results.
[86] M. Morton, chap. VII in G. E. Ham, ed., Copolymerization (Interscience Publishers, New York N.Y., 1964); S. Bywater, Advances in Polymer Sci. **4,** 66 (1965).
[87] S. Schlick and M. Levy, J. Phys. Chem. **64,** 883 (1960).
[88] A. Rembaum, F. R. Ells, R. C. Morrow, and A. V. Tobolsky, J. Polymer Sci. **61,** 155 (1962).
[89] A. A. Korotkov, L. A. Shibayov, L. M. Pyrakov, V. G. Aldoshin, and S. Ya. Fenkel, Vysokomol. Soed. **1,** 443 (1959).
[90] R. K. Graham, D. L. Dunkelberger, and E. S. Cohn, J. Polymer Sci. **42,** 501 (1960).
[91] D. Freyss, P. Remp, and H. Benoit, J. Polymer Sci. **2B,** 217
[92] M. Baer, J. Polymer Sci. **2A,** 417 (1964).
[93] D. H. Richards and M. Szwarc, Trans. Faraday Soc. **55,** 1644 (1959).
[94] M. Morton, A. A. Rembaum, and E. E. Bostick, J. Appl. Polymer Sci. **8,** 2707 (1964).
[95] K. Nore, H. Kawazura, T. Moriyama, and S. Yoshika, Makromolekulare Chem. **83,** 35 (1965).
[96] H. Yu, A. J. Bur, and L. J. Fetters, J. Chem. Phys. **44,** 2568 (1966); L. J. Fetters and H. Yu, Polymer Preprints **7,** 443 (1966).
[97] C. A. Uraneck, H. L. Hsieh, and O. G. Buck, J. Polymer Sci. **46,** 535 (1960).
[98] H. Brody, D. H. Richards, and M. Szwarc, Chem. Ind. (London) **45,** 1473 (1958).
[99] E. Schoenberg, J. Polymer Sci. **49,** S9 (1961).
[100] D. P. Wyman, V. R. Allen, and T. Altares, Jr., J. Polymer Sci. **2A,** 4545 (1964).
[101] P. Rempp and M. H. Loucheux, Bull. Soc. Chim. 1497 (1958).
[102] E. J. Goldberg, U.S. Patent 3,955,952 Sept. 25, 1962; Chem. Abstr. **58,** 645f (1963).
[103] M. H. Loucheux, G. Mayer, and P. Rempp, Compt. Rend. **252,** 2552 (1961).
[104] J. Trotman and M. Szwarc, Makromolekulare Chem. **37,** 39 (1960).
[105] D. Braun and W. Fischer, Makromolekulare Chem. **85,** 155 (1965).
[106] F. Dawans, J. Polymer Sci. **2A,** 3297 (1964).
[107] D. M Wiles and S. Bywater, Trans. Faraday Soc. **61,** 150 (1965).
[108] A. Rogi, J. E. Figueruelo, and E. Liano, J. Polymer Sci. **3B,** 171 (1965).
[109] A. V. Tobolsky and D. B. Hartley, J. Am. Chem. Soc. **84,** 1391 (1962).
[110] M. Szwarc and A. Rembaum, J. Polymer Sci. **22,** 189 (1956).
[111] A. Tsukamoto, J. Polymer Sci. **3A,** 2767 (1965).
[112] A. Zilkha, B.-A. Feit, and M. Frankel, J. Polymer Sci. **49,** 231 (1961).
[113] C. G. Overberger, E. M. Pearce, and N. Mayes, J. Polymer Sci. **34,** 109 (1959).
[114] P. Rempp, Polymer Preprints **7,** 141 (1966).

(Paper 70A5–414)

JOURNAL OF RESEARCH of the National Bureau of Standards—A. Physics and Chemistry
Vol. 70A, No. 5, September–October 1966

The Configurations $4d^n + 4d^{n-1}\,5s$ in Doubly-Ionized Atoms of the Palladium Group*

Yehuda Shadmi

The Hebrew University of Jerusalem, Jerusalem, Israel

(June 17, 1966)

Four hundred and eighty-three energy levels belonging to the low even configurations of the third spectra of the palladium group are predicted by the use of interpolation formulas for the interaction parameters.

Key Words: Configurations $4d^n + 4d^{n-1}\,5s$, energy levels, interaction parameters, palladium group, theoretical, third spectra.

1. Introduction

In the present paper we describe a systematic treatment of the low even configurations of the sequence [1] of the third spectra of the palladium group. This treatment is analogous to the treatments of the second spectra of the iron group [1],[2] the second spectra of the palladium group [2], and the third spectra of the iron group [3] described in three previous papers.

The approximation used in this work is, as in the the previous papers, the Slater approximation with several improvements. We have included the interaction between the configurations $4d^n$, $4d^{n-1}5s$, we have taken different values for the corresponding parameters B, C and α of the two configurations, we have considered the L(L + 1) correction as well as the spin-orbit interaction.

The main stages of this treatment are the following:

(a) The Slater approximation, improved by the above mentioned corrections, is used to calculate the energy levels of each spectrum. After diagonalizing ("Diag.") the energy matrices, the interaction-parameters are considered as free parameters and the best fit to the experimental material is achieved by least-squares calculations ("L.S."). We call this stage "the separate treatment."

(b) The corresponding interaction-parameters of all the spectra of the sequence are expressed as linear functions (in some cases, with a small quadratic correction) of the atomic number. Only the coefficients of these interpolation formulas ("general parameters") retain the role of free parameters. Thus, the whole sequence, containing several hundreds of energy levels, is treated as a single problem ("general treatment") with quite a small number of free parameters.

In the sequence from Y III to Cd III, theory predicts, for the configurations $4d^n + 4d^{n-1}5s$, 209 terms which split into 483 levels. Unfortunately, the experimental material is rather scarce. Only 56 terms splitting into 130 levels were found reliable and could be fitted with the calculated levels. In most spectra the number of known terms does not exceed the number of electrostatic-interaction parameters; thus, a separate treatment of one spectrum loses a great deal of its significance. Such separate treatments were performed only as an introduction to the interpolative treatment, which is rather reliable even in this case, since the number of parameters is reduced by the use of interpolation formulas for them.

In the following, we shall first give an account of the situation and the separate calculations in the various spectra, and then describe the general treatment.

Most of the experimental material used in this paper was taken from Moore's Atomic Energy Levels, [4] later referred to as AEL. Unless other sources are explicitly mentioned, it means that the experimental matter was taken from AEL.

2. Notations

The symbols for the parameters are the usual ones. The parameters A, B, C, ζ refer to the configuration d^n, while A′, B′, C′, ζ' refer to the configuration $d^{n-1}s$.

In the actual calculations of the separate treatment A′ was replaced by S′ = A′ − A. In the general treatment A and A′ were replaced by the centers of gravity of the configurations, M and M′, and the difference D′ = M′ − M was expressed by an interpolation formula like the interaction parameters.

The parameter $G = G_2(ds)$ measures the exchange interaction between d and s electrons, $H = R^2(dd, ds)/35$ is the parameter of the interaction between the configurations d^n and $d^{n-1}s$, and α is the parameter of the L(L + 1)-correction.

*An invited paper. This paper was partially supported by the National Bureau of Standards, Washington, D.C.

[1] We call "a sequence" all the atoms belonging to the same period with the same degree of ionization.

[2] Figures in brackets indicate the literature references at the end of this paper.

"Diag." is an abbreviation for "diagonalization," "L.S." is an abbreviation for "least-squares calculation."

3. The Mean Error

Two kinds of mean-error are used in this paper. The "level-mean-error," Δ, is defined by the formula

$$\Delta = \sqrt{\Sigma \Delta_L^2/(n-m)} \tag{1}$$

where the Δ_L are the differences between the observed levels and the calculated levels fitted to them, n is the number of observed levels, and m is the number of free parameters. The "term-mean-error," Δ', (the term, "mean error" as defined in this paper is identical to the concept, "residual standard deviation" used in statistical analysis) is defined by the formula

$$\Delta' = \sqrt{\Sigma \Delta_T^2/(n_T - m_E)} \tag{2}$$

where the Δ_T are the differences between the observed terms and calculated terms fitted to them, n_T is the number of observed terms, and m_E is the number of the free electrostatic parameters.

The calculation of Δ is easier, since our least-squares program furnishes $\Sigma \Delta_L^2$; the abbreviation "mean-error" means the level-mean-error.

In fact, Δ' is a more serious criterion of the precision of our approximations, as the levels belonging to the same term are strongly correlated, while in the definition of Δ they are considered independent.

4. Survey of the Various Spectra

Y III $-(4d+5s)$

This spectrum consists of two terms and needs for its description two electrostatic parameters, so that a separate treatment is meaningless. On the other hand in the general treatment it supplies reliable points for the interpolation formulae of D′ and ζ.

The observed and calculated levels are given in table 7.

Zr III $-(4d^2+4d5s)$

These configurations consist of 7 terms which split into 13 levels. In AEL 6 experimental terms, splitting into 12 levels, are reported; only the ^1S of d^2 is unknown.

Here, too, a separate treatment is not fully significant, since 6 electrostatic parameters are necessary. Nevertheless, a separate treatment was performed in order to get some preliminary information about the more stable parameters: D′, B, G, ζ, ζ'.

Initial values for the parameters were taken from Zr II [2]. In L.S. 1, the parameter H was frozen and the mean error was 4 because the number of free electrostatic parameters is equal to the number of known terms.

The parameters of the various stages of the calculation are given in table 1, the observed and calculated energy levels in table 8.

Nb III $-(4d^3+4d^25s)$

In these configurations theory predicts 15 terms which split into 35 levels. In a paper of L. Iglesias [5] 11 experimental terms, splitting into 28 levels are reported.

Parameters for Diag. 1 were prepared by comparison with the parameters of NB II and Zr II [2]. It turned out that the level assigned by Iglesias as $^2D_{3/2}$ is actually the $^2P_{3/2}$ of d^3.

In L.S. 1 we got a mean error of 34.

The estimates of parameters of the various stages of the calculation are given in table 2, the energy levels in table 9.

Mo III $-(4d^4+4d^35s)$

These configurations consist of 27 terms, which split into 72 levels. In AEL only the level $^5D_4$ and the 5 levels belonging to the ^5F of d^5s are reported. Since the ground level $d^4\,^5D_0$ is unknown, Rico and Catalan estimated the value of the $^5D_4$ to be 1500 cm^{-1}, and added to all the known levels an unknown additive constant x. (Note, there is no connection between the unknown numerical constant "x", introduced by Rico and Catalan, and the variable $x=n-6$ defined in eq (5a) in the section on the interpolative treatment.)

Because of these circumstances we did not even include Mo III in the General Least Squares (G.L.S.) calculation, but, using the improved coefficients of the interpolation formulae achieved in the G.L.S., we calculated the interaction parameters of Mo III. Then the matrices of d^4+d^3s were diagonalized with the use of the interpolated parameters, and thus, we obtained predictions for the levels of Mo III.

Using the calculated values of the $(^4F)^5F$ one gets for x the value 340. For $^5D_4$ we got the value 1807 cm^{-1} and this gives $x=307$. We suppose that the uncertainty of x is of the order of magnitude of the term-mean-error of the G.L.S. which is 91 cm^{-1}.

The predicted levels of Mo III are given in table 10.

Tc III $-(4d^5+4d^45s)$

In these configurations theory predicts 40 terms which split into 100 levels. Unfortunately, no level was observed. Using the results of the G.L.S. the interaction parameters of Tc III were interpolated, and then the energy matrices of these configurations were diagonalized. In this way the energy levels could be calculated.

The predicted levels of Tc III are given in table 11.

Ru III $-(4d^6+4d^55s)$

These configurations consist of 48 terms, which split into 108 levels. In AEL only 7 levels are reported: The ^5D of d^6, and the ^7S and the ^5S of d^5s.

Obviously, no separate treatment was performed, but in the G.L.S. these few data furnished more points for D′, G, and ζ. Of course, the main role of the G.L.S. in this case was to calculate all the levels of Ru III.

The observed and calculated energy levels are given in table 12.

Rh III $-(4d^7+4d^65s)$

In these configurations theory predicts 33 terms, which split into 82 levels. In AEL all these levels are reported. Only the b^2S of d^6s is considered doubtful.

Even at the preliminary stage of estimating parameters for the first diagonalization we had serious doubts as to the reliability of the experimental material. It is well known that the difference between two terms of d^6s having the same parent term of d^6 is determined by the parameter $G = G_2(4d5s)$. This parameter is very stable for all spectra of the transition elements and also does not change considerably for all spectra of the same sequence. In the present spectrum we could get for the parameter G values which were different from each other by about 1000 cm^{-1}, depending upon the choice of the parent term. Only the difference between $(^5D)^4D$ and $(^5D)^6D$ was consistent with the interpolated value of G.

Since the experimental levels did not seem reliable we decided to perform Diag. 1 with interpolated parameters and to use its results for a more detailed critique of the observed levels. We got a very bad fit. The deviations between the calculated levels and those reported in AEL were frequently more than 10000 cm^{-1}. In order to check if there exists any set of parameters which will give calculated values close to the observed ones we included in the first least-squares calculation ("L.S. 1a") 81 levels. Only the b^2S which is reported as doubtful was excluded. We got a mean error of 3094 cm^{-1}. In L.S. 1b only 33 levels were included. We did not include 42 levels belonging to $4d^65s$. The terms b^2D, a^2F, a^2H of $4d^7$ were also included. The mean error reduced to 273, but B′ and C′ assumed nonreasonable values. In L.S. 1c from the configuration d^6s only the levels of $(^5D)\ ^6D$ and $(^5D)\ ^4D$ were left. The values of B′ and C′ were frozen and we got a mean error of 235. It should be noted that in L.S. 1c we used 6 free electrostatic parameters and 2 frozen ones for the description of only 7 observed terms. Thus, the separate treatment lost its physical significance and we could not use it for further critique of the remaining reported levels.

In the G.L.S. calculations, it turned out that also the other doublets of $4d^7$ were doubtful. Finally, only 16 levels were included in the calculation: the ^4F and ^4P of $4d^7$ and the $(^5D)\ ^6D$ and $(^5D)\ ^4D$ of d^6s.

After these calculations had been finished, we had the opprotunity to discuss the results with A. G. Shenstone and he told us that he had reached similar conclusions by comparing the spectrum of Rh III to the isoelectronic spectrum of Ru II, which he analyzed later.

We hope that the predictions of the G.L.S. will help to revise the analysis of this spectrum.

The parameters of the various stages of the calculation are given in table 3, the levels are given in table 13.

Pd III $-(4d^8 + 4d^7 5s)$

In these configurations theory predicts 21 terms which split into 47 levels. In AEL 19 terms, splitting into 45 levels, are reported. Only the ^1S of $4d^8$ and the high ^1D of $4d^7 5s$ were not observed. The level assigned as $b\ ^3D_1$ is reported in AEL as doubtful. It also deviates by about 700 cm^{-1} from its calculated value, thus we did not include this level in the calculations.

In L.S. 1 the mean error was 157 and in L.S. 2 it reduced to 110. Because of the big distance between the configurations $4d^7 5s$ and $4d^8$ and the weak interaction between them the parameter H is not stable. Pd III is the only spectrum in the sequence in which the number of experimental levels is sufficient to make also the results of the separate treatment quite reliable.

The estimates of parameters of the various stages of the calculation are given in table 4. The observed and calculated levels are given in table 14.

Ag III $-(4d^9 + 4d^8 5s)$

These configurations consist of 8 terms which split into 18 levels. In AEL only the ^2S of d^8s is not reported, and the $^4P_{1/2}$ of d^8s is doubtful. Since also the deviation of this level from its calculated value is rather big, we excluded it from the calculations.

After performing Diag. 1 we saw that the level $^2P_{1/2}$ deviates by more than 1000 cm^{-1} from its calculated value. In L.S. 1a, where it was included, the mean error was 461. In L.S. 1B, from which it was excluded, the mean error reduced to 112. Hence, we did not include this level in the general least squares.

Not having a sufficient amount of experimental material the parameter H was frozen in L.S. 1a and 1b. After having an interpolation formula for the parameter H we could see that we forced H to assume a value which was much bigger than the correct one. Since in the configuration d^8s the parameters H and α can compensate each other, this also caused an unjustified increase of α.

The estimates of parameters of the various stages of the calculation are reported in table 5, the energy levels—in table 15.

Cd III $-(4d^{10} + 4d^9 5s)$

These configurations include only three terms which split into 5 levels. All are experimentally known.

There is no sense to perform any separate calculation of this spectrum. By including it in the G.L.S. we got an additional value for each of the parameters D′, G, ζ'.

The observed and calculated levels are given in table 16.

5. The Interpolative Treatment of the Whole Sequence

5.1. General Description of the Procedure

In the general (interpolative) treatment the whole sequence is considered as one system, and the coefficients of the interpolation formulas are given the role of free parameters. We call these coefficients "General Parameters."

The parameters B, B′, C, C′, G, H, and α are represented by linear expressions of the form

$$P(n) = \overline{P} + \Delta P \cdot x, \tag{3}$$

and the parameters D′, ζ, ζ′ by quadratic expressions of the form

$$P(n)=\overline{P}+\Delta P\cdot x+\Delta_2 P\cdot y, \tag{4}$$

where

$$x=n-6 \tag{5a}$$

and

$$y=x^2-10 \tag{5b}$$

Here n is the total number of electrons in the states $4d$ and $5s$. We consider only the coefficients $\overline{P}$, ΔP, and $\Delta_2 P$ as independent parameters (the "general parameters"). The substitution of x and y for n and n^2 is used in order to get fairly orthogonal parameters.

By fitting the interpolation-formulas to the parameters of the separate treatments we obtain a set of initial general parameters. Using these parameters, we diagonalized the matrices of all spectra of the sequences; this is the "General Diagonalization" ("G. Diag.").

In the "General Least-Squares" ("G.L.S.") the known levels of all the spectra are compared with the results of the General Diagonalization. In this unified least-squares calculation only the general parameters specified in table 6 and the normalization parameters $M(d^n)$ are considered as free parameters.

5.2. The Actual Calculations

As a consequence of the separate treatment which was described in the previous chapter we had for the general treatment only 56 reliable observed terms which split into 130 levels. Because of the relatively small amount of experimental material we were forced to use also the results of Zr III and Ag III (which are not quite reliable) for the calculation of the initial interpolation formulas. For the formulas of D′, ζ, and ζ′ even the information from Y III or Cd III was used.

In the G.L.S. we had 30 free parameters: 22 general parameters and 8 additive parameters $M(d^n)$. 25 of them are electrostatic interaction parameters and 5 are spin-orbit interaction parameters.

A total of 483 levels, belonging to 209 terms, were calculated. The *level mean error* of the G.L.S. is

$$\underline{\Delta_{G.L.S.}=77\ cm^{-1}},$$

and the *term-mean-error* is

$$\underline{\Delta'_{G.L.S.}=91\ cm^{-1}}.$$

The general parameters of the G. Diag. and the improved general parameters which were obtained in the G.L.S. are given in table 6.

6. Conclusions

We shall use the results in order to evaluate the relative importance of the various improvements to the Slater approximation used in the present paper. Generally speaking an interaction (or a correction-term) is important if, relative to other sequences of the transition elements [1–3] the parameter representing it has a large value and a small relative statistical uncertainty.

We see that the spin-orbit interaction is quite important, and it is certainly the most important correction in the right-hand side of the period. This fact can be seen also from the very mixed assignments given to the levels in tables 7 through 16.

The differences (B′−B), (C′−C), and (ζ′−ζ) are much bigger than the uncertainties of these parameters. This means that it is important to allow these parameters to assume different values for the configurations $4d^n$ and $4d^{n-1}5s$.

The estimates of the parameter α is considerably smaller than in the iron group, but its standard error is much smaller than its value. This means that it is still necessary in order to improve the fit between the theoretical and experimental levels.

Contrary to the results in the first [6] and second [2] spectra of the palladium group, the interaction between the configurations $4d^n$ and $4d^{n-1}5s$ is rather unimportant in the right hand side of the present sequence. This fact manifests itself in the large standard errors of H and the small values it assumes.

Out of 10 spectra of the sequence there are 8 in which the amount of experimental material is not sufficient for a reliable separate treatment. Thus, in this sequence the interpolative method is not only the more reliable one—practically it is the only method which enables us to predict the energy-levels for all the third spectra of the palladium group. We hope that these predictions will help in their experimental observation.

7. Tables of Results* Part A: Parameters

TABLE 1. *Parameters of* Zr III − ($4d^2+4d5s$)

	Diag. 1	L.S. 1*	G.L.S.
A	4840	4807±3	4741
S′	16560	16481±3	16593
B	530	525±0.3	532
C	1600	1829±2	1757
G	3000	2350±3	2454
H	400	fixed	376
α	25	23±0.4	34
ζ	450	410±1.4	411
ζ′	450	454±2.4	461
Δ	.....	4	.....

*In tables 1–6 the number following the ± sign is the L.S. standard error of the parameter estimate.

TABLE 2. *Parameters of* Nb III $-(4d^3+4d^25s)$

	Diag. 1	L.S. 1	G.L.S.
A	9260	9308 ± 26	9224
S′	25650	26330 ± 52	26485
B	550	563 ± 2	559
B′	550	593 ± 2	592
C	2200	2054 ± 10	2018
C′	2200	2188 ± 16	2210
G	2400	2386 ± 19	2424
H	400	383 ± 7	334
α	0	30 ± 1	33
ζ	560	544 ± 11	535
ζ′	560	589 ± 11	597
Δ	.....	34	.....

TABLE 3. *Parameters of* Rh III $-(4d^7+4d^65s)$

	Diag. 1	L.S. 1a	L.S. 1b	L.S. 1c	G.L.S.
A	11650	12717 ± 1790	11792 ± 1560	11621 ± 146	11895
S′	56750	62083 ± 2454	70184 ± 1570	57185 ± 222	56964
B	669	801 ± 104	651 ± 14	647 ± 21	667
B′	713	980 ± 52	1336 ± 74	fixed	716
C	3068	3616 ± 547	3288 ± 57	3293 ± 56	3062
C′	3194	3844 ± 290	2926 ± 76	fixed	3178
G	2296	2316 ± 297	2276 ± 35	2304 ± 33	2304
H	.....	.....	.....	.....	166
α	28	fixed	fixed	24 ± 17	29
ζ	1324	1110 ± 677	1146 ± 64	1141 ± 60	1291
ζ′	1450	1673 ± 490	1395 ± 78	1381 ± 102	1401
n	.....	81	33	22	16
Δ	.....	3094	273	235	.....

n = number of levels included in the L. S. calculations.

TABLE 4. *Parameters of* Pd III $-(4d+5s)^8$

	Diag. 1	L.S. 1	Diag. 2	L.S. 2	G.L.S.
A	8100	7613 ± 105	7600	7602 ± 90	7663
S′	65100	65836 ± 159	65836	65827 ± 121	65818
B	800	699 ± 13	699	695 ± 9	694
B′	800	747 ± 5	747	744 ± 3	747
C	2500	3221 ± 92	3221	3322 ± 67	3328
C′	3100	3429 ± 25	3429	3445 ± 18	3420
G	2270	2277 ± 24	2277	2274 ± 18	2274
H	385	146 ± 56	235	30 ± 70	124
α	40	31 ± 4	31	28 ± 3	28
ζ	1300	1664 ± 72	1664	1519 ± 43	1545
ζ′	1530	1681 ± 26	1681	1666 ± 18	1667
Δ	.....	157	.....	110	.....

TABLE 5. *Parameters of* Ag III $-(4d+5s)^9$

	Diag. 1	L.S. 1a	L.S. 1b	G.L.S.
A	1840	1595 ± 400	1689 ± 93	1655
S′	75290	75465 ± 480	75037 ± 115	75125
B′	770	841 ± 33	804 ± 8	778
C′	3210	3063 ± 319	3377 ± 78	3662
G	2270	2413 ± 127	2236 ± 33	2244
H	400	fixed	fixed	82
α	20	68 ± 37	50 ± 9	27
ζ	1730	1846 ± 261	1846 ± 61	1825
ζ′	1730	2031 ± 162	1978 ± 38	1959
Δ	.....	461	112	.....

TABLE 6. *General parameters in the third spectra of the palladium-group*

	G. Diag.	G.L.S.
$\overline{D}'$	48792	48746 ± 34
$\Delta D'$	8657	8666 ± 10
$\Delta_2 D'$	85	98 ± 5
$\overline{B}$	640	640 ± 4
ΔB	28	27 ± 1
$\overline{B}'$	691	685 ± 2
$\Delta B'$	34	31 ± 1
$\overline{C}$	2756.9	2803 ± 23
ΔC	232.4	262 ± 8
$\overline{C}'$	2939.9	2939 ± 14
$\Delta C'$	250.7	243 ± 6
$\overline{G}$	2318	2334 ± 10
ΔG	−24	−31 ± 6
$\overline{H}$	250	208 ± 24
ΔH	−40	−42 ± 6
α	30	31 ± 2
$\Delta\alpha$	0	−0.9 ± 0.7
$\overline{\zeta}$	1190	1193 ± 16
$\Delta\zeta$	221	215 ± 6
$\overline{\zeta}'$	1293	1291 ± 12
$\Delta\zeta'$	232	227 ± 4
$\Delta_2\zeta = \Delta_2\zeta'$	15.5	13 ± 2
Level mean error	.....	77
Term mean error	.....	91

Tables of Results Part B: Energy Levels

TABLE 7. *Observed and calculated levels of* Y III

Conf.	Term	*J*	Observed	G.L.S.	
				Calc.	O − C
4*d*	a^2D	3/2	0.0	18	−18
		5/2	724.8	802	−77
5*s*	a^2S	1/2	7466.2	7371	95

TABLE 8. *Observed and calculated levels of* Zr III

Conf.	Term	J	Observed	G.L.S.	
				Calc.	O−C
d^2	a^3F	2	0.00	−1	1
		3	681.0	683	−2
		4	1486.4	1488	−2
d^2	a^1D	2	5741.55	5725	16
d^2	a^3P	0	8062.07	8045	17
		1	8325.65	8312	13
		2	8838.21	8833	5
d^2	a^1G	4	11048.70	11067	−18
ds	$(^2D)a^3D$	1	18398.87	18382	17
		2	18802.79	18796	7
		3	19533.35	19532	1
d^2	^1S	0	(13832.0?)	24518	
ds	$(^2D)b^1D$	2	25066.25	25122	−56

TABLE 9. *Observed and calculated levels of* Nb III

Iglesias	Conf.	Term	J	Observed	G.L.S.		Calc. g
					Calc.	O−C	
	d^3	a^4F	3/2	0.0	63	−63	0.403
			5/2	515.8	565	−49	1.029
			7/2	1176.6	1208	−32	1.237
			9/2	1939.0	1949	−10	1.331
	d^3	a^4P	1/2	8664.3	8614	50	2.430
			3/2	8607.5	8562	45	1.629
			5/2	9593.7	9486	108	1.596
	d^3	a^2G	7/2	9236.1	9215	21	0.890
			9/2	9804.5	9761	44	1.098
	d^3	^2P	1/2		10753		0.904
a^2D		$^2P+{}^4P+{}^2D$	3/2	10912.2	10959	−46	1.307
	d^3	a^2H	9/2	12916.4	12856	60	0.925
			11/2	13263.8	13183	81	1.091
	d^3	$^2D+{}^2P$	3/2		12894		0.928
		^2D	5/2	13094.0	13041	53	1.203
	d^3	a^2F	7/2	19861.0	19907	−46	1.142
			5/2	19975.0	20061	−86	0.857
	d^2s	$(^3F)b^4F$	3/2	25220.2	25248	−28	0.403
			5/2	25735.2	25759	−23	1.029
			7/2	26463.7	26481	−18	1.238
			9/2	27373.5	27382	−9	1.333
	d^3	^2D	5/2		31463		1.197
			3/2		31785		0.800
	d^2s	$(^3F)b^2F$	5/2	33658.0	33650	8	0.894
			7/2	35079.2	35060	19	1.141
	d^2s	$(^3P)b^4P$	1/2	34514.5	34500	15	2.664
			3/2	34807.2	34797	10	1.704
		$^4P+{}^2D$	5/2	34989.8	34983	7	1.507
	d^2s	$(^1D)b^2D$	3/2	36535.7	36577	−42	0.832
		$^2D+{}^4P$	5/2	37114.7	37105	10	1.258
	d^2s	$(^1G)b^2G$	9/2	40875.2	40939	−64	1.112
			7/2	40943.9	40959	−15	0.891
	d^2s	$(^3P)^2P$	1/2		43004		0.672
			3/2		43729		1.328
	d^2s	$(^1S)^2S$	1/2		57154		1.997

TABLE 10. *Observed and calculated levels of* Mo III

Conf.	Term	J	Observed	G.L.S.		Calc. g
				Calc.	O−C	
d^4	^5D	0	(0.00)	40	(−40)	
		1	(243.10)	275	(−32)	1.500
		2	(669.60)	688	(−18)	1.499
		3	(1225.20)	1224	(1)	1.498
		4	(1873.80	1847	(27)	1.497
d^4	^3P	0	(11271.30)	11328	(−57)	
		1	(12509.80)	12554	(−44)	1.493
		2	(14357.30)	14373	(−16)	1.491
d^4	^3H	4	(12630.31)	12634	(−4)	0.843
		5	(13201.34)	13201	(0)	1.043
		6	(13741.54)	13701	(41)	1.167
d^4	^3F	2	(13927.76)	13923	(5)	0.675
	$^3F+{}^3G$	3	(13947.40)	13924	(23)	1.015
	$^3F+{}^3G+{}^3H$	4	(14295.85)	14233	(63)	1.185
d^4	$^3G+{}^3F$	3	(15672.25)	15835	(−163)	0.822
		4	(16143.15)	16224	(−81)	1.067
	^3G	5	(16763.14)	16629	(134)	1.190
d^4	^3D	3	(19390.90)	19391	(0)	1.329
		2	19783.28	19493	290	1.160
		1	(19995.50)	19806	(190)	0.509
d^4	^1I	6		19754		1.003
d^4	^1G	4		20377		1.008
d^4	^1S	0		22555		
d^4	^1D	2		23221		1.011
d^4	^1F	3		26903		1.005
d^4	^3P	2	(30992.50)	31086	(−93)	1.495
		1	(32292.70)	32323	(−30)	1.493
		0	(32887.80)	32976	(−88)	
d^4	^3F	4	(31932.50)	31970	(−37)	1.245
		3	(32142.80)	32252	(−109)	1.082
		2	(32126.50)	32112	(15)	0.672
d^3s	$(^4F)^5F$	1	(32419.44)	32439	(−20)	0.010
		2	(32844.04)	32854	(−10)	1.000
		3	(33453.10)	33459	(−6)	1.249
		4	(34226.01)	34227	(−1)	1.349
		5	(35130.10)	35122	(8)	1.398
d^4	^1G	4		36033		1.005
d^3s	$(^4P)^5P$	1	(42405.50)	42389	(17)	2.473
	$^5P+{}^3F$	2	(42665.90)	42652	(14)	1.378
	^5P	3	(43462.69)	43420	(43)	1.596
d^3s	$(^4F)^3F+{}^5P$	2	(42605.84)	42526	(80)	1.112
	$(^4F)^3F$	3	(43562.61)	43557	(6)	1.142
		4	(44656.23)	44646	(10)	1.231
d^3s	$(^2G)^3G$	3		46227		0.763
		4	(46557.96)	46544	(14)	1.053
		5	(46581.03)	46921	(−340)	1.185
d^4	^1D	2		47541		1.007
d^3s	$(^2P)^3P$	0		48707		
	$^3P+{}^3D$	1	(48753.45)	48636	(117)	1.159
		2	(49052.05)	48972	(80)	1.383
d^3s	$(^2H)^3H$	4		49460		0.835
		5		50272		1.048
		6		50459		1.167

TABLE 10. *Observed and calculated levels of* Mo III—Continued

Conf.	Term	J	Observed	G.L.S.		Calc. g
				Calc.	O−C	
d^3s	$^3D+^3P+^1P$	1		50200		0.946
	$^3D+^3P$	2		51289		1.284
	^3D	3		51204		1.333
d^3s	$(^2G)^1G$	4		52519		0.985
d^3s	$(^4P)^3P$	0		53082		
	$^3P+^1P+^3D$	1		52528		1.284
	$(^4P)^3P$	2		53858		1.487
d^3s	$(^2H)^1H$	5		54931		1.002
d^3s	$^1P+^3P$	1		55174		1.133
d^3s	$(a^2D)^1D$	2		56633		1.001
d^3s	$(^2F)^3F$	4		58811		1.249
		3		58960		1.084
		2		59121		0.672
d^4	^1S	0		61910		
d^3s	$(^2F)^1F$	3		64072		1.004
d^3s	$(b^2D)^3D$	3		71596		1.329
		2		71793		1.165
		1		71940		0.500
d^3s	$(b^2D)^1D$	2		76887		1.000

TABLE 11. *Calculated levels of* Tc III

Conf.	Term	J	G.L.S.	Calc. g
d^5	^6S	5/2	−2	1.997
d^5	^4G	5/2	19179	0.586
		7/2	19343	0.988
		9/2	19442	1.172
		11/2	19398	1.271
d^5	$^4P+^4D$	5/2	20987	1.510
		3/2	21308	1.564
		1/2	21759	2.207
d^5	^4D	7/2	23007	1.422
	$^4D+^4P$	5/2	23849	1.430
		3/2	23850	1.354
		1/2	23502	0.456
d^5	^2I	11/2	28153	0.933
		13/2	28521	1.077
d^5	$^2D+^2F$	5/2	29536	1.075
	$^2D+^4F$	3/2	30299	0.681
d^5	$^4F+^2G$	9/2	31308	1.292
	$^4F+^2F$	7/2	31291	1.182
	^4F	5/2	31746	1.015
	$^4F+^2D$	3/2	32463	0.534
d^5	$^2F+^4F$	7/2	32182	1.171
	$^2F+^2D$	5/2	33789	1.002
d^5	$^2H+^2G+^4F$	9/2	33612	1.028

TABLE 11. *Calculated Levels of* Tc III—Continued

Conf.	Term	J	G.L.S.	Calc. g
	^2H	11/2	34954	1.083
d^5	^2G	7/2	34555	0.915
	$^2G+^2H$	9/2	35662	1.034
d^5	^2F	7/2	36640	1.146
		5/2	36655	0.872
d^5	^2S	1/2	39605	1.997
d^5	^2D	3/2	44478	0.801
		5/2	44737	1.193
d^4s	$(^5D)^6D$	1/2	44705	3.322
		3/2	45063	1.864
		5/2	45607	1.656
		7/2	46287	1.585
		9/2	47069	1.553
d^5	^2G	9/2	49288	1.111
		7/2	49405	0.891
d^4s	$(^5D)^4D$	1/2	56604	0.053
		3/2	57168	1.205
		5/2	57959	1.367
		7/2	58847	1.427
d^5	^2P	3/2	58686	1.317
		1/2	58938	0.660
d^4s	$(a^3P)^4P$	1/2	61309	2.613
		3/2	62857	1.716
		5/2	65015	1.584
d^4s	$(^3H)^4H$	7/2	61772	0.670
		9/2	62063	1.001
		11/2	62579	1.141
		13/2	63139	1.228
d^4s	$(a^3F)^4F$	3/2	63738	0.419
	$(a^3F)^4F+^4G$	5/2	63609	0.928
		7/2	63808	1.156
		9/2	64055	1.278
d^5	^2D	5/2	64334	1.195
		3/2	64525	0.805
d^4s	$(^3G)^4G+^4F$	5/2	65388	0.692
		7/2	66037	1.041
		9/2	66416	1.188
	$(^3G)^4G$	11/2	66569	1.259
d^4s	$(a^3P)^2P+^4D$	1/2	68826	0.564
	$(a^3P)^2P$	3/2	71968	1.309
d^4s	$(^3H)^2H$	9/2	69062	0.933
	$^2H+^2I$	11/2	69934	1.071
d^4s	$(^3D)^4D$	7/2	69731	1.420
		5/2	69916	1.356
		3/2	69973	1.206
	$^4D+^2P$	1/2	70649	0.170
d^4s	$(a^3F)^2F$	7/2	70791	1.066
d^4s		5/2	71320	0.882
	$(^1I)^2I$	13/2	72399	1.079
	$^2I+^2H$	11/2	72703	0.949
d^4s	$(^3G)^2G$	7/2	72503	0.899
	$(^3G)^2G+(^1G)^2G$	9/2	73239	1.112
d^4s	$(^1G)^2G+(^3G)^2G$	9/2	74267	1.098
	$^2G+^2F$	7/2	74648	0.966
d^4s	$(a^1S)^2S$	1/2	76572	1.966
d^4s	$(^1D)^2D+(^3D)^2D$	3/2	76635	0.807
		5/2	77879	1.197
d^4s	$(^3D)^2D+(^1D)^2D$	5/2	77018	1.187
		3/2	78766	0.809
d^4s	$(^1F)^2F$	7/2	81046	1.153
		5/2	81264	0.891

TABLE 11. *Calculated levels of* Tc III—Continued

Conf.	Term	J	G.L.S.	Calc. g
d^4s	$(b^3P)^4P$	5/2	83340	1.585
		3/2	84675	1.697
		1/2	85616	2.650
d^4s	$(b^3F)^4F$	9/2	84019	1.330
		7/2	84506	1.227
		5/2	84501	1.019
		3/2	84305	0.442
d^4s	$(b^3F)^2F+{}^2G$	7/2	90827	1.039
	$(b^3F)^2F$	5/2	91454	0.860
d^4s	$(b^3P^2P$	3/2	91036	1.334
		1/2	92733	0.678
d^4s	$(b^1G)^2G$	9/2	91658	1.113
	$^2G+{}^2F$	7/2	92142	0.993
d^4s	$(b^1D)^2D$	3/2	104753	0.800
		5/2	104764	1.200
d^4s	$(b^1S)^2S$	1/2	120665	1.999

TABLE 12. *Observed and calculated levels of* Ru III

Conf.	Term	J	Observed	G.L.S.		Calc. g
				Calc.	O−C	
d^6	a^5D	4	0.0	−35	35	1.496
		3	1158.8	1139	20	1.498
		2	1826.3	1827	−1	1.498
		1	2266.3	2279	−12	1.498
		0	2476.0	2495	−19	
d^6	$^3H+{}^3F+{}^3G$	4		15028		0.994
	$^3H+{}^3G$	5		15326		1.066
	^3H	6		15081		1.162
d^6	^3P	2		15092		1.486
		1		18412		1.454
		0		19048		
d^6	$^3F+{}^3H$	4		16824		1.043
	$^3F+{}^3G$	3		16857		1.025
	^3F	2		17357		0.677
d^6	$^3G+{}^3H$	5		18612		1.167
	$^3G+{}^3F$	4		19611		1.062
		3		19878		0.814
d^6	^3D	1		22495		0.550
		2		22319		1.171
		3		22644		1.328
d^6	^1I	6		23289		1.004
d^6	^1G	4		24503		1.006
d^5s	$(^6S)a^7S$	3	27162.8	27177	−14	1.997
d^6	^1S	0		27242		
d^6	^1D	2		28412		1.008
d^6	^1F	3		31296		1.007
d^6	^2P	0		34942		
		1		35818		1.498
		2		38006		1.491
d^6	^3F	4		36927		1.244
		3		37559		1.079
		2		37008		0.671

TABLE 12. *Observed and calculated levels of* Ru III—Continued

Conf.	Term	J	Observed	G.L.S.		Calc. g
				Calc.	O−C	
d^5s	$(^6S)a^5S$	2	41111.7	41121	−9	1.992
d^6	^1G	4		42394		1.005
d^5s	$(^4G)^5G$	2		51433		0.345
		3		51551		0.924
		4		51674		1.152
		5		51743		1.266
		6		51703		1.332
d^5s	$(^4P)^5P+{}^5D$	3		53614		1.600
		2		53937		1.701
		1		54432		2.257
d^6	^1D	2		54879		1.013
d^5s	$(^4D)^5D$	4		55985		1.493
	$^5D+{}^5P$	3		57107		1.542
		2		57152		1.600
		1		56727		1.726
	^5D	0		56198		
d^5s	$(^4G)^3G$	3		60682		0.771
		4		60980		1.054
		5		60957		1.195
d^5s	$(^4P)^3P+{}^3D$	2		62624		1.323
		1		63453		1.033
	^3P	0		64541		
d^5s	$(^2I)^3I$	5		64001		0.847
		6		64093		1.030
		7		64422		1.143
d^5s	$(^4D)^3D+{}^5F$	3		65012		1.294
	^3D	2		66051		1.152
	$^3D+{}^3P$	1		66262		0.669
d^5s	$(^4F)^5F+{}^3P$	1		65273		0.316
	^5F	2		65408		1.054
	$^5F+{}^3D$	3		65724		1.275
	^5F	4		65554		1.336
		5		65454		1.382
d^5s	$^3D+{}^3F+{}^5F$	3		66565		1.216
	$^3D+{}^3F+{}^1D$	2		69516		1.006
	$^3D+{}^3F+{}^3P$	1		68811		0.497
d^5s	$^3F+{}^3D+{}^3P$	2		67522		0.984
	$^3F+{}^3G+{}^3D$	3		70165		1.040
	^3F	4		68919		1.241
d^5s	$(^2I)^1I+{}^3H$	6		68535		1.002
d^5s	$^3H+{}^3G$	4		70311		0.923
		5		72693		1.110
	$^3H+{}^1I$	6		72408		1.139
d^5s	$^3G+{}^3H$	5		70511		1.126
		4		72228		0.965
	$^3G+{}^3F$	3		71472		0.908
d^6	^1S	0		71104		
d^5s	$(a^2D)^1D+{}^3F$	2		73602		0.892
d^5s	$(^2F)^3F$	2		73625		0.705
	$^3F+{}^1F$	3		73412		1.059
		4		73715		1.227

TABLE 12. *Observed and calculated levels of* Ru III—Continued

Conf.	Term	J	Observed	G.L.S.		Calc. g
				Calc.	O−C	
d^5s	$(^4F)^3F+^1G$	4		74832		1.184
	$^3F+^1F$	3		74904		1.063
	^3F	2		76138		0.738
d^5s	$(^2F)^1F+^3F$	3		75145		1.050
d^5s	$(^2H)^1H$	5		76539		1.008
d^5s	$(^2G)^1G+^3F$	4		77177		1.071
d^5s	$(^2S)^3S$	1		77522		1.997
d^5s	$(^2F)^1F$	3		78799		1.027
d^5s	$(^2S)^1S$	0		82821		
d^5s	$(b^2D)^3D$	1		82910		0.502
		2		83073		1.161
		3		83477		1.311
d^5s	$(b^2D)^1D$	2		87968		0.999
d^5s	$(^2G)^3G$	5		88207		1.200
		4		88335		1.051
		3		88434		0.754
d^5s	$(^2G)^1G$	4		92963		1.001
d^5s	$(^2P)^3P$	2		99093		1.490
		1		99316		1.486
		0		99513		
d^5s	$(^2P)^1P+^3D$	1		103479		0.923
d^5s	$(c^2D)^3D$	3		105494		1.333
		2		105701		1.172
		1		106119		0.595
d^5s	$(c^2D)^1D$	2		110249		1.003

TABLE 13. *Observed and calculated levels of* Rh III

Conf.	Term	J	Observed	G.L.S.		Calc. g
				Calc.	O−C	
d^7	a^4F	9/2	0.0	−25	25	1.327
		7/2	2147.8	2124	24	1.236
		5/2	3485.7	3476	9	1.031
		3/2	4322.0	4328	−6	0.414
d^7—	a^4P	5/2	11062.3	11060	2	1.592
	$^4P+^2P$	3/2	10997.1	11085	−88	1.642
		1/2	12469.8	12519	−50	2.507
d^7	^2G	9/2		13092		1.093
		7/2		15229		0.893
d^7	$^2P+^2D+^4P$	3/2		16334		1.250
	$^2P+^4P$	1/2		18451		0.827
d^7	^2H	11/2		17317		1.091
		9/2		19500		0.931
d^7	^2D	5/2		18436		1.203
	$^2D+^2P$	3/2		21873		0.960
d^7	^2F	5/2		26798		0.863
		7/2		27889		1.140
d^7	^2D	3/2		42251		0.800
		5/2		43173		1.196
d^6s	$(^5D)a^6D$	9/2	43022.0	43010	12	1.552
		7/2	44394.4	44385	9	1.584
		5/2	45278.2	45274	4	1.654
		3/2	45876.6	45876	1	1.862
		1/2	46227.1	46230	−3	3.317

TABLE 13. *Observed and calculated levels of* Rh III—Continued

Conf.	Term	J	Observed	G.L.S.		Calc. g
				Calc.	O−C	
d^6s	$(^5D)a^4D$	7/2	54632.2	54576	56	1.418
		5/2	56125.7	56109	17	1.370
		3/2	57012.5	57013	0	1.200
		1/2	57531.3	57545	−14	0.023
d^6s	$(^3H)^4H$	13/2		62412		1.227
	$^4H+^4G$	11/2		62573		1.153
	$^4H+^4G+^4F$	9/2		62416		1.091
		7/2		62857		0.796
d^6s	$(a^3P)^4P$	5/2		62555		1.585
		3/2		65466		1.574
		1/2		67426		2.523
d^6s	$^4F+^4H$	9/2		64224		1.191
		7/2		64732		1.081
	$^4F+^4G$	5/2		64864		0.957
	$(^3F)^4F$	3/2		65263		0.492
d^6s	$^4G+^4H$	11/2		66126		1.236
	$^4G+^4F$	9/2		67620		1.175
		7/2		68041		1.020
		5/2		67796		0.668
d^6s	$(^3H)^2H$	11/2		69678		1.091
	$^2H+^2G$	9/2		69710		0.964
d^6s	$^2F+^2G+^4D$	7/2		70567		1.123
	$(^3F)^2F$	5/2		72351		0.871
d^6s	$^2P+^4D+^4P$	3/2		70583		1.345
	$^2P+^2S$	1/2		73950		0.842
d^6s	$(^3D)^4D$	1/2		70819		0.159
	$^4D+^2P$	3/2		71264		1.236
	^4D	5/2		70984		1.361
		7/2		71445		1.363
d^6s	$(^3G)^2G$	9/2		73708		1.089
		7/2		74718		0.909
d^6s	$(^1I)^2I$	13/2		74084		1.080
		11/2		74354		0.939
d^6s	$(a^1G)^2G$	9/2		76094		1.096
	$^2G+^2F$	7/2		76404		0.945
d^6s	$(3D)^2D$	3/2		77596		0.821
		5/2		77834		1.191
d^6s	$^2S+^2P+^4P$	1/2		79502		1.847
d^6s	$(a^1D)^2D$	5/2		80313		1.204
		3/2		80439		0.810
d^6s	$(^1F)^2F$	7/2		82984		1.157
		5/2		83130		0.886
d^6s	$(b^3P)^4P$	1/2		85311		2.601
		3/2		86279		1.718
		5/2		88927		1.579
d^6s	$(b^3F)^4F$	9/2		87320		1.328
		7/2		88264		1.221
		5/2		88099		1.013
		3/2		87453		0.412
d^6s	$(d^3P)^2P$	1/2		92424		0.687
		3/2		95311		1.330
d^6s	$^2F+^2G$	7/2		94021		1.093
	$(b^3F)^2F$	5/2		94542		0.862
d^6s	$(b^1G)^2G$	9/2		95741		1.114
	$^2G+^2F$	7/2		96104		0.940
d^6s	$(b^1D)^2D$	5/2		110016		1.200
		3/2		110018		0.801
d^6s	$(b^1S)^2S$	1/2		128531		1.999

223-178 O-66-5

TABLE 14. *Observed and calculated levels of* Pd III

AEL	Conf.	Term	J	Observed	G.L.S.		Calc. g
					Calc.	O−C	
	d^8	a^3F	4	0.0	2	−2	1.248
			3	3229.7	3227	3	1.083
			2	4687.3	4728	40	0.714
a^1D	d^8	$\underline{a^3P}+{}^1D$	2	10230.5	10330	−99	1.284
		^3P	1	13470.3	13394	76	1.500
			0	13699.1	13636	63	
a^3P_2	d^8	$\underline{a^1D}+{}^3P$	2	14634.3	14768	−133	1.168
	d^8	a^1G	4	17880.4	17824	56	1.002
	d^8	^1S	0		41196		
	d^7s	$(^4F)a^5F$	5	52915.9	52885	31	1.395
			4	55088.8	55040	49	1.344
			3	56741.5	56697	44	1.248
			2	57845.0	57806	39	1.002
			1	58527.3	58492	36	0.017
	d^7s	$(^4F)b^3F$	4	62560.9	62397	163	1.242
			3	65255.4	65181	74	1.151
			2	67079.4	66986	94	0.694
	d^7s	$(^4P)a^5P$	3	65708.0	65689	19	1.595
			2	65788.3	65817	−29	1.754
			1	67151.4	67195	−44	2.403
	d^7s	$(^2G)a^3G$	5	69985.8	70034	−49	1.185
		$\underline{^3G}+{}^3H$	4	71047.2	71027	20	1.022
		^3G	3	72786.1	72791	−4	0.759
	d^7s	$\underline{(^2P)^3P}$	2	72745.0	72859	−113	1.381
		$^3\underline{P}+{}^1P+{}^3D$	1	73002.6	73096	−93	1.259
		$\overline{(^2P)^3P}+$	0	74281.1	74320	−38	
		$\overline{(^4P)^3P}$					
	d^7s	$(^2H)a^3H$	6	74673.3	74741	−67	1.167
			5	75967.6	75971	−4	1.040
		$^3\underline{H}+{}^1G$	4	78581.1	78525	56	0.890
	d^7s	$^1G+{}^3H+{}^3G$	4	75403.0	75336	67	0.957
	d^7s	$(^4P)c^3P$	2	75455.0	75447	8	1.430
			1	76055.8	76193	−137	1.346
		$\overline{(^4P)^3P}+$	0	78732.5	78682	50	
		$\overline{(^2P)^3P}$					
	d^7s	$(a^2D)a^3D$	3	76231.4	76235	−4	1.331
		$^3\underline{D}+{}^1D+{}^3P$	2	78169.8	78125	45	1.176
		$^3D+{}^3P+{}^1P$	1	78120.0	78210	−90	1.049
	d^7s	$(^2H)a^1H$	5	80805.1	80802	3	1.012
	d^7s	$^1\underline{P}+{}^3D+{}^3P$	1	82620.3	82809	−189	0.925
	d^7s	$(a^2D)c^1D+$	2	83204.3	83113	91	1.074
		$^3P+{}^3D$					
	d^7s	$(^2F)c^3F$	2	85420.7	85494	−74	0.678
			3	85830.4	85940	−110	1.084
			4	86795.2	86937	−142	1.246
	d^7s	$(^2F)a^1F$	3	90684.3	90857	−173	1.004
	d^7s	$(b^2D)b^3D$	1	(103529.4?)	102858		0.501
			2	103549.6	103296	254	1.160
			3	104419.1	104124	295	1.327
	d^7s	$(b^2D)^1D$	2		108183		1.002

TABLE 15. *Observed and calculated levels of* Ag III

Conf.	Term	J	Observed	G.L.S.		Calc. g
				Calc.	O−C	
d^9	a^2D	5/2	0	23	−23	1.200
		3/2	4607	4587	20	0.800
d^8s	$(^3F)a^4F$	9/2	63250	63283	−33	1.332
		7/2	65764	65744	20	1.226
		5/2	68145	68146	−1	1.031
		3/2	69351	69360	−9	0.440
d^8s	$(^3F)a^2F$	7/2	71691	71579	113	1.151
	$^2F+{}^2D+{}^4P$	5/2	73934	73955	−21	1.135
d^8s	$^4\underline{P}+{}^2F$	5/2	76406	76415	−9	1.284
	$^4\underline{P}+{}^2D$	3/2	77413	77476	−63	1.426
	^4P	1/2	(79326?)	78938		2.656
d^8s	$^2D+{}^4P+{}^2P$	3/2	80131	80213	−82	1.189
	$^2\underline{D}+{}^4P$	5/2	82231	82363	−132	1.236
d^8s	$^2\underline{P}+{}^2D$	3/2	85182	85216	−34	1.212
		1/2	(87477)	85512		0.682
d^8s	$(^1G)a^2G$	9/2	85599	85703	−104	1.113
		7/2	85727	85760	−33	0.893
d^8s	$(^1S)^2S$	1/2		111864		1.994

TABLE 16. *Observed and calculated levels of* Cd III

Conf.	Term	J	Observed	G.L.S.		Calc. g
				Calc.	O−C	
d^{10}	a^1S	0	0.0	−72	72	
d^9s	$(^2D)a^3D$	3	80454.3	80540	−86	1.332
		2	82354.6	82361	−6	1.125
		1	86219.5	86237	−18	0.500
d^9s	$(^2D)a^1D$	2	88871.8	88834	38	1.042

An Additional Remark. The calculations reported in the present paper had been completed about five years ago and then the results were sent to several spectroscopy groups. Some weeks ago, after the stencils for the preprints of this paper had already been typed, we received from Rico a reprint of his paper [7] on the spectrum of Mo III. In table I of his paper he compares his observed levels with our theoretical calculations and the fit is quite good. Checking these results we found out, that by adding to all the calcu-

lated levels of Mo III 80 cm^{-1} the fit is very much improved and we get a mean error of 95 cm^{-1} with M(d^4) being the only free parameter. In table 10 we have added the observed levels of Mo III enclosed in brackets in order to indicate that they were not included in the G.L.S.

The author also was informed by L. Iglesias that now she is making a new analysis of Rh III. Hence, we already know that the calculations reported in the present paper actually help in the further analysis of the third spectra of the Pd group.

The author is grateful to the late G. Racah for his invaluable advice during all the stages of the present work.

The author is thankful to Prof. A. G. Shenstone for the thorough commom discussion of the spectra of Pd III and Rh III.

8. References

[1] G. Racah and Y. Shadmi, Bull. Res. Counc. of Israel **8F**, 1 (1959).
[2] Y. Shadmi, Bull. Res. Counc. of Israel, **9F**, 4 (1961).
[3] Y. Shadmi, Bull. Res. Counc. of Israel, **10F**, 3 (1962).
[4] C. E. Moore, Atomic Energy Levels, NBS Circular 467, Vol. II (1952) and Vol. III (1958).
[5] L. Iglesias, J. Opt. Soc. Am. **45**, 855 (1955).
[6] Y. Shadmi (not yet published).
[7] F. R. Rico, Anales Real Soc. Espanola Fisica Quimica, **LXI (A)**, 103 (1965).

(Paper 70A5–415)

JOURNAL OF RESEARCH of the National Bureau of Standards—A. Physics and Chemistry
Vol. 70A, No. 5, September–October 1966

Publications of the National Bureau of Standards*

Selected Abstracts

NBS standard frequency and time services, *NBS Misc. Publ. 236, 1966 edition (1966). 15 cents. (Supersedes previous editions.)*
Detailed descriptions are given of eight technical services provided by the National Bureau of Standards radio stations WWV, WWVH, WWVB, and WWVL. These services are: 1. Standard radio frequencies; 2. Standard audio frequencies; 3. Standard musical pitch; 4. Standard time intervals; 5. Time signals; 6. UT2 corrections; 7. Radio propagation forecasts; and 8. Geophysical alerts. In order to provide users with the best possible services, occasional changes in the broadcasting schedules are required. This publication shows the schedules in effect on January 1, 1966. Annual revisions will be made. Advance notices of changes occurring between revisions will be sent to regular users of these services upon request.

Statistical association methods for mechanized documentation. Symposium Proceedings Washington 1964, M. E. Stevens, V. E. Giuliano, and L. B. Heilprin, *NBS Misc. Publ. 269 (Dec. 15, 1965). $2.75.*
A Symposium on Statistical Association Methods for Mechanized Documentation was held in Washington, D.C., in March 1964. The Symposium was jointly sponsored by the Research Information Center and Advisory Service on Information Processing, Institute for Applied Technology, National Bureau of Standards, and by the American Documentation Institute. Topics covered include the historical foundations, background and principles of statistical association techniques as applied to problems of documentation, models and methods of applying such techniques, applications to citation indexing, and tests, evaluation methodology and criticism. This volume contains 22 of the papers included in the program, the abstracts of 4 additional papers that were presented, and the text of the talk given by R. M. Hayes at the banquet.

Photonuclear data index, *NBS Misc. Publ. 277 (Apr. 1, 1966). 55 cents.*
An index to experimental data on photonuclear reactions is presented. Organized by element and isotope, each entry in the index supplies quantitative information for a specific reaction on the ranges of excitation energy, source energy, detected particle energy, and emission angles for reaction produced covered in each reference. Information is also given on the type of measurement and detector used.

Bibliography on atomic transition probabilities, B. W. Glennon and W. L. Wiese, *NBS Misc. Publ. 278 (Apr. 22, 1966). 55 cents. (Supersedes Mono. 50.)*
A revised and updated bibliography on atomic transition probabilities is presented. The papers are arranged according to elements and stages of ionization, and the method employed and class of transitions are indicated behind each reference. Only articles on discrete transitions, both permitted and forbidden, are listed. Also included is a supplementary list of important papers dealing with transition probabilities from a general point of view, and a table of comprehensive papers not included in the element list.

Doors as barriers to fire and smoke, H. Shoub and D. Gross. *Bldg. Sci. Series* **3,** *(Mar. 25, 1966), 15 cents.*
A study was made of means for improving dwelling unit entrance doors as fire and smoke barriers. Existing combustible doors and frames could be modified to enhance their fire resistance, but it did not appear practical to raise them to the level of rated commercial fire door assemblies. Fire retardant paints, except those consisting of heavy, reinforced, intumescent-type coatings, provided little or no increase in fire resistance.
Several modifications of existing doors were not effective in preventing the transmission of smoke. However, controlling the pressure levels on both sides of a door, as by suitable venting, appeared to offer a means of reducing smoke penetration into an area.
It is recommended that current methods of fire tests of doors, and criteria relating to their fire smoke transmission be improved.

Selected values of chemical thermodynamic properties. Part 2. Tables for the elements twenty-three through thirty-two in the standard order of arrangement, D. D. Wagman, W. H. Evans, I. Halow, V. B. Parker, S. M. Bailey, and R. H. Schumm, *NBS Tech. Note 270–2 (May 6, 1966), 40 cents.*
Technical Note 270–2 is the second of a series of publications containing material prepared as a revision of the tables of Series I of National Bureau of Standards Circular 500, Selected Values of Chemical Thermodynamic Properties. This Note contains revised Tables 24 to 32, covering the elements silicon, germanium, tin, lead, boron, aluminum, gallium, indium, and thallium, and compounds of these elements following the Standard Order of Arrangement.
Tables for the first twenth-three elements and their compounds, and a discussion of the symbols, conventions, units of energy, and conversion factors used in this series are given in National Bureau of Standards Technical Note 270–1.

Nuclear and radiation standards of importance to the National Atomic Energy Program, H. W. Koch, J. H. Donnert, W. W. Havens, Jr., G. L. Rogosa, and L. Rosen, *NBS Tech. Note 283 (Mar. 31, 1966), 35 cents.*
A systematic approach to physical measurements in nuclear physics requires the establishment, availability, and use of standards. The standards of measurement may consist of standard cross sections, foils, counters, and evaluated nuclear data. Because of the fundamental importance of measurement standards, the Nuclear Cross Section Advisory Group has examined the definitions, requirements, characteristics, and availability of nuclear and radiation standards of importance to the national atomic energy program.

Some properties of the eigenfunctions and eigenvalues introduced by Bethe for the linear chain of atoms, H. Unruh, Jr., *NBS Tech. Note 328 (Apr. 19, 1966), 25 cents.*
The operations $S^2\psi$ and $S^{\pm}\psi$, in which ψ is an exact eigenfunction obtained by Bethe for the linear chain of localized spins, are discussed. The operations S^2 and $S^{\pm}$ are the usual square of the total angular momentum and the raising and lowering operators respectively. The results, valid for an arbitrary number of spin inversions, show, as expected, that all possible states of the system can be achieved by omitting all excitations associated with zero wave number but requiring each state to take all possible orientations in space.

Adsorption isotherms for polymer chains adsorbed from theta solvents, C. A. J. Hoeve, *J. Chem. Phys.* **44,** *No. 4, 1505–1509 (Feb. 15, 1966).*
In the case of interacting polymer chains near the interface, the first layer at the interface corresponding to the thickness of segments, is treated as a polymer solution to which the Flory-Huggins theory is applied. Interaction in other layers is assumed to be absent for Θ-solvents. On minimizing the free energy, adsorption isotherms are calculated. The amount of adsorbed polymer increases without limit and the fraction of segments in the first layer decreases to zero with increase in molecular weight and solution concentration. The root-mean-square distance of segments from the interface is also calculated and is found to vary approximately proportional to the square-root of the molecular weight, in good agreement with experiment.

Critical scattering of the perfluoroheptane-iso-octane system, G. W. Brady, D. McIntyre, M. E. Myers, Jr., and A. M. Wims, *J. Chem. Phys.* **44,** *No. 5, 2197–2198 (Mar. 1, 1966).*
The critical opalescence of mixtures of perfluoroheptane-iso-octane near and at the critical concentration has been examined by x-ray scattering measurements over a large angular range.
The measurements are discussed and shown to agree well with the assumed correlation function proportional to $e^{-Kr} \cdot r^{-1.1}$ near the critical temperature.

Polymer property-structure studies at the National Bureau of Standards; thermal stability, G. M. Kline, *Proc. European Plastics Congress, Milano, Italy, Sept. 20–23, 1964.*
Continuing studies at NBS of the thermal stability of polymers are summarized. Wall and Straus conclude, from a comparison of measured volatilization rates of pyrolyzed polystyrenes with computed theoretical rates, that a transfer mechanism reasonably explains the degradation behavior of polystyrene; "weak links" need not be invoked. Precise measurements of the molecular weight dependence of the degradation rates of polyisobutylene show very little MW dependence over a 50-fold range. The volatilization rate of gamma-irradiated polytrifluoroethylene was found to have been increased, reflecting a change in decomposition mechanism from a random one to a mechanism with possibly a large zip length. Irradiation and decomposition of polyvinyl fluoride and polyvinylidene fluoride, in the absence of air lead to an increase in volatilization rates, but with a stronger tendency than in PTFE for the formation of residues. The decomposition of polyvinylidene fluoride is characterized by greater HF production than in the case of polyvinyl fluoride. Crosslinking predominates over scission. The thermal stabilities of coordination polymers of bis(8-hydroxy-5-quinolyl)methane involving Mn, Co, Ni, Cu, and Zn were examined thermogravimetrically up to 1000 °C. The decomposition temperatures are markedly dependent on the atomic number of the metal.

Polymers and telomers of perfluoro-1,4-pentadiene, J. E. Fearn, D. W. Brown, and L. A. Wall, *J. Polymer Sci.* **4,** *Pt. A–1, 131–140 (1966).*
Perfluoro-1,4-pentadiene was prepared from 3,5,6-trichloro-octafluorohexanoic acid by pyrolysis and subsequent dechlorination with zinc in a high-boiling ether. This process also yielded three isomers of chloroheptafluoro-1,4-pentadiene. Polymerization studies showed that the monomer yielded rubbery samples, powdery samples, oils, and at least four dimers. There was also strong evidence that the 1,4-diene is converted into the 1,3-diene under conditions of polymerization.

The vaterite-type ABO_3 rare-earth borates, W. F. Bradley, D. L. Graf, and R. S. Roth, *Acta Cryst.* **20,** *Pt. 2, 283–287 (Feb. 1966).*
Approximate models for both the room temperature and high temperature modifications of the vaterite-type rare earth borate structure are deduced from X-ray powder diffraction data. A study of structure sensitive information, including optical properties and infrared absorption characteristics, leads to the conclusion that the low temperature form contains borate tetrahedra whereas the high temperature modification probably contains triangular borate ions inclined to the *c*-axis.

Accuracy and precision of standards, and measurements, W. A. Wildhack, Acta. *Imeko* **4,** *63–81 (1964).*
This paper reviews the accuracy of measurements and of calibration at the National Bureau of Standards, based on "accuracy charts" prepared for each of various areas of measurement. Accuracy charts, consisting of plots of accuracy vs. magnitude of the measured quantity for each of the more precise standards, are shown in connection with a discussion of the present status and future goals for measurement and calibration capabilities. Measurement areas included are length, mass, temperature, pressure, vacuum, force, resistance capacitance, inductance and voltage. The concept and utility of the accuracy chart itself are stressed, as a technique for a basis appraisal of capabilities and goals. The need for a more general agreement on expressions for accuracy is discussed, and recent work in this direction by NBS is reviewed.

Time-resolved electrical measurements in high current discharges, E. C. Cassidy, S. W. Zimmerman, and K. K. Neuman, *Rev. Sci. Instr.* **37,** *No. 2, 210–214 (Feb. 1966).*
A method for measurement of the resistive component of the instantaneous voltage across a sample installed in a high-voltage, high-current circuit is described. Simultaneous measurement of the current permitted time-resolved determination of electrical energy dissipation, power, and resistance of the sample. The system was calibrated calorimetrically, and measurements were made with exploding wire samples.

Experimental verification of superachromatism, R. E. Stephens, *J. Opt. Soc. Am.* **56,** *No. 2, 213–214 (Feb. 1966).*
To experimentally verify superachromatism a five-element prism, to deviate a beam of light approximately 30 degrees without dispersion or distortion, has been designed and constructed from three types of Schott glass. When tested on a spectrometer, viewing a narrow slit with a telescope magnification of approximately 30 times, no dispersion could be seen. Pointings on 7 isolated spectrum lines separated by a monochromator show a maximum dispersion of 3 seconds, 1 part in 36,000.

Force fields for the boron trihalides, I. W. Levin and S. Abramowitz, *J. Chem. Phys.* **43,** *No. 12, 4213–4222 (Dec. 15, 1966).*
The method of Edgell and Moynihan for determining Coriolis zeta constants from the infrared band contours of degenerate vibrational modes was verified for selected molecules and was then applied toward computing the zeta values for the E symmetry vibrations of the boron trihalide molecules. Since it is not feasible to define unique potential functions for the BX_3 species from only frequency data, general force fields were determined for the series by combining both the Coriolis zeta constants and the observed isotopic frequency data in a least-squares refinement scheme. The final force fields indicate that the sensitive stretch-bend interaction constant is a significantly large negative quantity that decreases as the series progresses from BF_3 to BI_3.

Interpretation of Brillouin spectra, R. D. Mountain, *J. Chem. Phys.* **44,** *No. 2, 832–833 (Jan. 15, 1966).*
When a fluid consists of molecules having internal degrees of freedom weakly coupled to the translational degrees of freedom of the fluid (phonons), it is not correct to refer to the phonons as isotropic fluctuations in the density. This is relevant to the interpretation of Brillouin scattered light in terms of the properties of the scattering fluid. An approximate expression for the ratio of the intensity of the unshifted component to that of the Brillouin components is presented and applied to CS_2.

Isotopic effects in the ν_3 fundamental of matrix-isolated BCl_3, J. J. Comeford, S Abramowitz, and I. W. Levin, *J. Chem. Phys.* **43,** *No. 12, 4536–4537 (Dec. 15, 1965).*
The spectrum of matrix isolated BCl_3 has been observed in the region of the ν_3 fundamental. The structure of each of the bands observed due to B^{10} and B^{11} isotopic species are interpreted as being due to the chlorine isotopic effect.

On the quantum-mechanical pair-correlation function of ^{4}He gas at low temperatures, S. Y. Larsen, K. Witte, and J. E. Kilpatrick, *J. Chem. Phys.* **44,** *No. 1, 213–220 (Jan. 1, 1966).*
The density independent part of the direct and exchange correlation functions for He^4, using the de Boer and Michels Lennard Jones potential, have been calculated at 2°, 1°, .1 °K. The necessary wave functions were obtained by numerical integration of the Schrodinger equation. The peak of the direct correlation function is much less than its classical value and occurs at a slightly larger radius. The tail (large *r*) agrees very well with the form given by the Wigner-Kirkwood expansion. The exchange correlation function which represents the entire effect of the spin and statistics of the system vanishes very rapidly with increasing temperatures.

Spectral distribution of scattered light in a simple fluid, R. D. Mountain, *Rev. Mod. Phys.* **38,** *NO. 1, 205–214 (Jan. 1966).*
The spectral distribution of light scattered by density fluctuations in a dense, monatomic, one-component fluid is calculated from the time dependence of the density fluctuations predicted by the linearized, hydrodynamic equations of irreversible thermodynamics.

The results of Landau and Placzek are verified and a procedure for deriving correction terms is discussed with the dispersion in the velocity of thermal sound waves obtained as an illustration. Particular attention is paid to the critical region. The properties of carbon dioxide are used to estimate the spectral distribution of critical opalescence. A comparison is made between light-scattering and sound-propagation experiments. Space dispersion near the critical point in the pressure and the thermal conductivity is examined briefly. Finally, some of the experimental problems involved in measuring the spectral distribution of the scattered light are discussed.

Spin-lattice relaxation in some rare-earth trichlorides, B. W. Mangum and R. P. Hudson, *J. Chem. Phys.* **44,** *No. 2, 704–713 (Jan. 15, 1966).*

Studies of *spin-lattice relaxation* of the ions Ce^{3+}, Nd^{3+}, Sm^{3+}, Ho^{3+}, and Er^{3+} present in low concentrations (0.2 to 2 percent) in the host lattice of $LaCl_3$ have been made in the liquid helium region by the pulsed-microwave method. The variation of the relaxation time, τ, with temperature permits separation of the contributions to the relaxation from the two-phonon (resonant and non-resonant) and single phonon processes.

The substances studied are not"well-behaved"; features such as non-exponential decays and variability of the derived values for the splitting between the ground and first excited levels are discussed. Some of the ions exhibit a significant variation of τ with concentration and Nd^{3+} shows an interestingly large anisotropy of τ in the Raman process.

The crystal structure of the strontium and lead tetraborates, $SrO \cdot 2B_2O_3$ and $PbO \cdot 2B_2O_3$, A. Perloff and S. Block, *Acta Cryst.* **20,** *Pt. 2, 274–279 (Feb. 1966).*

$SrO \cdot 2B_2O_3$ and $PbO \cdot 2B_2O_3$ are isostructural. These compounds crystallize in the orthorhombic system, $P2_1nm$, with two formula units in a cell of dimensions $a = 4.237$, $b = 4.431$, $c = 10.706$ Å for $SrO \cdot 2B_2O_3$ and $a = 4.244$, $b = 4.457$, $c = 10.840$ Å for $PbO \cdot 2B_2O_3$. A detailed structure analysis was carried out for the Sr compound only.

The structure was solved by conventional Patterson and electron density syntheses utilizing the heavy atom to establish the initial phases. Least squares refinement on three-dimensional data yielded a final R-factor of 7.1 percent.

The results reveal an unusual type of borate framework. All boron atoms are tetrahedrally coordinated. The unusual feature is the occurrence of an oxygen atom common to three tetrahedra.

Although the tetrahedra form a three-dimensional network by corner sharing the borate network gives the appearance of a layer-like structure because there are comparatively few links in the *c* direction. The layers can be described in terms of chains (parallel to *a*) of six membered rings having B-O edges in common. These chains are joined by non-ring oxygens to form layers which are parallel to the *a b* plane.

The Sr coordination is not clearly defined. There are nine nearest neighbor oxygens at distances ranging from 2.52–2.84 Å. There are six more oxygens at 3.04–3.20 Å which could conceivably be considered as part of the Sr coordination sphere.

Search methods used with transistor patent applications, J. R. Cornog and H. L. Bryan, Jr., *IEEE Spectrum, pp. 116–121 (Feb. 1966).*

As the world has become more technically oriented, the number of patent applications has been increasing also too rapidly for the Patent Office to assimilate them comfortably with current techniques. When an application for a patent is received, it must be evaluated as to novelty by a specialist who searches the prior art for similar patents. Previously, all such searches were done manually, which meant that the examiner had to rely entirely on his knowledge and experience. In an effort to remedy the situation the Office has instituted mechanized search methods. In order to ascertain the differences in patterns of thinking associated with manual and mechanized searches, a study was carried out in which a patent application in the transistor art was searched both manually and by a mechanized method. The mechanized search in this case permitted more patents to be analyzed more quickly but, being completely literal, it does not allow for hunches or browsing.

Acid-base behavior in methanol-water solvents, R. G. Bates and R. A. Robinson (*Proc. Intern. Symp. Electrochemical Society, Toronto, Canada, May 4–6, 1964*), *Book, Chemical Physics of Ionic Solutions, ch. 12, pp. 211–235 (John Wiley & Sons, Inc., New York, N.Y., 1966).*

Data for (a) the standard potential of the cell Pt; H_2 (g., 1 atm), HX (in methanol-water solvents), AgX;Ag (where X = Cl, Br, or I); (b) the activity coefficients and relative partial molal heat content of HX in methanol-water media; and (c) the pK and related thermodynamic quantities for the dissociation of weak acids in these solvents have been collected and critically examined. When the observed solvent effects on pK for acids of different charge types are corrected for changes in the electrostatic energy of dissociation, one obtains a fairly uniform solvent parameter. The change of this parameter as methanol is added to the solvent confirms the view that enrichment with methanol produces a more basic mixture up to a composition of about 80 wt. % methanol, after which the total basicity declines as the water concentration becomes low. A standard activity scale for methanol-water solvents, based on the unit pH^*, is proposed.

Combustion and reaction calorimetry of several compounds of interest in a light element program, G. T. Armstrong (*Proc. 3d Meeting of the ICRPG Working Group on Thermochemistry, El Segundo, Calif., May 17–18, 1965*), *Chemical Propulsion Information Agency I, No. 82 (U), 81–88 (July 1965).*

The heat of formation of beryllium fluoride has been determined in our laboratory by K. L. Churney, by direct combination of the elements. Using two samples of different purities and particle sizes, he obtained concordant results, despite marked differences in the completeness of reaction. The heat of formation is −242.89 kcal mol^{-1}, with a standard error of 0.29 kcal mol^{-1} computed from seven determinations (preliminary figures). A study of the heat of solution of beryllium metal powder in HF(aq) in a rotating bomb calorimeter has been initiated, and the experimental procedures have been worked out for obtaining valid heat measurements.

Kinetics of desorption of the beta-nitrogen states chemisorbed on tungsten, T. E. Madey and J. T. Yates, Jr., *J. Chem. Phys.* **44,** *No. 4, 1675–1684 (Feb. 15, 1966).*

The kinetics of desorption of the strongly chemisorbed β_1 and β_2 nitrogen states on tungsten have been studied. Independent techniques of isotopic mixing and flash-filament desorption have been employed. The rate of production of $^{14}N^{15}N(g)$ from $^{14}N_2(g)$ and $^{15}N_2(g)$ in a steady state flow experiment is completely accounted for by the kinetically determined rate of desorption from the chemisorbed layer. β_1-nitrogen appears to desorb by first order kinetics. β_2-nitrogen desorbs in a complex manner with higher order kinetics. The apparent β_2 desorption order decreases markedly as temperature increases. A superposition of two or more unresolved substates in the β_2 state is postulated. The temperature variation of desorption order can be accounted for by a lack of achievement of equilibrium between the spatially-separate β_2 substates during desorption at scan rates of 12.5 °K/sec or greater.

Above 1500 °K, where the steady state coverage of nitrogen is very low, a sticking coefficient of less than 0.02 has been measured. The sticking coefficient is nearly constant in the range 1500–1700 °K and over a 25-fold pressure range.

Photoionization mass spectrometry of NO, R. M. Reese and H. M. Rosenstock, *J. Chem. Phys.* **44,** *No. 5, 2007–2009 (Mar. 1, 1966).*

The photoionization of NO has been studied in the 1360–600Å range with mass analysis. All autoionization peaks found here below 900Å have been assigned to diffuse lines observed in absorption by Huber (7). In the 1130–900Å range several new vibrational progressions are deduced. Photoionization, Autoionization, Rydberg series, Nitric Oxide.

The reaction between $O(^3P)$ and condensed olefins below 100 °K, A. N. Hughes, M. D. Scheer, and R. Klein, *J. Chem. Phys.* **70,** *No. 3, 798–805 (Mar. 1966).*

The addition of oxygen atoms to condensed simple olefins has been studied in the 77 to 90 °K temperature range. The ground state $O(^3P)$ atoms were generated in the gas by dissociation of O_2 on rhenium or tungsten surfaces heated to 2300 °K.

At 90 °K and oxygen pressures below 40 millitorr, the major products were found to be the unfragmented epoxides and carbonyls. Above 50 millitorr ozonides and oxygenated products characteristic of rupture at the double bond were observed. Above 100 millitorr only the ozonides and its fragments were produced. At 77 °K, the ozonolysis reaction occurred at much lower oxygen pressures. Comparison of these results with those obtained in the gas phase at 300 °K indicates that the low temperature environment efficiently removes the excess energy from the excited biradical formed in the primary act of O atom addition to the double bond. In all cases studied, fragmentation was less extensive than in the comparable gas phase process.

Titrimetric and equilibrium studies using indicators related to Nile Blue A, M. M. Davis and H. B. Hetzer, *Anal. Chem.* **38,** *451–461 (Mar. 1966).*
The behavior of Nile Blue A and several closely related dyes in nonaqueous spectrophotometry and titrimetry was explored. Nile Blue A was used as the salt, the anhydro-base, and the oxazone. The other dyes were the chloride or anhydro-base having an alkyl, aralkyl, or aryl group attached to the 5-amino nitrogen in place of hydrogen. The arylamino derivatives, though less basic than Nile Blue A, are much stronger than Methyl Yellow and are useful reference bases in aprotic solvents. Their applicability in determining stoichiometry and the relative strengths of strong and moderately strong acids is discussed. The strengths of the indicators relative to sulfonephthaleins and other common acid-base indicators are different in aqueous and non-aqueous solvents, pointing to a useful role in non-aqueous differentiating titrations.

Thermodynamic property computations for systems analysis, J. G. Hust and R. B. Stewart, *ASHRAE J., pp. 64–69 (Feb. 1966).*
Methods for calculating thermodynamic properties from equations of state and zero pressure properties are reviewed. The calculation of entropy of gases, saturated fluids, and liquids is considered in detail. Particular attention is given to the determination of the two phase boundary and thermodynamic consistency of the calculated properties.
A method of iterative solution for implicit variables and its application to thermodynamic calculations are discussed. In addition methods of least squares are considered. Normal equations resulting from the usual minimization procedure are compared with corresponding equations of the constrained least squares problem. Discussion is also included on a technique for fitting related thermodynamic data simultaneously.

Critical configurational entropy at glass transformation, S. S. Chang, A. B. Bestul, and J. A. Horman, *Proc. VII Intern. Conf. Glass, Brussels, Belgium, 1965, pp. 26.1–26.15 (Gordon & Breach, New York, N.Y., 1966).*
When an equilibrium supercooled liquid transforms to a glass, the amount of configurational entropy which it possesses at the glass transformation is trapped into the glass. By two different methods, and a distinguishable variation of one of them, it is shown experimentally that the value of this configurational entropy at glass transformation for most glasses for which data exist to evaluate it is near 0.7 cal deg^{-1} per "bead" as defined by Wunderlich. These beads are equivalent to molecular chain links for polymers. The above stated result is obtained first by evaluating configurational entropy from experimental data on molecular configurational relaxation times, using a reinterpretation of the Williams-Landel-Ferry equation, for the temperature dependence of such relaxation times, in terms of configurational entropy rather than free volume. Secondly, the configurational e tropy at glass transformation is evaluated independently as the calorimetrically determined residual entropy of the glass at absolute zero temperature. In addition the above results imply a fixed value for the ratio of the glass transformation temperature to the reference temperature at which configurational entropy would vanish for an equilibrium supercooled liquid. This implication would provide a third method of evaluating configurational entropy at the glass transformation if the necessary reference temperature could be determined experimentally by a non-calorimetric method. The implications of the configurational entropy reinterpretation of the Williams-Landel-Ferry equation are examined.

Analysis of the spectrum of neutral erbium (Er I), N. Spector, *J. Opt. Soc. Am.* **56,** *No. 3, 341–349 (Mar. 1966).*
First results of a continuing analysis of Er I are given: 30 low levels belonging to the odd configurations $4f^{11}5d6s^2$ and $4f^{11}5d^26s$, as well as 138 high levels of even parity are assigned J-values. More than 300 absorption lines are classified. The connection of the odd levels to the $4f^{12}6s^2$ configuration is established, using transitions in the infrared. The energy matrices in intermediate coupling for the subconfiguration $f^{11}(^4I)d$ have been calculated and are given. The theoretical formulas were adjusted by a least-squares fit to 19 observed levels designated as $4f^{11}(^4I_{7_{1/2}, 6_{1/2}})5d6s^2$ resulting in new values for 6 electrostatic and 2 spin-orbit interaction parameters. The rms error was 186 cm^{-1}. Calculated percentage compositions in various coupling schemes show the $J_1 = j$ type to be the best for these levels.

ESR measurement of metastable atomic nitrogen in helium-nitrogen afterglows, K. M. Evenson and H. E. Radford, *Phys. Rev. Letters* **15,** *No. 24, 916–917 (Dec. 1965).*
The ESR (electron spin resonance) spectra of the $^2D_{5/2}$ and $^2D_{3/2}$ levels of atomic nitrogen were observed in the afterglow from He–N_2 microwave discharge. An X band (9.2 GHz) ESR spectrometer in conjunction with a high velocity flow system was used to observe the signals. Maximum concentrations were observed at N_2 pressures of 0.13 Torr mm with 3.2 Torr mm of added helium and at time less than 10 msec from discharge. The g factors of the $^2D_{3/2}$ and $^2D_{5/2}$ levels were found to be respectively 0.8802 ± 0.0004 and 1.2005 ± 0.0006.

Excitation of molecular rotation by slow electrons II, S. Geltman and K. Takayanagi, *Phys. Rev.* **143,** *No. 1, 25–30 (Mar. 4, 1966).*
A previous study is here extended to consider the effects on rotational excitation of the nonvanishing electronic spin of O_2 and the short range static fields of the H_2, N_2, and O_2 molecules. The spin effect is found to be negligible, while the effect of short range interactions can be quite large in certain energy regions. This permits a qualitative explanation of the heretofore unexplained ratio of the observed electron relaxation rates in oxygen and nitrogen.

Nucleation in polymers, F. Gornick and J. D. Hoffman, Ind. Engr. *Chem.* **58,** *No. 2, 41–53 (Feb. 1966).*
This article is a review of current theories and experimental data on homogeneous nucleation and crystal growth with chain folding in linear polymers.

Possible importance of internal excitation in ion-molecule reactions in the F region, L. Thomas and R. B. Norton, *J. Geophys. Res.* **71,** *No. 1, 227–230 (Jan. 1, 1966).*
The apparent electron loss rate in the F region is determined by ion-molecule reactions involving O^+ ions and O_2 or N_2 molecules. The present paper considers whether a dependence of the rate coefficients on internal excitation of the reactants could be important in the ionosphere and examines briefly the excitation and deactivation processes involved. Particular attention is paid to vibrational excitation of N_2 molecules and it is suggested that excitation by electron impact may be important especially during conditions of high electron temperature as might be expected during magnetic disturbances and aurorae.

Results of some recent transport calculations for electrons and bremsstrahlung, M. J. Berger and S. M. Seltzer, (*Proc. 2d Symp. Protection Against Radiations in Space, Gatlinburg, Tenn., Oct. 12–14, 1964, ed. A. Reetz, Jr.), Natl. Aeronaut. Space Admin. Spec. Publ. 71, pp. 437–448 (1965).*
Illustrative results are given for three types of problems: (1) the transmission of electrons through thin and thick foils, with emphasis on the effect of energy loss straggling; (2) the energy dissipation by electrons in a semi-infinite water phantom, for an incident broad beam (depth dose distribution) and for an incident pencil beam (distribution as function of two spatial variables); (3) the production of bremsstrahlung in thick targets. The data presented for the first two problems are entirely theoretical and result from a Monte Carlo calculation. Similar calculations for the third problem are compared with recent experiments.

Spin independence, W spin, parity, and SU(6) symmetry, H. J. Lipkin and S. Meshkov, *Phys. Rev.* **143,** *No. 4, 1269–1274 (Mar. 25, 1966).*

The assumption of strict spin independence of strong interactions between elementary particles forbids all three meson and meson-baryon-baryon couplings, such as $\rho\pi\pi$, $NN\pi$, and $N^*N\pi$. It is shown that these catastrophies may be avoided, even in the nonrelativistic limit, by adopting a modified definition of spin-independence, i.e., W-spin independence. A nonrelativistic definition of W-spin is obtained which requires only a trivial change to yield the relativistic description. The consequences of the assumption of W-spin independence are explored.

Other NBS Publications

J. Res. NBS 70B3 (Math. and Math. Phys.), No. 3 (July-Sept. 1966), 75 cents.

Error bounds for asymptotic solutions of differential equations. I. The distinct eigenvalue case. F. Stenger.

Error bounds for asymptotic solutions of differential equations. II. The general case. F. Stenger.

On the approximation of functions of several variables. B. Mond and O. Shisha.

Finding a rank-maximizing matrix block. A. J. Goldman and M. Newman.

On certain discrete inequalities and their continuous analogs. A. M. Pfeffer.

J. Res. NBS 70C3 (Engr. and Instr.), No. 3 (July-Sept. 1966), 75 cents.

Some harmonic properties of an oscillating Fabry-Perot interferometer. M. Gadsden and H. M. Williams.

Precise reflection coefficient measurements with an untuned reflectometer. W. E. Little and D. A. Ellerbruch.

A versatile ratio instrument for the high ratio comparison of voltage or resistance. A. E. Hess.

Console for the rapid and precise comparison of volt boxes. P. H. Lowrie, Jr.

Corrosion rates of binary alloys of nickel and iron measured by polarization methods. W. J. Schwerdtfeger.

The effect of cold-drawing on the creep behavior of a nickel-4.2 percent aluminum alloy. W. D. Jenkins and W. A. Willard.

Magnetic transformation and the influence of plastic strain on the shear modulus of Fe-Cr-Ni alloys. R. P. Mikesell and R. P. Reed.

Report of the 50th National Conference on Weights and Measures 1965, NBS Misc. Publ. 272 (Apr. 1, 1966). $1.00.

List of errata to accompany the first, second, and third printings of NBS Applied Mathematics Series 55, Handbook of Mathematical Functions with Formulas, Graphs, and Mathematical Tables, ed. M. Abramowitz and I. A. Stegun (April 1966). This errata is free to holders of AMS55, upon request from the Publications Section, A617 Administration Building, National Bureau of Standards, Washington, D.C. 20234.

Weather resistance of porcelain enamels. Effect of exposure site and other variables after 7 years, M. A. Rushmer and M. D. Burdick, Bldg. Sci. Series 4 (May 2, 1966), 20 cents.

Some properties of the calcium aluminoferrite hydrates, E. T. Carlson, Bldg. Sci. Series 6 (June 1, 1966), 20 cents.

Quarterly radio noise data. December, January, February 1964–65, W. Q. Crichlow, R. T. Disney, and M. A. Jenkins NBS Tech. Note 18–25 (Mar. 14, 1966), 40 cents. (Formerly Central Radio Propagation Laboratory of the National Bureau of Standards, now Environmental Science Services Administration, Boulder, Colo.)

Spark source mass spectrograph program July 1964 to June 1965, P. J. Paulsen and P. E. Branch, NBS Tech. Note 286 (Apr. 15, 1966), 25 cents.

Measurement philosophy of the pilot program for mass calibration, P. E. Pontius NBS Tech. Note 288 (May 6, 1966), 30 cents.

An introduction to sampled data and switching logic, T. L. Davis, NBS Tech. Note 334 (Apr. 1, 1966), 40 cents. (Formerly Central Radio Propagation Laboratory of the National Bureau of Standards, now Environmental Science Services Administration, Boulder, Colo.)

Composition, work and interrelation of international and national organization engaged in the standardization of dental materials and therapeutic agents, G. C. Paffenbarger and M. Kumpula, Intern. Dent. J. **15,** No. 4, 571–587 (Dec. 1965).

Crystal imperfections in magnesium fluoride, D. J. Barber, J. Appl. Phys. **36,** No. 10, 3342–3349 (Oct. 1965).

Dental application of polymers: a review, G. M. Brauer, J. Am. Dental Assoc. **72,** 1151–1158 (May 1966).

Dislocations and stacking faults in rutile crystals grown by flame-fusion methods, D. J. Barber and E. N. Farabaugh, J. Appl. Phys. **36,** No. 9, 2803–2806 (Sept. 1965).

Effect of reactions with the atmosphere during fatigue of metals, J. A. Bennett (Proc. Sagamore Conf. Fatigue, Sagamore, New York, Aug. 15, 1963), Book, Fatigue: An Interdisciplinary Approach, pp. 209–227 (Syracuse University Press, Syracuse, N.Y., 1964).

Electrometric method of *p*H determination, R. G. Bates, Book, Standard Methods of Chemical Analysis, 6th edition, IIIA. Instrumental Analysis, ed. F. J. Welcher, ch. 26, pp. 521–532 (D. VanNostrand Co., Inc. Princeton, N.J., 1966).

Field-ion microscopy of ruthenium at 77 °K, A. J. Melmed and R. Klein, J. Less-Common Metals **10,** 225–228 (1966).

Growth of large sodium chloride crystals from solution for color-center studies, P. M. Gruzensky, J. Chem. Phys. **43,** No. 11, 3807–3810 (Dec. 1965).

Melting, flow, and thermal expansion characteristics of some dental and commercial waxes, M. Ohashi and G. C. Paffenbarger, J. Am. Dental Assoc. **72,** 1141–1150 (May 1966).

Recrystallization of anodic alumina films, D. J. Barber, J. Electrochem. Soc. **112,** No. 11, 1143–1145 (Nov. 1965).

Rubber and rubber products, M. Tryon and E. Horowitz, Book, Standard Methods of Chemical Analysis, 6th edition, IIIB. Instrumental Analysis, ed. F. J. Welcher, ch. 59, pp. 1664–1763 (D. VanNorstrand Co., Inc., Princeton, N.J., 1966).

The concentration dependence of the sedimentation coefficient of polystyrene in dilute solution, I. H. Billick, preprint American Chem. Soc. **5,** No. 2, 855–860 (1964).

ADI auxiliary publications program, R. W. Zimmerer, IEEE Trans. Microwave Theory Tech. **MTT-13,** No. 6, 883–884 (Nov. 1965).

A precision pulse-operated electronic phase shifter and frequency translator, J. Barnes and A. Wainwright, Proc. IEEE **53,** No. 12, 2143–2144 (Dec. 1965).

Can infrared inprove visibility through fog? A. Ashley and C. A. Douglas, Illum. Engr. **61,** No. 4, 243–250 (Apr. 1966).

Condensate collection as a measuring technique for studying the cooling capacity of air-conditioning units, P. R. Achenbach and J. C. Davis (Proc. XI Intern. Congress of Refrigeration, Munich, Germany, 1963), Book, Progress in Refrigeration Science and Technology II, 1281–1286 (Pergamon Press Inc., New York, N.Y., 1963).

Cryogenic coil for megajoule energy storage, V. Arp, Proc. Intern. Symp. Magnet Technology, ed. H. Brechna and H. S. Gordon, pp. 625–629 (U.S. Atomic Energy Commission, 1965).

Design considerations for a Kossel microdiffraction camera, D. L. Vieth and H. Yakowitz, Rev. Sci. Instr. **37,** No. 2, 206–209 (Feb. 1966).

Heating performance of air-to-air heat pumps at two Air Force housing projects, P. R. Achenbach, C. W. Phillips, and W. T. Smith, ASHRAE J. **70,** 390–407 (1964).

Kinematic locator for crystal alignment, B. G. Simson and R. D. Deslattes, Rev. Sci. Instr. **37,** No. 3, 300–301 (Mar. 1966).

Laboratory study of the effect of solar radiation on cooling load of stationary refrigerated vehicles, P. R. Achenbach and C. W. Phillips (Proc. XI Intern. Congress of Refrigeration, Munich, Germany, 1963), Book, Progress in Refrigeration Science and Technology III, 1631–1635 (Pergamon Press Inc., New York, N.Y., 1963).

Measuring the cooling load of refrigerated vehicles by free evaporation of liquid nitrogen, P. R. Achenbach, C. W. Phillips, and R. W. Penney, Suppl. Bull. Intern. Inst. Refrigeration, Commission VII, 3, 115–124 (1965).

Infrared reflectance of frost, H. J. Keegan and V. R. Weidner, J. Opt. Soc. Am. Letter **56,** No. 4, 523–524 (Apr. 1966).

Lightness change of grays induced by change in reflectance of gray background, H. Takasaki, J. Opt. Soc. Am. **56,** No. 4, 504–509 (Apr. 1966).

Thoughts on weights and measures, M. W. Jensen, Soap and Chemical Specialties **VLII,** No. 4, 99 (Apr. 1966).

Field emission ultramicrometer, R. D. Young, Rev. Sci. Instr. **37,** No. 3, 275–278 (Mar. 1966).

Microscopic visualization of dose distributions, W. L. McLaughlin, Intern. J. Appl. Radiation Isotopes **17,** 85–96 (1966).

Multiple scattering corrections for proton range measurements, M. J. Berger and S. M. Seltzer, Natl. Acad. Sci.–Natl. Res. Council Publ. 1133, #5. Studies in Penetration of Charged Particles in Matter. Nuclear Science Series Report **39,** pp. 69–98 (1964).

Nuclear giant quadrupole resonance, R. Ligensa, W. Greiner, and M. Danos, Phys. Rev. Letters **16,** No. 9, 364–367 (Feb. 28, 1966).

** Publications for which a price is indicated are available by purchase from the Superintendent of Documents, U.S. Government Printing Office, Washington, D.C. 20402 (foreign postage, one-fourth additional). The NBS nonperiodical series are also available from the Clearinghouse for Federal Scientific and Technical Information, Springfield, Va. 22151. Reprints from outside journals and the NBS Journal of Research may often be obtained directly from the authors.*

★ U.S. GOVERNMENT PRINTING OFFICE : 1966 OL—223–178

UNIVERSITY MICROFILMS INC
SERIALS SECTION
313 NORTH FIRST ST
ANN ARBOR MICH

UNITED STATES
GOVERNMENT PRINTING OFFICE
DIVISION OF PUBLIC DOCUMENTS
WASHINGTON, D.C. 20402

OFFICIAL BUSINESS

POSTAGE AND FEES PAID
U.S. GOVERNMENT PRINTING OFFICE

JOURNAL OF RESEARCH of the National Bureau of Standards
A. Physics and Chemistry

Vol. 70A, No. 5 September–October 1966

Contents

	Page
Orientation of calcium molybdate ($CaMoO_4$) and other single crystals having the scheelite structure. E. N. Farabaugh, H. S. Peiser, and J. B. Wachtman, Jr.	379
Crystal structure of $BaGe[Ge_3O_9]$ and its relation to benitoite. C. Robbins, A. Perloff, and S. Block.	385
A rotating cylinder method for measuring normal spectral emittance of ceramic oxide specimens from 1200 to 1600 °K. Howard E. Clark and Dwight G. Moore.	393
Electron absorption spectrum of cobalt(II)-doped trisphenanthroline-zinc nitrate dihydrate. Curt W. Reimann.	417
Procedures for homogeneous anionic polymerization. Lewis J. Fetters.	421
The configurations $4d^n+4d^{n-1}$ 5s in doubly ionized palladium group. Yehuda Shadmi.	435
Publications of the National Bureau of Standards.	447

Library of Congress Catalog Card Number: 62–37059

For sale by the Superintendent of Documents, U.S. Government Printing Office, Washington, D.C. 20402. Price $1.00 (single copy).
Subscription price: $5 a year; $1.00 additional for foreign mailing.
UNITED STATES GOVERNMENT PRINTING OFFICE, WASHINGTON : 1966